Time-resolved and Static NMR Characterization of the Structure and Folding Kinetics of the Diels-Alder Ribozyme

Dissertation
zur Erlangung des Doktorgrades
der Naturwissenschaften

vorgelegt beim Fachbereich Biochemie, Chemie und Pharmazie
der Johann Wolfgang Goethe-Universität
in Frankfurt am Main

von

Vijayalaxmi Manoharan

aus

Chennai, Indien

Frankfurt am Main
2009
D30

Dem Fachbereich Biochemie, Chemie und Pharmazie der
Johann Wolfgang Goethe-Universität als Dissertation vorgelegt.

Dekan: Prof. Dr. Dieter Steinhilber
1. Gutachter: Prof. Dr. Harald Schwalbe
2. Gutachter: Prof. Dr. Beatrix Süß

Datum der Disputation: 2009

This thesis was prepared under the supervision of Prof. Dr. Harald Schwalbe between June 2005 and June 2009 at the Institute for Organic Chemistry and Chemical Biology of the Johann-Wolfgang Goethe-University of Frankfurt.

Acknowledgement

Many people have made this work possible. I dedicate this thesis to those who have been directly and indirectly behind it and who have made an impact in my life through their contributions.

To my advisor Prof. Dr. **Harald Schwalbe**

Thank you for your support and guidance. Your constant feedback and encouragement and ability to provide a macro perspective to my work have been invaluable.

To Dr. **Jens Wöhnert**, Dr. **Boris Fürtig,** Dr. **Jonas Noeske** - the RNA guys

I was lucky to have the smartest guys I have known with me in my graduate career. Your tremendous support definitely made my initiation into this world much smoother. Jens - the trouble shooter- who I have constantly consulted with even when he was 1000s of miles away! Your pithy explanations have saved me hours in the laboratory. Somehow you made it all sound so simple! I can't thank you enough for your support. Boris -who worked with me on this project from the very beginning - You have shown me how constant diligence definitely pays off. Thank you for tirelessly and patiently sharing your expertise. Jonas - I and my RNA are grateful to you for your patience and support in the lab. My RNA have definitely had it easy because of you.

Prof. Dr. **Andres Jäschke** and his group

For providing this fruitful collaboration on the Diels-Alder ribozyme. Thank you for your time and input on this project and for the numerous perusals and insightful remarks that finally made the publication of the work possible. I would also like to acknowledge his generosity in sharing RNA and ligand with me.

Dr. **Judith Klein-Seetharaman** and her group

For the nurturing in your laboratory during my programmer days and your encouragement and support that have got me where I am today. Thank you for generously hosting me in Pittsburgh for a year.

Dr. **Johannes Gottfried Zimmermann** - A perfect world will be filled with Zims! Zim, your good spirits are amazing. Your patience and support at the spectrometers were invaluable. Dr. **Christian Richter** - with his impressive technical expertise. Thank you for your excellent support at the spectrometers. **Elke Stirnal**, who has a way with RNA, thank you for the innumerable HPLC runs.

Anna Paulus and **Elena Hartmann** - Many a late nights at the lab were made cozy only because of Anna's presence in her office. Thanks so much for being there when we needed you - for finding the 'rat hole' which I really really adored. :) - for clarifying the numerous bureaucratic procedures and making our lives easier and for lots and lots of good conversations. Elena, your

enthusiasm is infectious. It was always good fun to be around you. I thank you two for being such good supports in our life.

Gerd Nielsen and Dr. **Henry Jonker**. I can not imagine my four years there without you guys in it. The coffee breaks - the lunch breaks - the laughs - the beer hour - the Alte Papier Mühle - the walks in the Taunus - Bad Soden barbecues - the stroopwaffels. I hope we stay connected. Henry, thanks for always having an open door – be it help with spectrometers, critical discussions or for just bouncing ideas.

Sridhar Sreeramulu and Dr. **Santhosh Gande**. For providing the home away from home. Countless couch crashes, cookouts in coffee room, movie nights, lab nights, weekends in lab. You guys made it so much fun. I have learnt so much from you two. Sridhar, your drive and commitment to your work is amazing. Thank you for always having the time and good ideas when I turned to you with mini crises. Dr. **Raja K. Muruga Poopathi** and **Jitendra Kumar** - I appreciate the interest you have always shown in my work and your invaluable inputs and encouragement. Also memorable are the days spent at your homes. Thanks for making me so welcome.

Dr. **Kai Schlepckow** – for stimulating discussions and of course for saving me from lab work by generously sharing his hoard of DMN. Dr. **Jürgen & Iris Graf** – my time in Frankfurt was definitely enriched by your presence. Thanks for the good conversations, awesome food and wine. **Jan-Peter Ferner** - your enthusiasm in everything to do with RNA and relaxation is cool.

Dr. **Nicole Schmut and Max Stadler** – who have contributed so much of their valuable time for the smooth running of the lab. Dr. **Christian Schlörb** and **Martin Hähnke**, **Daniel Mathieu** and **Fabian Hiller** for being such competent and cheerful computer administrators in addition to being good researchers. Dr. **Elke Duchardt**, Dr. **Julia Wirmer,** Dr. **Steffen Grimm,** Dr. **Karla Werner, Neda Bahktiari, Janina Buck, Christian Gerum,** Dr. **Hamid Nasiri** and **Jörg Rinnenthal,** the original guys and fellow colleagues. **Anna Wacker, Senada Nozinovic, Anke Reining, Katja Barthelmes**, **Melanie Koschinat**, **Friederike Heinicke, Tanja Machnik, Anna Lena Lieblein, Florian Buhr, Jochen Stehle and Robert Silvers –** the youngsters leading the show now.

Dr. **Karin A Heidemann, Teresa Jimenez, Stephan Rehm, Carlos & Stefanie Mauricio**. for the Clubkeller nights (and mornings!) the Lokalbahnhof and parties. Your warmth and hospitality definitely helped me find my footing there. Dr. **Jesse & Ralf Bidinger**– for opening your home to us and for the many a good evenings around your kitchen table. **Sofia and** Dr. **Radhan Ramadass** – for the many late nights and many many debates about everything under the sun.

To my loved ones in Pittsburgh – my crazy nephews who bring perspective into my life. My family there and in India, who are happy that the end is in sight at last. **Oznur Tastan,** for the numerous brunches, the sleep-overs, the

workathons and most of all, for the constant companionship, encouragement and support.

And to **Andreas Christoph Zollmann** – my husband - for being a pillar by my side.

Contents

Abstract

Despite the well-known importance of ribonucleic acids (RNA) in cell biology, it is astounding to realize the pace at which new fundamental functions of RNAs have been discovered. One of the fundamental reasons for the multitude of functions of RNA is the property of RNA to adopt different conformations or folds. The primary sequence of RNA, a linear polymer built from four different repetition units, can fold into alternate secondary structure motifs which in turn form alternate long-range interactions in complex tertiary structures. Ligands such as metal ions or small molecular weight metabolites and also proteins or peptides can bind to RNA and induce the changes in tertiary conformation.

For example, in the cell, RNA participates in gene regulation in the form of riboswitches. Riboswitches are found in untranslated regions of messenger RNA (mRNA) and adopt alternate conformations depending on the presence or absence of specific metabolites. If a metabolite is present above a specific concentration, it induces a conformational change in the respective riboswitch by binding and thereby alters gene expression. Another example is the RNA thermometer which participates in the cell translational mechanism by a similar strategy. Translation initiation requires the binding of RNA thermometers to the ribosome. The ribosome binding region is located in the 5' untranslated region of mRNA. At low temperatures this region is prevented from binding to the ribosome by forming basepairs. At higher temperatures, these basepairs dissociate allowing ribosome binding and subsequent translation.

Therefore, the characterization and delineation of the kinetics and pathway of RNA folding is important to understand the function of RNA and is an important contribution to fundamentally understand RNA's role in the cell. RNA conformational transitions occur over a wide range of timescales. Depending on the timescale, various biophysical techniques are used to study RNA conformational transitions. In these biophysical studies, achieving good structural and temporal resolution constitute frequently encountered challenges or limitations. For example, single molecule FRET spectroscopy provides high temporal resolution in the milliseconds at high sensitivity but

lacks atomic resolution. Recent advances in the field of Nuclear Magnetic Resonance (NMR) spectroscopy have enabled the elucidation of tertiary folding events to be characterized with atomic resolution.

This thesis involves the use of NMR spectroscopy to characterize the folding of RNA molecules. Kinetics experiments require rapid initiation of the kinetics followed by monitoring of the reaction. In this thesis, two different folding initiation techniques have been applied and coupled to the subsequent detection of RNA folding using NMR spectroscopy, namely, **photocaging** and **rapid mixing**.

The method of photocaging is well established (Kuhn and Schwalbe, 2000) and builds on the following principle: A photolabile moiety is attached to a molecule that prevents a specific interaction. Upon irradiation of the molecule with the photolabile group using laser light at a specific wave length, at which the molecule of interest is not absorbing, the protecting group is released. In our group, together with the group of S. Pitsch, ETH Lausanne, we could "cage" RNA at its equilibrium state by a photolabile molecule (similar work has been carried out in the group of A. Heckel).

Rapid and traceless release of the photolabile precursor compound by a laser pulse releases the RNA to fold into its native state; the build-up of the native state of the RNA is monitored by NMR signals that are uniquely characteristic for the native state of the RNA. By optically coupling a laser source to an NMR magnet, the above procedure can take place *in situ* and the kinetics recorded by NMR.

Several different molecules can be caged: The photocage can be attached to RNA. Then, a modified photolabile nucleotide can be placed at strategic positions of a target RNA whose folding properties is to be studied. The photocage can also be attached to a ligand: if folding is dependent on ligand binding then the ligand can be modified to carry a photosensitive unit whose degradation allows binding to RNA.

In this thesis, an alternative method for photocaging is introduced. Here, metal ions essential for folding of the RNA are photocaged using the photolabile chelating agent Dimethyl-nitrophen (DMN). Photolysis of DMN releases the metal ion, thereby RNA folding is initiated. In the rapid-mixing technique, one of (several) components required for proper folding of the RNA

is rapidly injected into an NMR sample *in situ* by the use of a pneumatic injection device.

The Diels-Alder ribozyme family developed in the laboratories of A. Jäschke, Univ. Heidelberg, was investigated by time-resolved NMR experiments using the above techniques. The Diels-Alder ribozyme is an *in vitro* selected RNA that catalyzes the cycloaddition of anthracene dienes and maleimide dienophiles (Seelig and Jäschke, 1999). Several considerations lead to the selection of this ribozyme:

- The Diels-Alder ribozyme is a non-natural catalyst obtained by *in vitro* selection. It exhibits an interesting pseudoknot architecture, usually found in natural ribozymes, as the basis of its catalytic activity.
- Tertiary folding of the RNA into its catalytic active pseudoknot form is Mg^{2+} - dependent, and therefore is an excellent candidate for the metal ion photocaging method as well as the rapid-mixing technique.
- The catalytic properties of the ribozyme were already well described by a host of biochemical methods including probing and mutation studies of both the catalyst and substrates. Moreover, the crystal structure of the RNA in its catalytic state, both product bound and unbound had been determined giving a static image of the equilibrium native conformations. Imino proton resonances are good tools for structure probing (Hobartner and Micura, 2003b). Initial static NMR experiments indicated significant changes in imino-proton chemical shifts on addition of metal ions in the presence of an Diels-Alder adduct thereby providing defined ‘start’ and ‘end’ states for monitoring kinetics.
- At the time of the start of this study, this ribozyme was also being investigated by independent groups using complementary biophysical techniques such as Fluorescence Resonance Energy Transfer (FRET) and Electron Paramagnetic Resonance (EPR). Subsequently, these studies provided valuable information on the conformational landscape of the folding kinetics and the role of metal ions in it.

In the present study, three ribozymes from the Diels-Alder family were investigated. The wild-type A27 WT was the first studied molecule by the photocaging technique. Metal ion induced tertiary folding was found to be too fast for NMR monitoring. Therefore, a single nucleotide mutant, G27 MUT was chosen and investigated using both methods to initiate RNA folding. This mutant also had the same tertiary conformation as the wild-type according to the crystal structure but with 30% less catalytic reactivity. Another single nucleotide mutant G40 MUT was also identified for kinetic investigation based on its similarity to G27 MUT. This mutant was interesting as it differed from G27 MUT only in the location of the G and the A nucleotides on the two pairing strands located in one of the helices of the tertiary fold, but this causes an similar apparent reduction in reactivity from the wild-type by 70%.

Static NMR results showed that both mutants display conformational heterogeneity in the absence of metal ions. This conformational heterogeneity in the apo-state of the two mutant ribozymes significantly influences their folding rates and also folding pathways. The metal ion induced rates of folding for both mutants were dependent on disruption of unfavorable non-native basepairs in the apo state of the Diels-Alder ribozyme. The time-resolved experiment using rapid mixing techniques showed biexponential kinetics for both mutants. The folding rates observed differed by three orders of magnitude from the A27 WT folding.

A model based on the characterization of the free and metal-bound forms of the ribozymes is proposed to account for the difference in the folding rates of the wild type and the two ribozymes. Evidence is provided that the reactivity is modulated due to local dynamics around the catalytic pocket for the G27 MUT ribozyme.

CHAPTER I

1. Introduction

1.1. RNA

Although nucleic acids were first discovered in the cell nuclei in the 1870s by Johann Friedrich Miescher (Dahm, 2005), the discovery of the ribonucleic acids, 'RNA', by Phoebus Levene happened only in the 1910s (Bédoyère, 2005; Regis, 2008). Levene's work established the defining element, the sugar component of the two types of nucleic acids. Even though it was soon clear that RNA-containing molecules, the ribosome in the cytoplasm of the cell, were essential for protein synthesis, subsequent profiling of RNA was only based on the discovery of the messenger RNA (mRNA). Originally called DNA-like RNA (Volkin and Astrachan, 1956), their significance as the messengers of genetic material were deduced by François Jacob and Jacques Monod who named them messenger RNA in the 1960s (Jacob and Monod, 1961). RNA molecules thus climbed up a notch in importance in the cell cycle. However, it was still considered to be only a temporary entity, a copy of the indispensable molecule, the DNA. The next important milestone in the story of RNA is the discovery that RNA could also function in the manner of proteins, carrying out important biological function. It was found that RNA were capable of assuming complex tertiary folds with the discovery of the compact tertiary fold of tRNAs (Fresco et al., 1966). The discovery in 1982 of the self-splicing pre-ribosomal RNA (rRNA) of the ciliate *Tetrahymena,* the first example of an RNA molecule acting as a catalyst that forms an active site for biochemical reactions, led to coining the term 'ribozyme' (Kruger et al., 1982). Quickly after, several other natural ribozymes were discovered. Most notable among these are ribonuclease P (RNase P) responsible for the pre-processing of tRNAs (Guerrier-Takada et al., 1983), Group I (Cech, 1990) and Group II introns (Fedorova and Zingler, 2007), Hammerhead ribozyme (Prody et al.,

1986), VS RNA (Saville and Collins, 1990), hairpin ribozyme (Ferre-D'Amare, 2004) and the spliceosome (Valadkhan and Manley, 2001; Valadkhan et al., 2007). In 2000, definite proof of the ribosome, arguably the most important molecular entity in living cells, being a ribozyme was provided by the determination of the atomic-level picturing of the site of peptidyltransferase, which showed it to be entirely composed of RNAs with no proteins in its vicinity (Nissen et al., 2000). In addition, it became increasingly clear that RNA molecules have important roles in the living cell apart from their roles in protein synthesis.

In a living cell, RNAs performing functions unrelated to mRNA, tRNA and rRNA are collectively called non-coding RNAs (ncRNA) (Eddy, 2001; Hannon et al., 2006; Storz, 2002). They are involved in gene silencing (Hammond et al., 2000), RNA modification (Maas and Rich, 2000) and processing, protein stability (tmRNA) (Gillet and Felden, 2001), translocation (Keenan et al., 2001; Walter and Blobel, 1982) and DNA replication (Theimer and Feigon, 2006), to name just a few. In particular the discovery of RNA interference (RNAi) which results in gene silencing or even in the expulsion of sequences from the genome is an important milestone in that it can be exploited therapeutically. Riboswitches are RNAs that act as gene expression regulators by directly binding with cellular metabolites, ribosomal subunits and proteins (Mironov et al., 2002; Nahvi et al., 2002; Soukup and Soukup, 2004; Winkler et al., 2002a; Winkler et al., 2002b; Winkler et al., 2004). RNA catalysts using a multitude of methodologies in their functionality were identified. Several groups demonstrated on the hepatitis delta virus ribozyme that an RNA can act as a general base catalyst (Ferre-D'Amare et al., 1998; Nakano et al., 2000; Perrotta et al., 1999). Several excellent reviews have been written highlighting their significance in the cellular life cycle and also its implications to our understanding of the origin of life on earth (Doudna and Cech, 2002). Increasingly, RNA motifs were found that mimic protein motifs. Indeed, the discoveries of the manifold functions of the RNA lead to speculation of RNA as the precursor molecule to both DNA and proteins (Gilbert, 1986; Woese, 1968).

1.2. *In vitro* selection and non-natural RNAs

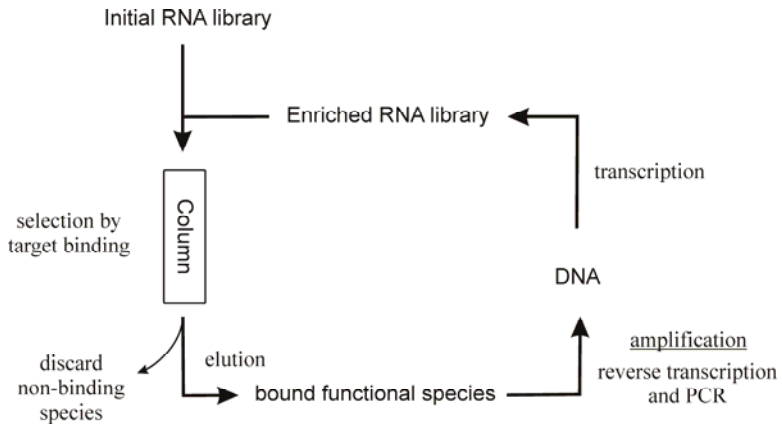

Figure 1: A schematic representation of the in vitro selection cycle.

In parallel to the discoveries of natural ribozymes, *in vitro* selection (Beaudry and Joyce, 1990; Ellington and Szostak, 1990; Szostak JW, 1993; Tuerk and Gold, 1990) played an important role in understanding and exploring the capabilities of RNA. Advances in this field were also partly fueled by the intense speculation of an 'RNA world' where it is postulated that RNA molecules alone could have possibly performed all essential processes for life to exist. In general, *in vitro* selection experiments involve the isolation of innovative peptides, proteins and nucleic acids depending on their performance of a given function (Figure 1). Efficient sequences identified from a huge library of sequences are first selected and amplified. Next, they undergo a number of further stringent selection rounds. In this manner, the best sequences for a given function are identified (Famulok and Jenne, 1998). Since both genotypic (the genome) and phenotypic (the expressed features of the genome in relation to a given environment) information are embedded in catalytic nucleic acids they are better suited for this procedure (Breaker, 1997). Several novel oligonucleotide catalysts for reactions including phosphorylation (Lorsch and Szostak, 1994), aminoacylation (Illangasekare et al., 1995), transesterification (Carmi et al., 1996; Jenne and Famulok, 1998), DNA cleavage (Carmi et al., 1996), amide bond formation (Zhang and Cech,

1997) and Diels-Alder reaction (Seelig and Jäschke, 1999; Tarasow et al., 1997) have been identified.

Another application of *in vitro* selection is to select mutants of an unstable wild type. This selection is applied when mutants are better suited for characterization because of their more stable structure and are therefore investigated to help understand the wild type (Juneau et al., 2001). Another important application area is the development of antiviral drugs. For example, to target the Hepatitis C virus (HCV), a cleaving ribozyme, the Hammerhead ribozyme, was designed to carry a domain that binds to the HCV IRES domain. The first step in this *in vitro* selection procedure was identification of binding domains. This was done by attaching a strand of randomized oligonuleotides to the Hammerhead ribozyme and selecting against binding to the IRES domain of HCV. Subsequently the selected ribozymes were again run through selection procedures for cleavage activity (Romero-Lopez et al., 2005). The process is called *in vitro* evolution when the element of mutation is added to it, due to its mimicry of the Darwinian evolution of nature. A comprehensive review focusing on the development of nucleic acid enzymes by directed *in vitro* evolution is found in the review by Joyce (Joyce, 2004). An example of directed *in vitro* evolved ribozymes is the well studied and the first reported RNA ligase ribozymes (Bartel and Szostak, 1993). Selection and evolution techniques are strategies to identify molecules with tailored functionality that are orthogonal to the more traditional, so called rational design strategies of molecules. In Synthetic Biology, the molecule capable of regulating gene expression at the translational level was evolving. A complementary segment of the ribosome binding region was introduced into the 5'-UTR of a mRNA to induce hairpin formation and thereby inhibit ribosomal docking and translation. Subsequent rescue of translation was performed by introducing a ncRNA designed to bind with the hairpin loop which induces structural modifications that are favorable for ribosome binding (Isaacs et al., 2004). With the development of these sophisticated techniques, currently, there exists a sizable repertoire of functional RNAs.

The advantage of *in vitro* selection lies in its ability to directly select against a desired function. Aptamers with initial favorable functional properties are bound to the ligand which is subsequently isolated to retrieve the aptamers. One of the disadvantages is the low specificity of binding. This low specificity is an inherently built-in weakness of the selection procedure and especially an issue in antiviral drug therapy where recent reports highlight the existence of this problem (Kleinman et al., 2008).

The diversity of functions of RNA molecules is attributed to the structural versatility of RNA molecules. This finding seems surprising as RNA, like DNA, are made up of only four building blocks (Figure 2b) and therefore it was long believed that their structural repertoire must be limited, at least in comparison to proteins which have 20 highly varied amino acids. However, RNAs are able to undergo conformational transitions by binding proteins or peptides or other cofactors (Draper, 1999; Leulliot and Varani, 2001; Williamson, 2000) Folding of the RNA, including secondary structure motifs, tertiary structure and assembly of large complexes with other RNA and proteins, are highly sensitive to pH, temperature and ions making it very complex. Differentiating the structural and chemical effects of these factors from experimental results remains a challenge (Butcher, 2001; DeRose, 2002).

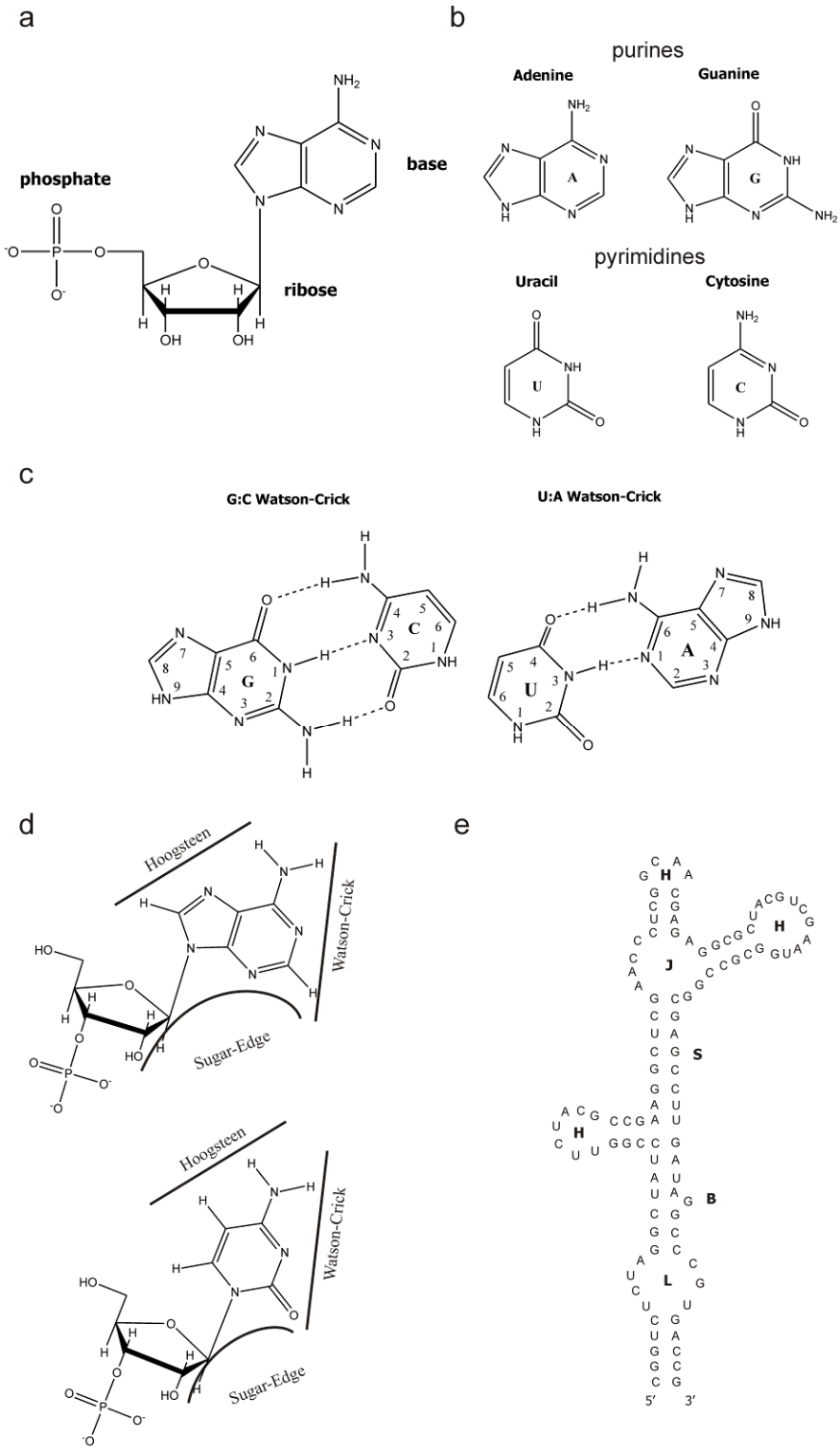

Figure 2: a) Constitution of a nucleotide. b) All four bases that differentiate the four nucleotides. c) Hydrogen bonded Watson-Crick basepairs. d)The three edges of purines and pyrimidines that are available for base pair interactions (Lescoute and Westhof, 2006). e) Secondary structure representation of an RNA primary sequence displaying the various possible secondary structures. S-Stem, H-Hairpin Loop, J - Junction, B- Bulge and L- internal Loop.

1.3. Structure and Mechanism

The field of Structural Biology tries to understand the molecular architecture of organisms. In comparison to the structure determination of protein enzymes, RNA enzymes have proven difficult to study. This is due to the difficulties encountered in the crystallization of these molecules in their active form. Often the crystallized structures are not in accord with the results from previous chemical studies, as in the case of the well studied Hammerhead ribozyme (Blount and Uhlenbeck, 2005b; McKay, 1996; Verma et al., 1997). The Hammerhead ribozyme is a self-cleaving ribozyme found in plant viruses made up of three helices and a junction region that is highly conserved. Several biochemical experiments pointed to the important role of a divalent metal in the cleavage activity. For example, experiments based on sulfur substitution of the scissile phosphate oxygen lead to a metal ion coordinated mechanism hypothesis (Koizumi and Ohtsuka, 1991). The crystal structures of the ribozyme on the other hand did not show any metal ions close to the active site, thus indicating a conformational change prior to cleavage (Pley et al., 1994; Scott et al., 1995). Structures of other ribozymes, e.g. the *in vitro* selected leadzyme, obtained from NMR studies showed high conformational flexibility of their active sites (Hoogstraten et al., 1998; Legault et al., 1998). In general ribozyme structures were found to adopt an architecture where scaffolding for the internal active core are provided by stable helices with Watson-Crick basepairs while the internal core itself remains less rigid to accommodate substrate entry and product release as most catalytic activities occur by strategic positioning of substrates.

The RNA primary structure, the nucleotide sequences, leads to secondary structure formation following intrinsic canonical Watson-Crick base-pairing properties. The next level of organization, the tertiary structure, is mediated either by the presence of metal ions or protein cofactors or by inherent propensity of long-range, non-Watson-Crick type interactions of nucleotides. Although most RNAs commonly require divalent metal ion cofactors for these tertiary native structures, exceptions exist. For example, the Hepatitis Delta Virus (HDV) does not require metal ions for its native tertiary

structure, although in this case metal ions are found in the active site and are essential for the catalytic activity.

1.3.1. RNA Structure Detection

RNA akin to DNA is made up of four nucleotides (Figure 2b). DNA is able to form only helices, and its functionalities are limited. RNA forms more readily several non-canonical interactions including the G.U wobble base pair and also triple basepairs. The pair wise basepair interactions in turn show several variations based on their bonding patterns. The most common hydrogen-bonding pattern, the Watson-Crick base pair is shown in Figure 2c. These hydrogen bonds involve the 'Watson-Crick edge' of the nucleobases. The two other edges that are also sometimes involved in base pair hydrogen-bonding are the 'Hoogsteen or CH edge' and the 'Sugar edge' involving the 2`- hydroxyl group (Figure 2d). In addition, the two glycosidic bonds may be oriented to form either the *cis* or *trans* forms. Cis is where both bonds are found on the same side if a line drawn between the nucleobases and parallel to them and the trans form occurs when the glycosidic bonds appear on either side of the line (Leontis and Westhof, 2001). These features give it a surprisingly large repertoire of interactions to draw from for its 3D structure. The most common secondary structure elements found in RNA include helices or stems, hairpins, loops, bulges and junctions (Figure 2d). These are the building blocks that form the complex tertiary conformation of the RNA with the aid of cofactors. The most common motif of tertiary structures is the pseudoknot. Since first proposed to occur in the 3' terminal of some viral RNAs in plants (Pleij et al., 1985), the pseudoknots have been found to be a ubiquitous feature of many complex RNA structures (Dam et al., 1992; Tzeng et al., 1992; van Belkum et al., 1985). Pseudoknots are formed when nucleotides from a loop region base pair with complementary nucleotides in a single strand or loop region outside of its own stem thereby forming additional stem and loop regions.

Standard biophysical procedures for structure detection, apart from the two atomic resolution techniques X-ray crystallography and Nuclear Magnetic Resonance spectroscopy (Felden, 2007; Furtig et al., 2003), include low resolution techniques such as SAXS (Lipfert and Doniach, 2007), fluorescence

and FRET spectroscopy. In addition, Raman (Leulliot et al., 1999) and CD spectroscopy (Meroueh and Chow, 1999) probe sensitive changes in structure by mutation studies. Some of the classical biochemical techniques that often complement the biophysical techniques are discussed below.

Biochemical structure detection methods

Chemical footprinting methods have been used extensively to probe the structures of RNAs at nucleotide resolution (Ansel-McKinney and Gehrke, 1997). In probing experiments, chemical reagents like diethylpyrocarbonate (DEPC) and dimethylsulfate (DMS) can be used as probes to infer structural details. DEPC modifies N7 of adenine and DMS alkylates N3 of cytosine or N1 of adenine. Therefore, if adenosine nucleotides are part of structures they are unavailable for modification to these chemical probes, and thus report on structure of the RNA (Peattie and Gilbert, 1980). Classical methods also include the use of RNA modifying enzymes like RNAses which differentiate between single stranded and double stranded regions of the RNA. In comparison to enzyme probing and chemical footprinting, hydroxyl radical footprinting is a versatile probing method due to the small size of the probing reagent and non sequence specific reactivity. Hydroxyl radicals are usually generated by radiolysis of water using synchrotron X-ray beams but can also be chemically generated. These radicals attack the C4` position of the sugars leading to the subsequent breakage of the phosphodiester backbone (Tullius and Dombroski, 1986). They have been extensively used in RNA secondary and tertiary structure probing (Latham and Cech, 1989). Other methods namely SHAPE chemistry and oligonucleotide hybridization techniques are discussed in the following sections.

Structure probing in vivo

Although a wealth of information about the structure, folding pathway and function of RNA is available, they are not based on *in vivo* or physiological cell conditions. Most studies are conducted *in vitro*, in carefully controlled environments outside the cell. These *in vitro* conditions can have significant impact on structure and dynamics of RNA, and can therefore be quite different

from the biological environment of the cell. RNA has the ability to adopt multiple conformers with small differences in ΔG, therefore, different conformers can be significantly populated at room temperature (Hobartner and Micura, 2003a). Therefore, the ability of RNA to correctly achieve its native fold *in vivo* is of great interest. Studies based on RNA activity measurements indicate that RNA folding is similar in both *in vitro* and *in vivo* conditions. However, the opposite behavior has also been observed (Schroeder et al., 2002). An example of the latter case was shown in the *Tetrahymena* pre-rRNA. Here, based on activity measurements, it was found that misfolded mutant structures formed *in vitro* were not formed and function was not impaired under *in vivo* conditions (Nikolcheva and Woodson, 1999). Two possible explanations have been proposed to explain this ability of avoiding misfolding by the RNA based on exchange kinetics between the non-functional alternate folds (Mahen et al., 2005). RNA chaperone aided rapid exchange kinetics of alternate folds of the RNA would enable it to achieve its functional fold more rapidly; misfolded species would therefore be trapped by higher activation barriers to refolding (Herschlag, 1995; Woodson, 2000), while slow exchange kinetics support a sequential fold which depends on the transcriptional 5' to 3' polarity where sequences upstream determine the fold of the RNA (Diegelman-Parente and Bevilacqua, 2002; Heilman-Miller and Woodson, 2003; Koduvayur and Woodson, 2004; Pan et al., 1999). In the light of these outstanding questions, *in vivo* probing of the RNA structure is important.

One method used in the *in vivo* probing of structure of RNA is probing with dimethylsulfate (DMS) (Waldsich and Schroeder, 2005). DMS methylates the N7 position of guanine and N1 of adenine and N3 of cytidine. The modified sites are then mapped by primer extension, which yields a pattern of protected nucleotides. The limitations of this complex approach have been discussed comprehensively (Waldsich and Schroeder, 2005). Another approach is SHAPE chemistry. SHAPE (selective 2`- hydroxyl acylation analyzed by primer extension) is based on the reactivity of 2`- hydroxyl group to acylating agents to form bulky adducts. Since nucleotides that are inhibited by base pair interactions do not react favorably with these agents, flexible nucleotides can thus be identified. Nucleotides bound to the acylating agents

are subsequently identified by reverse transcriptase primer extension experiments, since the bulky adducts terminate extension (Merino et al., 2005).

As is the case with proteins, the function of RNA is strictly correlated to its three dimensional fold. In RNA, this statement implies both the final folded form as well as the kinetics of attaining this final fold. For example, gene regulation by riboswitches depends on the folding of its aptamer domain, making the characterization of the folding kinetics an important component of its functional characterization (Schwalbe et al., 2007). Many interactions, including base stacking, non-Watson-Crick base pairing and the neutralization of phosphate backbone negative charges by ions, stabilize the RNA tertiary structure (Neidle, 2008; Saenger, 1984). Given the growing database of highly functional three-dimensional folds of RNA, the dynamics investigation of RNA is an important research area that contributes immensely to understanding the functional mechanisms involved.

1.4. RNA Folding

From a biological point of view, it is of interest to deduce the structure as well as the way in which these structures are actually formed. Complementary biophysical and biochemical tools are used to deduce the complexity of RNA folding as well as their dynamics due to the wide range of time-scales involved in their folding (Pyle and Green, 1995). The earliest investigations of RNA folding were concerned with the folding of the tRNA molecules where it was found that local secondary structures form within 10-100 μs. These finding were based on temperature-jump and NMR experiments on small RNA hairpins and tRNA (Cole and Crothers, 1972; Coutts, 1971; Woodson, 2000). Tertiary interactions were formed more slowly in the 10-100 ms timescale (Crothers et al., 1974; Lynch and Schimmel, 1974; Riesner et al., 1973). Metal ions were found to be the most common cofactor required for RNA folding.

Ions and RNA folding

Due to the high negative charge of the RNA phosphodiester backbone, structure formation requires charge compensation through positive counterions.

Mg^{2+} and K^{+} are the most common divalent and monovalent ions used for folding investigations. Particular efforts have been made to differentiate the structural contributions of ions from their contributions to catalytic activity by using combinations of biophysical and biochemical techniques (Fedor, 2002). The ion-RNA interaction is mainly governed by electrostatic forces. However, radii and the charge also affect their behavior in the form of steric effects and hydration energies (Draper et al., 2005). This has been demonstrated in cases where the RNA is shown to fold into the native 'functional' structure in the presence of either Mg^{2+} or Ca^{2+}. Catalytic activity is, however, impaired in the presence of Ca^{2+} (Grosshans and Cech, 1989; Seelig and Jäschke, 1999). The ion dependence of RNA folding is very specific for the given RNA sequence. For example, in the kinetic studies of the L-21 *Sca*I ribozyme derived from the Tetrahymena group I intron, two separate folding regions were distinguished by varying the ion concentration in the micromolar range. The P4-P6 involved tertiary structure region was formed at 0.7 mM Mg^{2+}, while P3, P7 and P2.1 tertiary interactions were at 0.85 mM (Laggerbauer et al., 1994).

Proteins and RNA folding

Binding of RNA to RNA chaperone proteins, promotes functional structure formation. This binding, however, is found to be non-specific. The absence of these chaperones, nevertheless, leads to 'kinetic traps'. Kinetic traps are stable intermediates that an RNA forms with non-native base pairing and thus inhibiting the function of the RNA (Herschlag, 1995; Treiber and Williamson, 1999). The first group of RNAs to have demonstrated a need for chaperones is the group I introns. A DEAD-box protein, CYT-19, together with CYT-18 was found to promote group I intron splicing *in vivo* and *vitro* by non-specifically binding to group I intron RNAs. The binding was found to destabilize non-native RNA structures that constitute kinetic traps in the CYT-18-assisted RNA-folding pathway (Mohr et al., 2002). In a yeast mitochondrial group I intron that is dependent on a protein for activity, the protein merely shifts the folding equilibrium to the native state by stabilizing interactions with a partially folded structure (Weeks and Cech, 1996). In other cases, RNA-protein binding have been shown to benefit one or both partners since otherwise disordered domains undergo conformational stabilization

through some kind of induced-fit mechanism (Williamson, 2000). An example where RNA binding induces structure and conformational change in its protein binding partner is the case of the L11 ribosome protein which binds to 23S rRNA for mediating GTPase activity in the ribosome (Ilin et al., 2005). Kink-turns are RNA motifs that have been found to bind proteins and provide an interesting example for induced fit of an RNA on protein binding. It was shown by FRET studies that a ribosomal L7Ae protein binds to K-turn motif containing RNA and induces a strongly kinked conformation from an elongated dynamic conformational state (Turner et al., 2005).

RNA misfolding

RNA chains adopt secondary structures very rapidly. The tertiary structure formation of RNA can proceed rapidly, if all base-pairing and secondary structure interactions are consistent with the tertiary fold and if tertiary fold is accompanied by formation of only new basepairs. The situation is different when incorrect secondary structure base pair interactions have to be broken first in order to attain the correct tertiary fold. Such a situation has been observed in the case of tRNA, where the secondary structure was other than the cloverleaf conformation. It was found that the timescale of secondary structure formation is independent of sequence and temperature. However, the helix unfolding rates are sequence dependent, as this directly affects the stability of basepairs and are also strongly varied by temperature (Craig et al., 1971; Porschke and Eigen, 1971). Although, the consensus that the overall folding pathways of RNAs are similar to protein folding, one major difference is the presence of persistent RNA folding intermediates. These are stable alternate folds that inhibit native folds (Draper, 1996).

CHAPTER II

2. RNA Folding Detection

For kinetic studies, folding must be initiated by switching from denaturing to native conditions. In proteins, urea or guanidinium hydrochloride are often used as chemical denaturants. Since most RNAs require divalent or monovalent ions for tertiary structure formation, a switch from low to high salt concentrations was one of the first strategies used to probe folding in RNA. For example, tRNAs adopt an ensemble of conformations with different non-cloverleaf base pairings at low salt concentrations (Cole et al., 1972). The increase in salt conditions acts as a switch and initiates tertiary native structure formation as demonstrated on investigations of tRNAs folding using Mg^{2+} and Na^{+} ions (Cole et al., 1972; Lynch and Schimmel, 1974). Also, pH jumps have been used to study tRNA renaturation (Hawkins et al., 1977). This approach in combination with stopped flow and UV absorbance measurements enabling real-time monitoring of kinetics was used to study secondary structure refolding kinetics (Nagel et al., 2002). Here, an acidic solution was used to denature the RNA. The refolding is initiated by addition of a neutralizing alkaline solution and the exponential change in UV absorbance was monitored. A third initiation methodology is temperature jump (Menger et al., 2000). Figure 3 gives a schematic representation of the timescales that can be investigated using various initiation and detection technologies some of which are discussed briefly below.

Small angle x-ray scattering – SAXS

Small angle x-ray scattering measures the scattering of x-rays by a given sample that is placed in the x-ray beam path. The scattering angles are small, typically in the 0.1-10 ° range. The resulting intensity of the scattering is measured as a function of the angle between the incoming beam and the scattered beam and the structure is modeled from the observed scattering

pattern. Reporting the changes in dimension and shape of the molecule over time allows sampling of the rugged folding landscape of RNAs as is demonstrated in the compaction during the folding of the *Tetrahymena* group I ribozyme (Rick Russell, 2002; Russell et al., 2000).

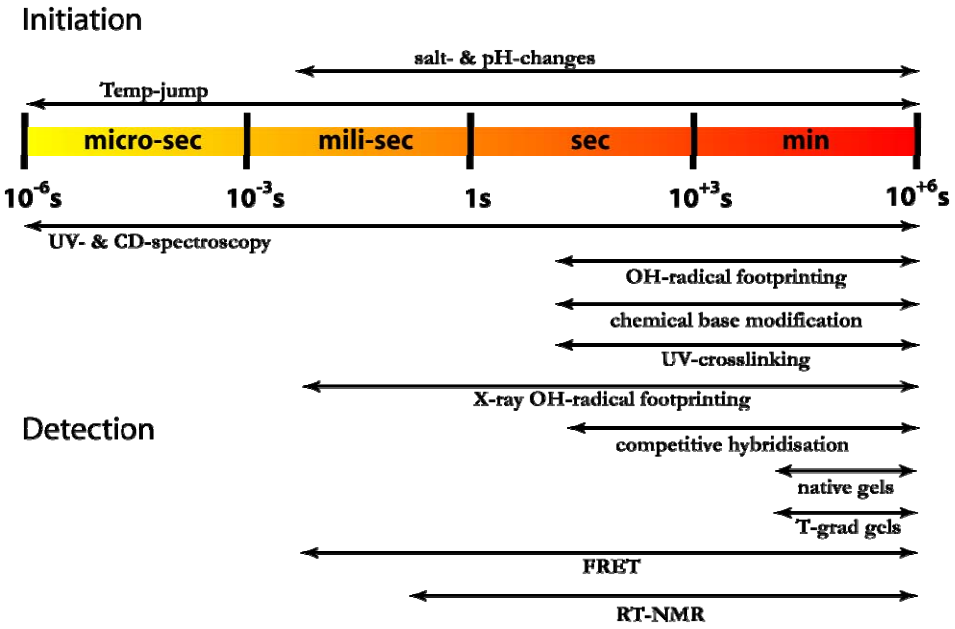

Figure 3: An overview of the currently applied techniques for initiation and detection of RNA folding. (Figure reproduced from Fürtig et al., 2007)

Stopped flow EPR

Electron paramagnetic resonance spectroscopy studies molecules containing unpaired electrons. In the presence of a magnetic field, the resonance absorption of microwave radiation by unpaired electrons or paramagnetic ions or free radicals is the basis of this technique. When these are introduced as probes in biological molecules, local structural features, ligand interactions and metal ion binding sites can be studied (Qin and Dieckmann, 2004). The advantages of this method lie in the small concentrations required for the experiments. However, there are size limitations on the molecules that can be studied, since probe attachment requires chemical synthesis where current techniques allow synthesis of up to only 100 nucleotides. Kinetic studies can be conducted by using continuous wave EPR (CW EPR) to monitor

a folding process. For example, the metal ions dependent folding of the hammerhead ribozyme used the dynamics of attached spin-labels to monitor the folding by CW EPR (Edwards and Sigurdsson, 2005). Till date the tumbling dynamics of a 20-mer stem loop 3 of the HIV-1 RNA and the effect of interaction of HIV-1 nucleocapsid Zn-finger protein (NCp7) on its kinetics has been studied using stopped-flow EPR (Xi et al., 2008).

***FRET* - Fluorescence resonance energy transfer**

FRET is based on the transfer of energy between a donor dye and an acceptor dye. This transfer of energy is distance dependent and the efficiency (E) of this process is given by the equation $E = Ro^6/(Ro^6 + r^6)$, where Ro is the distance at which energy transfer is 50% and is called the Förster distance and r is the distance between the donor and acceptor molecules. A typical FRET experiment involves attaching a donor and acceptor to vantage positions (about 10-100 Å apart) on the molecule studied and directly monitoring the excitation energy transfer between the donor and acceptors which takes place due to their dipolar interaction. The energy transfer is a function of the distance between the donor and acceptor and their orientation. Thus, monitoring the FRET efficiency over time can report on conformational changes of the ribozyme (Kobitski et al., 2007; Walter et al., 2001; Zhuang and Rief, 2003). Advances in single molecule studies have enabled capturing of transient intermediate states in the folding pathway and also the presence of multiple folding pathways (Zhuang et al., 2000).

Hydroxyl radical footprinting

This method is based on oxidation of the ribose C4` positions by hydroxyl radicals causing cleavage of the phosphodiester backbone. If one end of the molecule is labeled then the cleavage products can be analyzed by gel electrophoresis to obtain a pattern of solvent accessible nucleotides which yield structure information. The advantage of this method is that only small sample concentrations are required, usually in the picomole to nanomole range. This method has been comprehensively reviewed earlier (Brenowitz et al., 2002). The most commonly used methodology is the Fe-EDTA-catalyzed generation of hydroxyl radicals (Hampel and Burke, 2001). For increased

structure resolution of the data, tethered Fe(II)-EDTA radicals are used to obtain site-specific information (Huq et al., 1999). Here, the size and amount of cleaved fragments relate to the distance in the three-dimensional structure thus reporting on structural information of the neighborhood of the tethered Fe(II)-EDTA. By using synchrotron x-ray beams comparable generation of hydroxyl radicals by radiolysis of water can be obtained (Price and Tullius, 1992; Sclavi et al., 1997). Use of this technique in combination with a stopped-flow apparatus leads to millisecond time resolution footprinting giving real-time folding information on the *Tetrahymena* ribozyme (Sclavi et al., 1998a; Sclavi et al., 1998b). This technology therefore bears some analogy to hydrogen exchange experiments in proteins where the solvent exposed amide nitrogens are mapped. Other tools (Brenowitz et al., 2002) include the use of peroxonitrite footprinting as was demonstrated in the folding kinetics study of the Varkud satellite ribozyme (Hiley and Collins, 2001).

Kinetic oligonucleotide hybridization assays

In this method, when a complementary oligonucleotide strand of the domain of interest is introduced into the system, hybridization occurs if the domain is 'available' as in the case of unstructured regions. If it is already structured, then no hybridization is observed. For example, Figure 4 shows the induction of folding in an RNA that folds via an intermediate. Stage 1 shows the mostly unstructured RNA, stage 2 the intermediate RNA and stage 3 the higher order folding of the RNA. During the hybridization assay, when folding is induced, oligonucleotide probes that are complementary to the domains of interest (shown in red, green and blue in Figure 4) are introduced into the system along with RNase H. If the domains complementary to the probe are unstructured in the RNA, hybridization occurs. RNase H selectively cleaves the RNA strand of an RNA:DNA hybrid and thus by varying the incubation time of probe and enzyme, stages of the folding process can be delineated. This method is used to probe slow folding kinetics as in the case of the RNase P RNA (Zarrinkar et al., 1996).

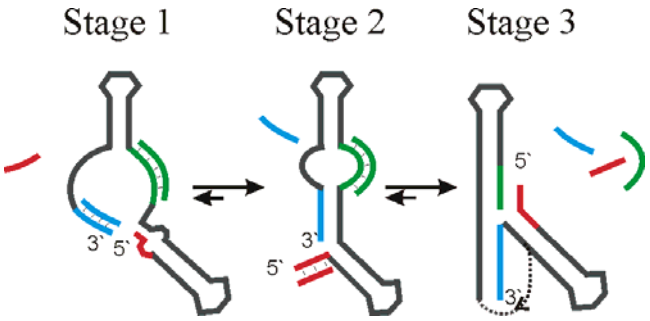

Figure 4: Schematic representation of oligonucleotide hybridization assay on folding of an RNA.

Temperature gradient gel electrophoresis

When a sequence adopts differing folds, its mobility in electrophoresis experiments can also differ. This property is used to detect various stages of an RNA folding as demonstrated in the kinetic analysis of the PSTVd(−)-strands during their synthesis (Repsilber et al., 1999).

Local 'region' specific dynamics

Apart from the kinetics that is involved in structure formation of a ribozyme, local dynamics are also common which are central to many of the functions performed by ribozymes. For example, the catalytic site of RNA in general should display a degree of flexibility which is a prerequisite for substrate entry and binding and product dissociation. Therefore specific methods that capture the dynamics of these regions are required (Al-Hashimi, 2005). These dynamics, displayed at the atomic level, are important in order to understand the role that the structure of an RNA plays in its function. By using NMR, dynamics over several time scales can be detected (Al-Hashimi and Walter, 2008). For example, information may be tapped from spin relaxation and is a powerful tool in the study of dynamics of secondary structure regions like the RNA loops and bulges in the pico-femto second time scale (Akke et al., 1997).

2.1. Nuclear Magnetic Resonance Spectroscopy

Nuclear Magnetic Resonance spectroscopy is an invaluable tool to study the structure and function of proteins and nucleic acids (Furtig et al., 2003). Solving the basic structure of molecules is a very well established

technique now. Incorrect conformations during protein folding are believed to result in several diseases (Soto, 2003). Consequently, considerable effort is also directed towards the study of structure and kinetics of unfolded and partially folded or misfolded proteins and RNA. The identification of rare high energy conformers and low population conformers or intermediates in the folding pathway (Akasaka, 2003; Korzhnev et al., 2004; Neudecker et al., 2006) are prime examples of innovation in this branch of the field. The current repertoire of NMR techniques enables the study of dynamics and conformational motion of molecules in a wide range of timescales (Furtig et al., 2007). Other biophysical methods can only report on conformational dynamics on a global level while in NMR, residue specific information can be determined.

2.1.1. Time-resolved NMR using rapid-mixing Technique

If the folding of the RNA can be initiated by a cofactor such as metal ions or ligands, then the most conventional method to initiate folding is rapid mixing of two solutions, one containing RNA and the other the cofactor. Rapid-mixing is a standard method to investigate numerous chemical and biological reactions. The most general method of achieving mixing is by turbulence where the two solutions mix completely before the reaction progresses considerably that is: $\tau_{mix} << \tau_{reaction}$. One obvious limitation is the 'dead time' of mixing. This is the time taken for complete mixing to take place before the initiated folding can be detected by a suitable technology. Therefore the choice of methodology depends on the timescale being studied.

The mixing methods used can be roughly categorized into continuous flow (CF) and stopped flow (SF) methods. In the continuous-flow setup, a turbulent flow of the two solutions creates a jet and the detector records the reaction at discrete points along the jet. The kinetic trace is then decoded by using information from the detection position on the jet stream and the velocity of the jet. In stopped-flow methods, using two syringes, the two solutions are pushed into a T-mixer where rapid turbulent mixing takes place. When sufficient amounts of the solutions have been injected into the mixer, the flow is 'stopped' and detection begins (Nölting, 2006). In NMR, time-resolved kinetics information was initially obtained using stopped-flow devices for

proteins (Hoeltzli and Frieden, 1995, 1996). Mixing of the solutions inside the NMR magnet considerably reduced the mixing time and this method was first demonstrated on bovine α-lactalbumin (Balbach et al., 1995).

2.1.2. Time-resolved NMR using Photocaging Technique

For a complete review of time-resolved NMR using this technique, please refer to the review by Fürtig et al., 2007. In this section, those research reports pertinent to the context of this thesis are discussed.

Conventional kinetics experiments were based on rapid-mixing devices (discussed in previous section). These techniques were applied to study protein folding where a reactant was used to initiate the folding event. For example, bovine α-lactalbumin in a denatured state was injected into a refolding buffer in excess EDTA and its folding was studied by recording 1D spectra. A time resolution of 2.4s was possible for the folding event (Balbach et al., 1995). This technique can be directly applied to RNAs that have suitable folding 'triggers'. However, as in the case of bistable RNAs (Hobartner and Micura, 2003b; Hobartner et al., 2004) where a given sequence can adopt two conformations leading to a heterogeneous equilibrium state, folding initiation is not so straightforward. In these cases an artificial trigger mechanism is required. The basic idea here is to hold the RNA in one conformation, trigger the folding of the second conformation by some external force and monitor its formation. One such method is the use of 'caged' nucleotides (Hobartner and Silverman, 2005). Here, a nucleotide that is required for proper folding of one of the conformations is prevented from base-pairing by modifying it with a photolabile group, thereby disrupting the folding of that conformation (Wenter et al., 2005). When this photolabile group is removed, ideally in a traceless manner, by a laser pulse, the nucleotide is free for base pair interaction, thus initiating the refolding of the conformation we want to study. The whole process can be performed inside the NMR magnet by guiding the laser required for the photolysis using optical fibers (Kuhn and Schwalbe, 2000). This method has been employed in the investigation of the folding kinetics of a 20 nucleotide bistable RNA and the conformational dynamics of the cleavage activity of a minimal hammerhead ribozyme (Furtig et al., 2008; Fürtig et al.,

2007; Wenter et al., 2005, 2006). The main disadvantage of this method is that the caged RNA must be chemically synthesized.

Using the same caging principle, a ligand or a metal ion that is a requisite for the folding of an RNA can also be photocaged thus providing the trigger for folding initiation (Furtig et al., 2007). An example of a caged ligand is the kinetics study of a guanine sensing riboswitch where a photocaged hypoxanthine was used as a ligand (Buck et al., 2007). In the case of metal ion caging, a suitable cage compound is DM-nitrophen (Kaplan and Ellis-Davies, 1988). DMN is an EDTA-analogue whose dissociation constant for Ca^{2+} is very high. (K_D = 5 x 10^{-9} M) (Kaplan and Ellis-Davies, 1988; McCray et al., 1992). When DMN is photolysed, the dissociation constant of binding of its photo products is higher (K_D = 3 x 10^{-3} M) thus making available the Ca^{2+} ions for folding. The ion release time after a laser pulse is 10 μs; up to 90% of DMN is photolysed in a solution containing 1 mM DMN; therefore the constraint for time resolution was only the NMR data acquisition time. This procedure was first demonstrated on a protein bovine α-lactalbumin (Kuhn and Schwalbe, 2000). One of the main advantages of this method of photocaging is that the RNA could be obtained using conventional *in vitro* transcription and therefore there are no size limitations on the molecule studied. However, a major drawback of this method could be the metal ion concentrations required for complete folding. As the ion concentration required for folding increases, so does the amount of the cage molecule required. This directly affects the percentage photolysis that can be achieved using a laser pulse without overheating the solution.

2.1.3. Comparison of time-resolved NMR techniques

Two folding initiation techniques were used in order to study folding by time-resolved NMR spectroscopy. The pros and cons of each of these techniques are discussed below

Prerequisites:

For the rapid mixing technique, the folding initiation component should be identified which, when mixed with the molecule, induces folding. For example, in the case of proteins changes in the denatured state of a molecule

can be achieved by rapid dilution of the denaturant or by changes in pH. In the case of RNA divalent ion concentration can be changed to induce folding.

In the case of photocaging technique a suitable photolabile cage should be identified. The criteria for such compounds are, short release time ($\tau_{release}$) on laser irradiation, the irradiation time ($\tau_{irradiate}$) should fall within or ideally less than the folding time of the molecule and non-interference of released photolabile byproducts with the system being studied.

Molecules:

Depending on the caging technique used, there exist limitations on the size of the molecule that can be studied by the photocaging method. When the RNA molecule is the caged entity, size of the molecule is limited by the solid phase chemical synthesis technology. Therefore this method is limited to only small RNAs. In the case of divalent metal ion caging, larger RNAs require high concentrations of Ca^{2+} or Mg^{2+}. Therefore the concentration of the photolabile chelator also increases, leading to low deprotection yields. However, this may be offset by the use of high monovalent ion concentrations which have been reported to cause a decrease in the concentration of divalent metal ions required for tertiary folding of some molecules. Ligand photocaging is limited only by the size of the ligand. The size of the molecule is not a limitation in the rapid-mixing technique.

In this thesis, a well defined system, the Diels-Alder ribozyme, is investigated to detect the kinetics of folding using time-resolved NMR. The investigation of this RNA included conventional solution-state NMR experiments and the recently established techniques for probing real-time kinetics of folding by time-resolved NMR spectroscopy by photocaging of metal ions and rapid mixing of metal ions. The properties and characteristics of the ribozyme are introduced in the next chapter.

CHAPTER III

This chapter includes material that has been published: *Metal-Induced Folding of Diels-Alderase Ribozymes Studied by Static and Time-Resolved NMR Spectroscopy.* Manoharan, V, Fürtig, B, Jäschke, A, Schwalbe, H. *J. Am. Chem. Soc.*, 2009, 131 (17), pp 6261–6270

3. Diels-Alder Ribozyme

3.1. Background

The Diels-Alder reaction is one of the most important reactions in synthetic organic chemistry. It is a cycloaddition reaction between a conjugated diene and a dienophile substituted alkene to form a substituted cyclohexene system. Much effort has been directed towards developing catalysts that improve both, rate and selectivity of the cycloaddition (Auclair et al., 2000; Guimaraes et al., 2005; Katayama et al., 1998; Ose et al., 2003; Pindur et al., 1993; Watanabe et al., 2000). Among these catalysts, several classes of biological macromolecular catalysts have been developed, including catalytic antibodies (Braisted and Schultz, 1990; Hilvert et al., 1989; Lerner et al., 1991), a DNA-based hybrid catalyst (Roelfes and Feringa, 2005) and two ribozymes (Seelig and Jäschke, 1999; Tarasow et al., 1997). The Diels-Alder ribozyme investigated here is an *in vitro* selected RNA developed in the Jäschke lab that catalyzes the cycloaddition of anthracene dienes and maleimide dienophiles (Seelig and Jäschke, 1999). From the sixteen independent RNA sequence families isolated from the initial combinatorial RNA library ($2x10^{14}$ species, 120 randomized positions) (Jäschke, 2001), thirteen contained a common small secondary structure motif consisting of an asymmetric bulge and at least three helices. A minimal 49mer RNA was identified based on this secondary structure and shown to act as a true catalyst by accelerating the bimolecular reaction in solution (Seelig et al., 2000). The

catalysis was found to depend strongly on divalent cations such as Mg^{2+} or Mn^{2+}. The ribozyme performs the reaction with high enantioselectivity (>95% ee) and multiple turnovers with a k_{cat} of 20 min^{-1}. Initial chemical substitution analysis of the RNA-substrate interactions pointed to hydrophobic and van-der-Waals interactions (Stuhlmann and Jaschke, 2002) between the ribozyme and the substrate while hydrogen bonding and metal ion coordination appeared to be less important in the catalysis.

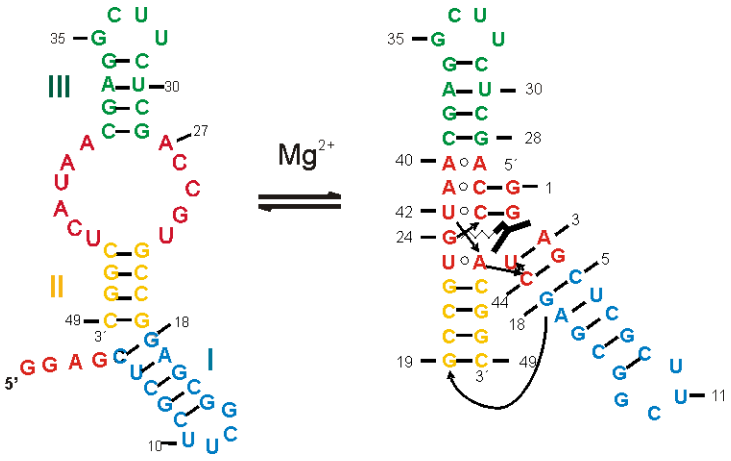

Figure 5: The predicted conformation of the Diels-Alder ribozyme in its free form and complex active form in the presence of Mg^{2+} and reaction product.

Mutation and structure probing studies further characterized the complex structure of the ribozyme revealing the participation of the conserved asymmetric bulge region in the catalytic site and proposed a pseudoknot fold (Keiper et al., 2004). It was proposed that the presence of the two reactants of the Diels-Alder reaction within the confined space of a cavity provided by the ribozyme drives the reaction (Kim et al., 2002). Also, at high Mg^{2+} ion concentrations, the ribozyme showed no major changes on substrate or product binding, consistent with a pre-formed structure of the ribozyme (Keiper et al., 2004). The crystal structure of the ribozyme in its product bound and unbound state was determined and confirmed all the previous studies (Serganov et al., 2005). The structures of the bound and unbound ribozyme were found to be virtually identical supporting the pre-formed architecture hypothesis. The catalytic site, hydrophobic in nature, was found centered around the junction of three helices forming the pseudoknot architecture with no metal ion binding

sites in its vicinity (Serganov et al., 2005). As was predicted, the conserved bulge region lined the catalytic pocket aided by base-pairing interactions of the opposite strands of the bulge and a four nucleotide long 5' single strand segment. The catalytic pocket showed two openings of differing sizes, the more favorable larger 'front' door and a smaller 'back' door. Surprisingly, in the product-bound crystal structure, the product was bound with the sterically demanding side in first, an orientation that could be possible only with a backdoor entrance. This initial hypothesis of a backdoor entrance was later confirmed to be the case (Wombacher et al., 2006). For the determination of the crystal structure, crystallization was performed with the Diels–Alder product covalently linked to the ribozyme comprising an 18-atom flexible tether which was attached to the RNA close to the backdoor in the product bound crystal structure. Experiments comparing the tethered version and the true catalytic version showed opposite enantiomers being formed under similar conditions. By varying the tether length, it was shown that longer tethers gave the same enantiomer product as in the true catalysis experiment, whereby the longer tether winds around the RNA backbone to position the product at the larger 'front' door (Serganov et al., 2005).

On the basis of these results biophysical techniques like single-molecule FRET and EPR spectroscopy have been used to gain more insight into the folding and dynamics of the ribozyme. The EPR spectroscopic study indicated different affinities and occupation for five metal(II) ion binding sites (Kisseleva et al., 2007) and a recent study of the dynamics using single-molecule FRET spectroscopy provided insight into the distribution of conformers and the structural dynamics of the wildtype ribozyme (Kobitski et al., 2007). Three states, the unfolded, intermediate and folded states, were identified and proposed to correspond to (largely) random coil, and states with secondary structure and complex native fold, respectively. The population of these states was shown to depend on the Mg^{2+} concentration and the entire RNA was shown to fluctuate permanently between these states. From the crystal structure of the wildtype ribozyme in the presence of Mg^{2+} ions it was seen that substrate binding had no effect on the structure of the ribozyme. Therefore we decided to study the folding of the ribozyme into its catalytically

active form by controlled introduction of divalent ions and monitoring the folding reaction.

3.2. Introduction

For this study, three sequences of the Diels-Alder ribozyme family were characterized: the best catalyst (A27 WT), a single-nucleotide mutant (G27 MUT) with ~70% catalytic efficiency relative to the wildtype ribozyme and a single-nucleotide mutant (G40 MUT) with 30% catalytic efficiency relative to the wildtype ribozyme. For G27 MUT, the single mutation is at the junction of stem III and asymmetrical bulge region of the ribozyme in its free form. For both forms of the ribozyme, crystal structures are available of the product-bound complex at resolutions of 3.3 Å for A27 WT and 3.0 Å for the G27 MUT. For the A27 WT, a crystal structure of the ribozyme without a bound product is also available at a resolution of 3.5 Å (Serganov et al., 2005).

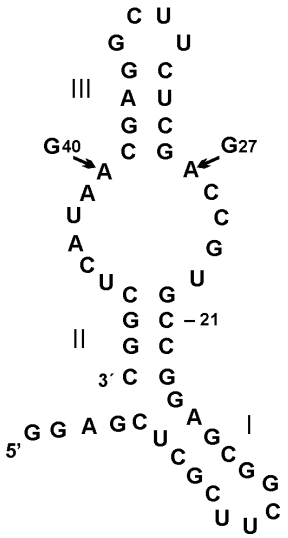

Figure 6: Secondary structure of the wild type Diels-Alder ribozyme family as predicted by mfold (Mathews et al., 1999; Zuker, 2003), with the two mutants marked.

3.3. Results

In order to delineate the folding pathway of the ribozyme, the start and end states of the pathway have to be determined. Therefore, the first steps were to characterize the free forms and the complex forms of the ribozymes by static

NMR spectroscopy. All NMR experiments conducted for free form characterization were on the ribozymes without divalent metal ions.

3.3.1. Characterization of the Diels-Alder ribozymes in their free form conformations by static NMR

3.3.1.A. A27 WT Free form Characterization

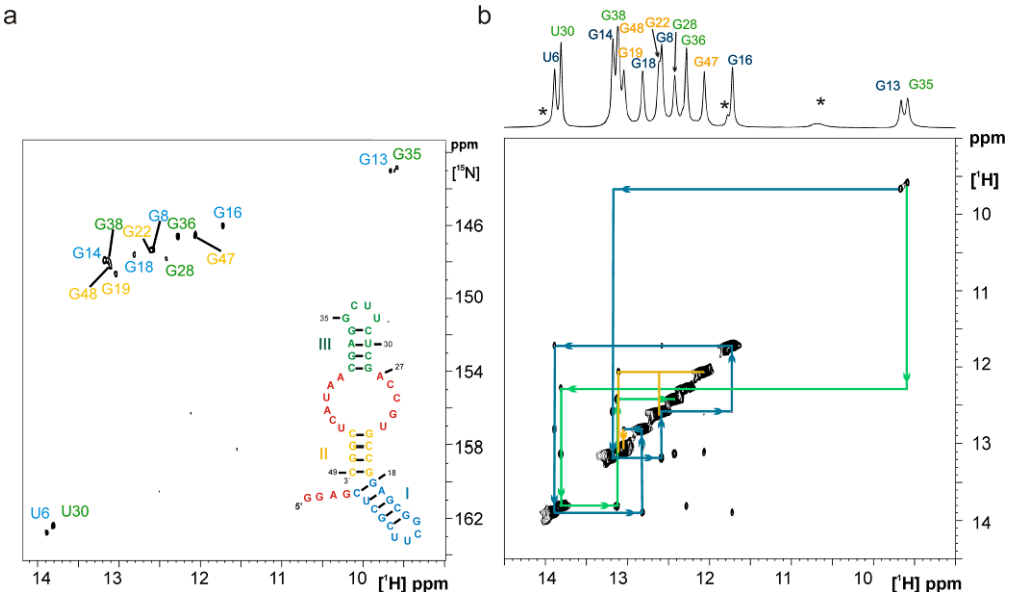

Figure 7: a) Natural abundance ^{1}H, ^{15}N HSQC of the imino region of the A27 WT ribozyme in its free form state. The inset shows the secondary structure of the free form of the ribozyme as predicted by mfold with initial ΔG = -23.50 kcal/mol b) NOESY spectrum of the A27 WT ribozyme, T=283K, 800 MHz field, conc. 0.9mM, measured over 41 hours. Sequential walk for the assignment is also shown. Each segment of the walk is color-coded according to those used in the free-state layout that is given in the inset in a. The projection at the top gives the labels of all the identified imino resonances. '' denotes all unassigned peaks.*

From the natural abundance ^{1}H, ^{15}N HSQC eleven GC, two GU (G13, G35) and two AU (U6, U30) basepairs were observed for the WT ribozyme in the absence of ligand and divalent cations. In the ^{1}H, ^{1}H NOESY spectrum, stems I and III could be readily assigned with the aid of the imino protons of the G forming the GU base pair within the tetra-loop (G13/G35) since it resonates characteristically at approximately 10 ppm and upfield to the other imino resonances. Typically, the imino U resonances cannot be observed in GU basepairs. Given the free-state secondary layout by mfold (inset in Figure 7)

we confirmed the presence of blue and green stems I and III. Two imino cross-peaks are observed from G18 which forms the end of blue stem I and therefore we conclude that the stems I and II are stacked to some degree. On this basis we assign this crosspeak as belonging to the imino proton of G19 of yellow stem II. No other crosspeak is observed from G19. A sequence of 3 GC basepairs corresponding to the rest of the yellow stem II is observed and was assigned with the aid of NOE crosspeaks between imino-imino and imino-aromatic protons.

Dynamics in free-form. At 283K, the wild type ribozyme shows a spectrum characteristic for a single RNA fold. At elevated temperature of 293 K and above, however, the wild type ribozyme showed a heterogeneous conformation in the free state as revealed by shoulders in the peak shapes observed by 1D imino region spectra and shown in Figure 8. The temperature induced changes in the conformation were reversible.

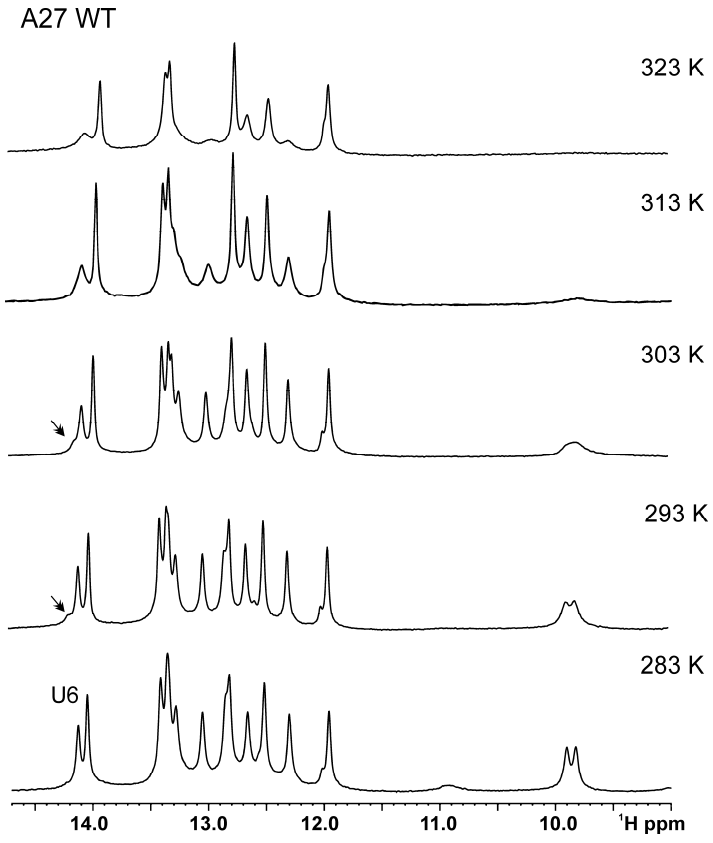

Figure 8: Imino region of the temperature gradient 1D spectra of A27 WT. The arrows show the minor secondary fold detected at higher temperatures.

3.3.1.B. G27 MUT Free form Characterization

The ^{1}H, ^{15}N HSQC of the G27 MUT showed all resonances already observed in the ^{1}H, ^{15}N HSQC of A27 WT. In addition, several cross peaks with weaker intensities were observed. From the HNN-COSY experiment, it can be inferred that all basepairs belonged to Watson-Crick basepairs (Figure 9d). In Figure 9e, each NOESY sequential walk within a stem can be identified by starting from the NOE crosspeaks between the loop G imino proton (G13 of stem I, and G35 of stem III) and the protons of the two G nucleotides (G14 of stem I, and G36 of stem III) of the closing base pair of the stem. Another useful and distinct characteristic of the 2D imino NOESY spectrum is the resonance pattern of imino protons of the U residues in the Watson-Crick AU base pair at around 14 ppm with a strong NOE with the H2 of its adenine base pair. Combining the above given information along with the position of the AU base pair in each stem, we were able to identify stems I and III distinctly with certainty. A third sequential walk was identified that also seemed to fit the base pairing pattern of blue stem I, but without the connectivity to a loop. This is shown by the dotted blue line in Figure 9e. As seen from the spectra, the chemical shift pattern is remarkably similar to the sequential walk of the blue stem I. The chemical shifts of nucleotides that have already been identified as stem I and the additional set of crosspeaks differs only marginally and the difference in chemical shifts become smaller for those nucleotides close to the loop. The signal from G14 which forms the closing basepair of the loop, resonates in a heavily overlapped region and thus doubling, if present, could not be observed. The absence of doubling of resonances from G13 from the loop may be due to the fact that the UUCG tetraloop motif is very stable thermodynamically (T_M ~70°C: (Varani, 1995)). Quantifying the two U6 peaks belonging to the two conformations gave a ratio of approximately 3:1 for the two species of the population. We conclude that the free form of the ribozyme exists in two conformations which are differentiated in the blue stem I.

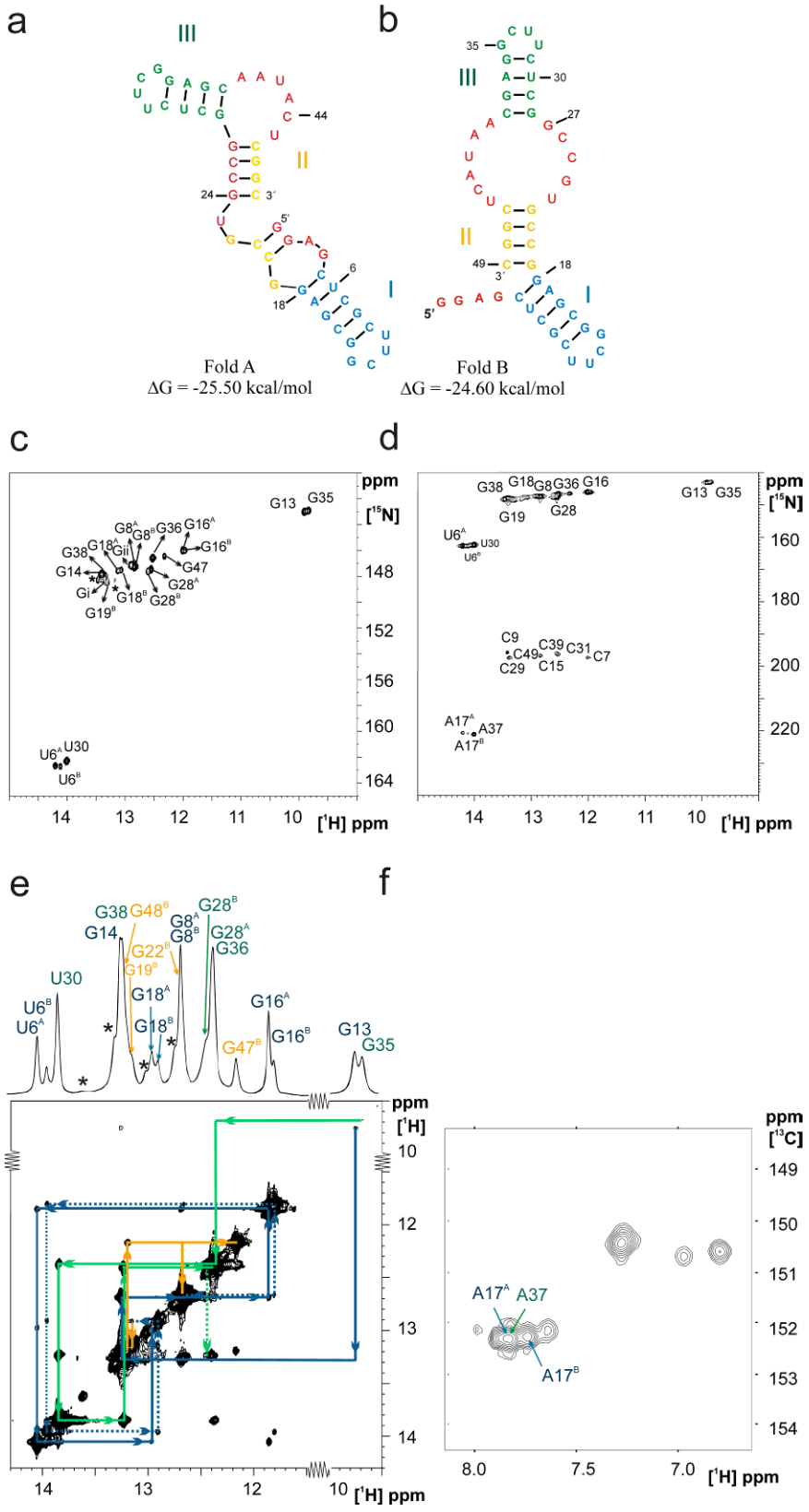
a
b
Fold A
ΔG = -25.50 kcal/mol
Fold B
ΔG = -24.60 kcal/mol
c
d
ppm
[15N]
[1H] ppm
e
f
[13C]

*Figure 9: a) and b) The first two lowest energy free forms of the mutant ribozyme predicted by mfold (Mathews et al., 1999; Zuker, 2003). c) and d) show the ^{1}H, ^{15}N HSQC and HNN-COSY spectra of the G27 MUT ribozyme in its free-state in the absence of ligand and divalent cations measured at 288 K with an RNA concentration of 0.5 mM (Experiment parameters - entries 2 and 5 in Table 4). The * denotes unassigned peaks. And peaks are labeled with superscripts A and B where peaks from the two folds show differences in chemical shifts. e) ^{1}H ^{1}H NOESY spectrum of the labeled G27 MUT ribozyme, T=288 K, 800 MHz field, conc.: 0.6 mM, measured over 45 hours (Experiment parameters entry 4 in Table 4). The sequential walk for the assignment of the free-state ribozyme is indicated. Each segment of the walk is color-coded according to the color code of the free-state conformations that is given in the secondary structure conformations in panels a and b. The dotted blue line denotes the sequential walk assigned to stem I of fold B given in b. f) ^{1}H, ^{13}C HSQC spectrum of G27 MUT in its free state displaying only the adenine H2C2 crosspeaks of the aromatic region (Experiment parameters entry 6 in Table 4).*

In the figure peak labels with superscripts denote the fold the resonance belongs to. This is further supported by the following observations: The intensities of the peaks as apparent from the 1D resonance of the imino region (projection on top of Figure 9e) reveal both strong and weak peaks. In addition, eight adenine H2/C2 crosspeaks can be identified instead of the expected six crosspeaks in the aromatic region of the ^{1}H, ^{13}C-HSQC with differing intensities as shown in Figure 9f.

G18 of stem I of the fold B shows a very weak crosspeak to another G downfield of 13.1 ppm which is assigned as G19 belonging to stem II. Similar to A27 WT this indicates some degree of stacking of the basepairs that G18 and G19 are involved in. Due to severe overlap in this spectral region, no crosspeaks could be detected from G19 to further assign the yellow stem II. This was also the case with the A27 WT ribozyme. One G nucleotide in the not well-resolved spectral region downfield of 12.5 ppm showed crosspeaks with two Gs downfield of 13 ppm and 12 ppm. Similar to A27 WT, this G nucleotide was tentatively assigned as G47 belonging to the stem II and shown as a yellow walk in Figure 9e, using imino-aromatic NOE crosspeaks. Fold B of G27 MUT had exactly the same resonance pattern as that found in the A27 WT ribozyme including the stacking interaction between stems I and III. Combining this information with the mfold conformation predictions for both the ribozymes, we could conclude that the G27 MUT ribozymes' fold B was the same as the A27 WT conformation.

Dynamics of G27 MUT in free state. The free form conformation of G27 MUT showed increased dynamics in stem II. The imino proton resonance spectra may also provide information about the dynamics of the RNA. Their linewidths increase as the hydrogen bonding strengths of the respective basepairs weaken. Figure 10 (left) shows the ^{1}H linewidth distribution of imino resonances of the free form G27 MUT extracted from the ^{1}H,^{15}N HSQC spectrum. The bars with thick black lines correspond to resonances from fold B. The linewidth of the imino G19^{B} proton of the G27 MUT minor conformation (marked by an arrow in Figure 10) is almost twice the average value. We conclude that G19 in fold B is involved in weak hydrogen bonding interactions. As A27 WT did not show major linewidths variations (20 ± 3 Hz) Figure 10 to the right, the increased linewidth of the G19^{B} imino proton in the G27 MUT is likely not due to "fraying" of terminal basepairs, but hints at additional line broadening induced by conformational exchange that is on a slower time scale than fraying motions.

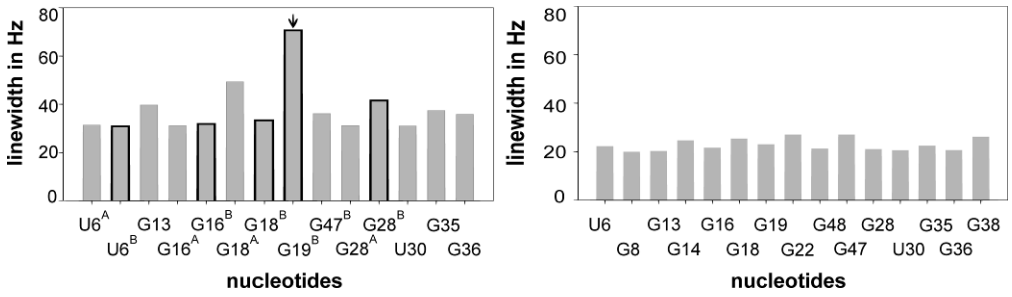

Figure 10: Bar chart showing the linewidths extracted from ^{1}H,^{15}N HSQC spectra of the imino protons of the free G27 MUT ribozyme at 283 K in a and A27 WT in b. Bars with dark borders denote fold B (panel b in Figure 9) linewidths. The arrow labels G19^{B} linewidth.

3.3.1.C. G40 MUT free form characterization

The G40 free-form conformation was characterized by measuring ^{1}H, ^{1}H NOESY and ^{1}H, ^{15}N HSQC spectra. The two helices I and III could be readily assigned by the NOESY sequential walk. Once again the yellow helix II could be identified by the stacking of G19 on G18 from blue stem I. This identifies the conformation to be similar to the WT free form. Based on peak intensities, G47 and G48 belonging to yellow helix II from this conformation

could also be assigned. As seen before in G27 MUT, an additional sequential walk made up of low intensity crosspeaks could be identified for the blue helix I. The mfold prediction for G40 MUT at 310 K shows the first two minimum energy conformations at ΔG = -27.60 kcal/mol and ΔG = -22.50 kcal/mol (Figure 11).

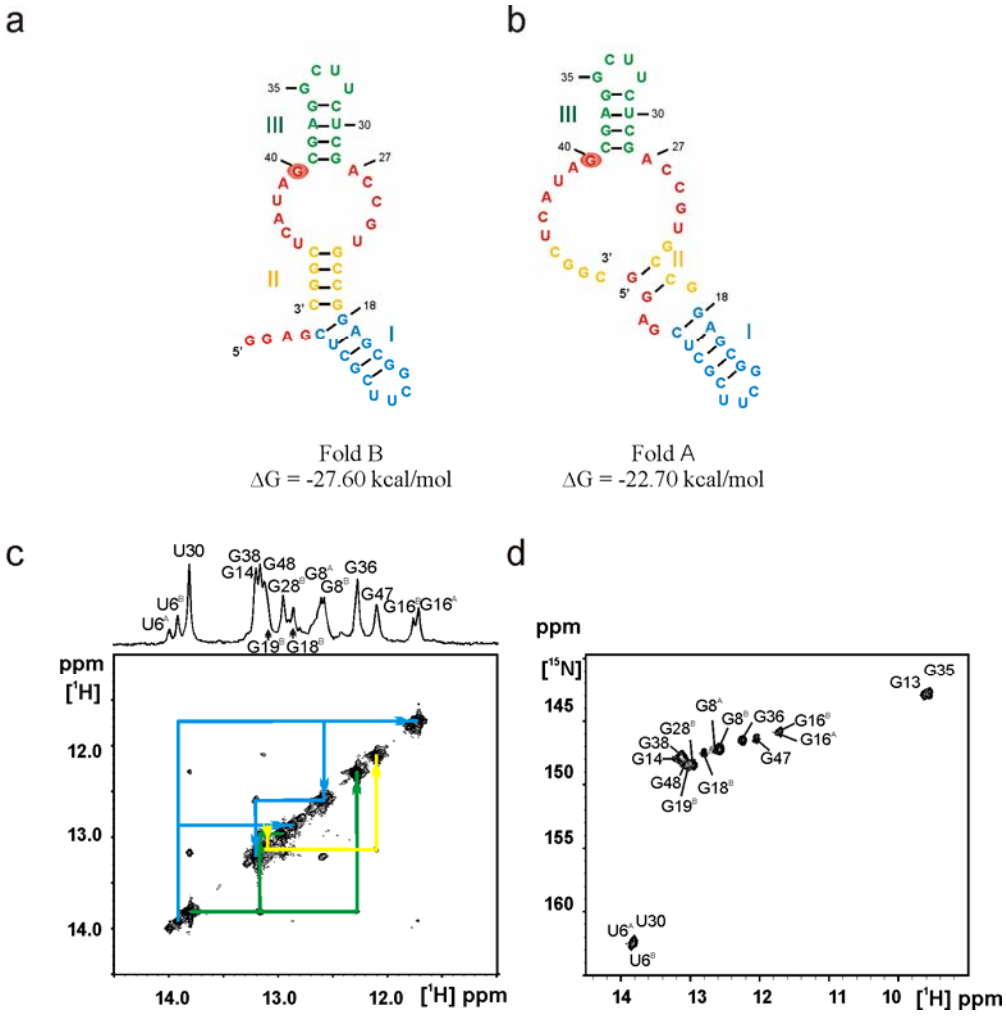

Figure 11: a) and b) The first two lowest energy free forms of the mutant ribozyme predicted by mfold c) and d) show the ^{1}H, ^{1}H NOESY and ^{1}H, ^{15}N HSQC spectra of the G40 MUT ribozyme in its free-state in the absence of ligand and divalent cations. ^{1}H, ^{1}H NOESY was measured at 288 K with an RNA concentration of 0.3 mMs, 800 MHz field over 48 hours. And peaks are labeled with superscripts A and B wherever resonances show dual conformation and therefore show differences in chemical shifts. The sequential walk for the assignment of the free-state ribozyme is indicated. Each segment of the walk is color-coded according to the color code of the free-state layout that is given in the secondary structure conformation in Figure 6 (Experiment parameters entries 7 and 8 in Table 4).

The difference between these two conformations lies in the yellow helix II. The less populated fold A shows only a two base pair yellow helix II with a base pairing pattern different from the majority populated fold B. The low spectral resolution between the two conformations in the ^{1}H, ^{15}N HSQC spectrum did not allow for linewidth analysis of the two conformations. In addition, even those peaks that were resolved, e.g. $U6^{A}$, displayed very low S/N ratio. We could not identify G22 from the closing base pair of the yellow helix from the NOESY sequential walk of the fold B which is the WT free form. This indicates dynamic properties of the yellow helix and therefore agrees with the mfold predictions.

Thus, we conclude that the free-form characterization of G40 MUT at 283 K showed a heterogeneous conformation state with at least two conformations, fold A and fold B, identified by NMR with an experimental population ratio of 1:4 with a difference of ΔG_{exp} of 0.76 kcal/mol. In the absence of ligand and metal ions, the major fold B was identified to be similar to the WT free form conformation using assignments from ^{1}H, ^{1}H NOESY and $^{1}H,^{15}N$ HSQC experiments.

3.3.1.D. Summary

In summary (Figure 12), we found that the wild type ribozyme, the best catalyst A27 WT, displays the most stable homogeneous free form conformation in the absence of ligand and divalent metal ions. This was confirmed by ^{1}H, ^{1}H NOESY and $^{1}H,^{15}N$ HSQC experiments. We observed that the two mutants exist at least in two conformations at lower temperatures with different ratios. G27 MUT exists in a ratio of 3:1 where the less stable fold B was similar to the wild type conformation. In G40 MUT the ratio was approximately 1:4 and the more stable Fold B was found to be similar to the wild type fold. A27 WT also displayed conformational heterogeneity at higher temperatures albeit not very significant (Figure 8).

Figure 12: a, b and c show the minimum energy secondary structures as predicted by mfold and validated by ^{1}H, ^{1}H NOESY and $^{1}H,^{15}$ N HSQC NMR experiments for A27 WT, G27 MUT and G40 MUT ribozymes. The $^{1}H,^{15}N$ HSQCspectra with the assignments for all three ribozymes are also given.

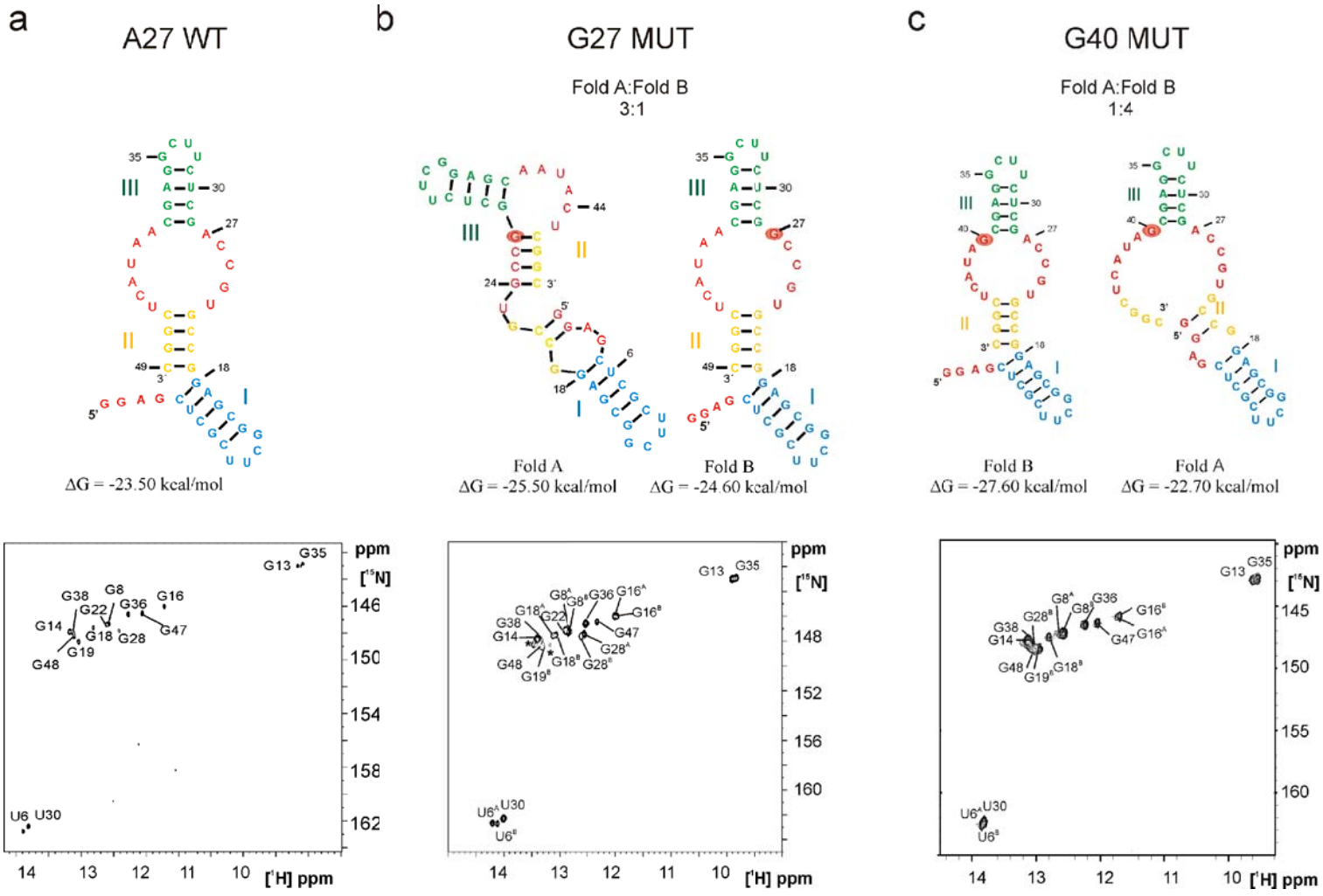
a
A27 WT
ΔG = -23.50 kcal/mol
b
G27 MUT
Fold A:Fold B
3:1
Fold A
ΔG = -25.50 kcal/mol
Fold B
ΔG = -24.60 kcal/mol
c
G40 MUT
Fold A:Fold B
1:4
Fold B
ΔG = -27.60 kcal/mol
Fold A
ΔG = -22.70 kcal/mol
ppm
[15N]
[1H] ppm

3.3.2. Characterization of the Diels-Alder-ribozyme (WT & mutants) in complex with product & divalent cations by static NMR spectroscopy

The Diels-Alder ribozyme is active only in the presence of divalent ions. We therefore performed Ca^{2+} titrations to characterize the changes in the free form induced by divalent ions for the A27 WT and G27 MUT ribozymes. Initial experiments showed that even at high divalent ion concentrations line broadened free form resonances were still present in conformational equilibrium with the tertiary complex form. Therefore, a previously identified (Stuhlmann and Jaschke, 2002) reaction inhibition product, AMDA (anthracene-maleimidocaproic acid Diels-Alder adduct), was used to hold the ribozyme in its complex form.

The A27 WT ribozyme showed 1D imino resonance (Figure 13b) characteristic of the tertiary complex conformation on addition of 4mM Ca^{2+}. The residual imino peaks from the free form that are still observed in the presence of metal ions are exchange broadened indicating conformational dynamics. This broadening may be due to exchange with a minor secondary fold that is observed at higher temperatures (Figure 8). Addition of ligand (AMDA) to this conformational ensemble shifts the equilibrium to the tertiary complex conformation. A residual population of ribozymes in the free form was still present even at higher concentrations of Ca^{2+}.

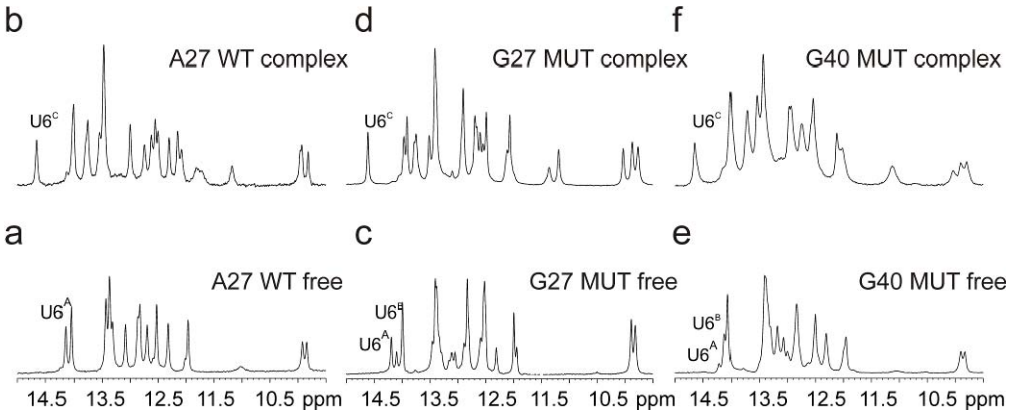

Figure 13: a and b show the free form and complex form in presence of Ca^{2+} for A27 WT at 291K. c and d show free and complex form of G27 MUT. e and f show free and complex form of G40 MUT at 288K.

Three conformations were identified for G27 MUT in the absence of the ligand AMDA. The line broadening of the folds A and B show that folds A and B become dynamic and their relative population is changed. In addition, the appearance of a signal $U6^{C\text{-like}}$ could be detected at a similar resonance position as in the complex. However, no non-Watson-Crick basepairs that characterize the complex ribozyme for both A27 WT and G27 MUT were detected. To induce the RNA conformation present in the complex, both divalent ions and the Diels-Alder product are necessary as discussed in the following section.

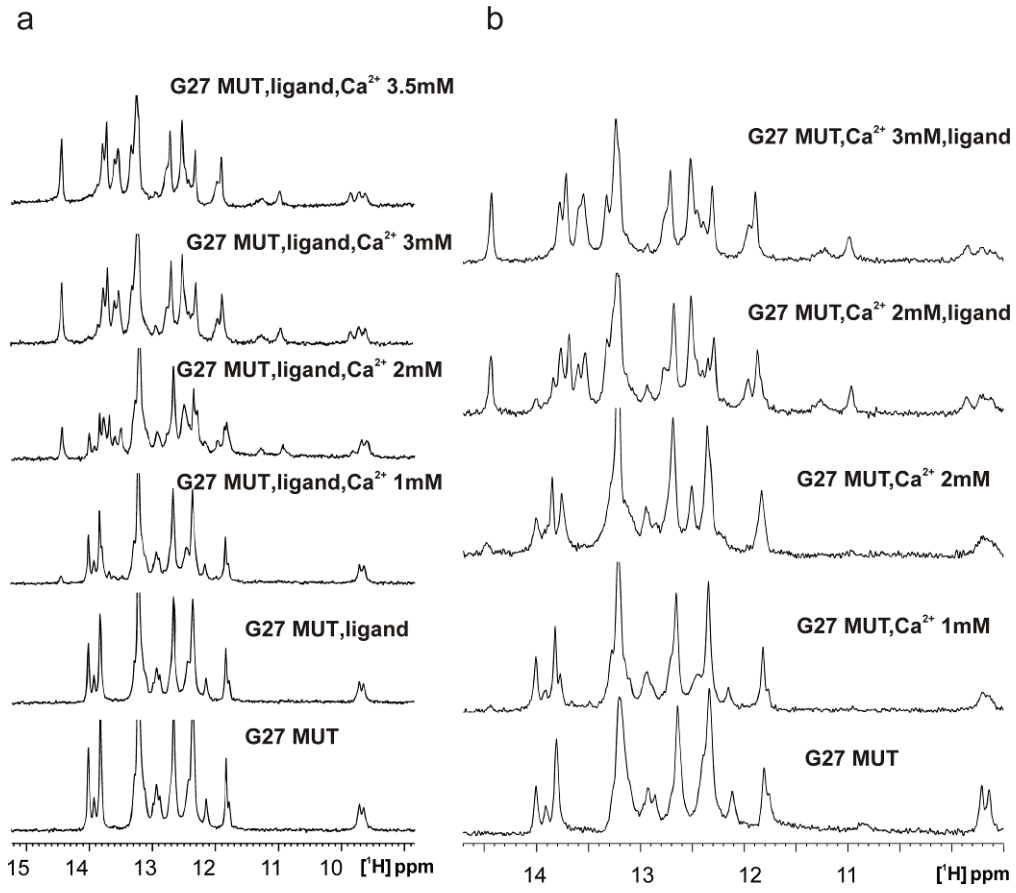

Figure 14: a) Titration of G27 MUT with ligand and Ca^{2+}. The final concentration of RNA was 0.3 mM and of ligand ~ 0.4 mM. b) Effect of addition of ligand to RNA (~0.280 mM) and Ca^{2+} (~2 mM). Significant stabilization of tertiary complex was exhibited only on addition of ligand though tertiary structure formation was initiated on addition of metal ions. On the other hand, ligand alone in the absence of metal ions showed no binding to the RNA. All measurements were at 283 K at a ^{1}H frequency of 600 MHz and 128 accumulated scans of spectral width of 24 ppm with 2048 complex data points.

On addition of Ca^{2+} imino resonances characteristic of tertiary complex similar to the WT were observed for G40 MUT. Residual free form imino resonances were exchange broadened indicating conformational dynamics. Throughout this text, complex form denotes that the RNA is bound with metal ions and ligand. We substituted Ca^{2+} for Mg^{2+}, as Ca^{2+} significantly increased the stability of the complex between RNA and divalent ions and revealed favorable well-resolved NMR spectra. In addition, Ca^{2+} was a better choice for the photocaging method due to the lower affinity of Mg^{2+} to DMN compared to Ca^{2+}. In order to determine the influence of ligand and Ca^{2+} ions on folding, titration of Ca^{2+} was carried out in steps of 1mM in the presence and absence of ligand (Figure 14 shows titration on G27 MUT). It was observed that Ca^{2+} initiated folding but significant stabilization of the complex was achieved only on addition of ligand (Figure 14d). It was also observed that the ligand alone in the absence of Ca^{2+} did not show any binding to the RNA (Figure 14a).

3.3.2.A. A27 WT tertiary complex characterization

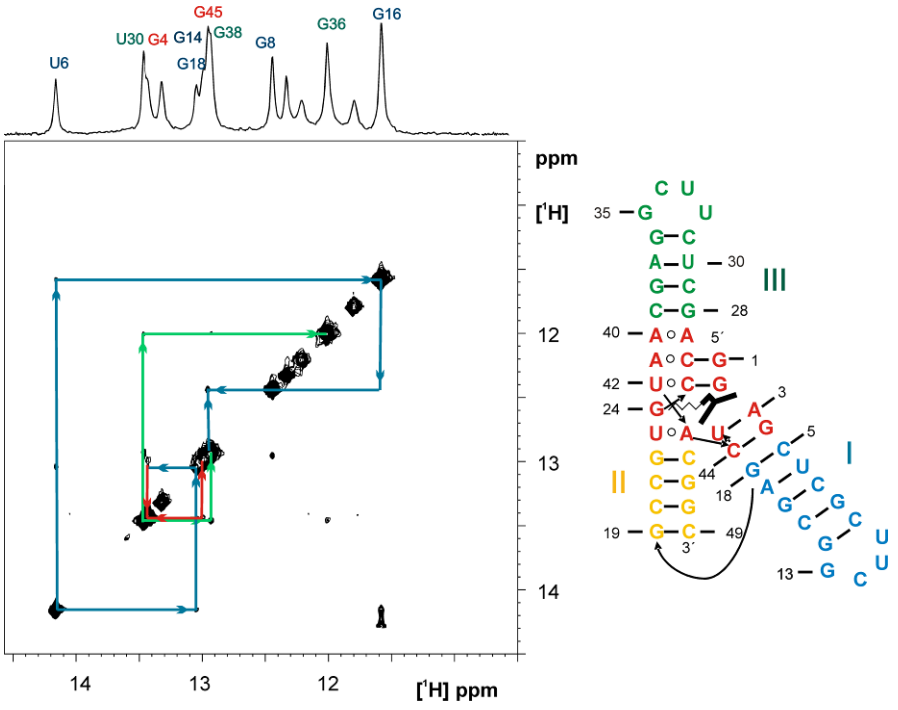

Figure 15: ^{1}H ^{1}H NOESY spectrum of the unlabeled A27 MUT ribozyme with 1D projection on top measured at T=288 K, 900 MHz field, conc.: RNA=0.4 mM, Mg^{2+}=5 mM, AMDA=0.6 mM measured over 60 hours. The sequential walk for the assignment of the ribozyme is indicated. Each segment of the walk is color-coded

according to the color code of the free-state layout that is given in the secondary structure conformation on the right as determined by x-ray crystallography (Serganov et al., 2005).

The tertiary complex structure of A27 WT was first characterized. To obtain the catalytically active tertiary complex, the RNA was titrated with Mg^{2+} and the ligand. By using the position of U6 and U30, stems I and III were identified in the NOESY spectrum. G14, G8, G16, U6, G18, G4 and U45 are assigned in blue stem I and its extension and G36, U30 and G38 are assigned in green stem III. The assignment of G4 and U45 indicating the basepairing of the 5' single tetranucleotide stretch with one of the strands of the asymmetrical bulge confirms the presence of tertiary structure interactions as in the crystal structure.

3.3.2.B. G27 MUT tertiary complex characterization

Complex of G27 MUT in solution is in agreement with crystal structure. The assignment of the stems I and III (blue and green) of the complex structure is straightforward when using the information from a NOESY, a $^{1}H,^{15}N$ HSQC and an HNN-COSY. Similar to the free form, the starting point is the characteristic chemical shift of the G nucleotide of the UUCG tetraloop resonating upfield of 10ppm. From here, we can follow the two characteristic crosspeaks between the imino proton resonances of G belonging to the two UUCG loops (G13, G35) and G of the closing GC base pair (G14,G36). The two walks are shown in green and blue, corresponding to the two helices of the x-ray structure shown in Figure 16b.The two helices are easily differentiated by the position of the AU base pair in the stem. In the green stem it is only one GC base pair away from the loop while in the blue it is three GC basepairs away. In the complex form, blue stem I was extended by stacking of two basepairs formed by interaction of A3 and G4 of the 5'-terminal tetranucleotides with U45 and C44 of the conserved bulge region. In the NOESY spectrum, this assignment is shown by the red lines continuing from the blue line that ends at G18 (Figure 16a). In the crystal structure of the RNA-ligand complex, the green stem III was also extended by a non-canonical basepair and two three-base interactions formed by the zippering up of the

bulge region by the 5' single stranded end. Of this extension, only the U42-C25 basepair could be resolved in the NMR spectra. No imino neighbor was detected from G28 to G27 in the NOESY. We attribute this finding to be due to imperfect stacking as observed in the crystal structure. Only a very weak peak was observed at the expected GA basepair resonance region upfield of 11 ppm, the correlation peaks are exchange broadened.

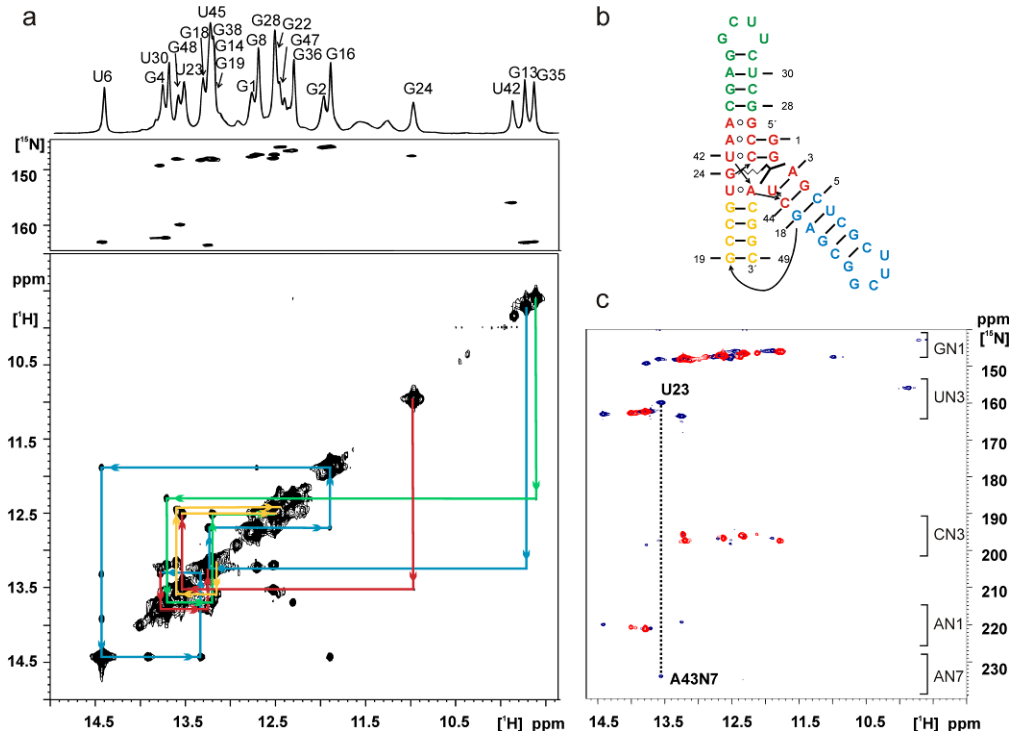

Figure 16: a) Imino region (15-9 ppm) of the G27 MUT product complex of ^{1}H, ^{1}H NOESY spectrum aligned with ^{1}H, ^{15}N HSQC with the assignment shown (see entries 10 and 11 of Table 4 for NMR parameters). Resonances of G13 and G35 appear folded in the ^{1}H,^{15}N HSQC. b) Complex structure base-pairing constellation as determined by x-ray crystallography (Serganov et al., 2005). Color coding is the same as for the free form. c) Superposition of the HNN-COSY spectra of the free G27 MUT ribozyme in red and the ribozyme in complex with Ca^{2+} and ligand in blue (NMR parameters are given in entries 12 and 13 in Table 4). The characteristic resonance regions of the base nitrogen atoms of the nucleotides are indicated. The dotted line highlights the reverse Hoogsteen-type basepair between U23 and A43.

To assign the catalytic core in the complex, we considered the resonance upfield of 11 ppm which could be identified as a G from the ^{1}H,^{15}N HSQC and which could *a priori* belong to a non Watson-Crick basepair or even an unpaired G (Varani et al., 1996). A crosspeak from this G to a U imino

proton, downfield of 13.5 ppm, was observed in the NOESY experiment. This U residue was unambiguously identified as belonging to a reverse Hoogsteen AU base-pair from $^{1}H,^{15}N$ HSQC and HNN-COSY experiments. The HNN-COSY showed that Watson-Crick side of this U nucleotide was hydrogen bonded with N7 of an A nucleotide (dotted line in Figure 16c). This pattern fits that of G24 and U23-A43 of the conserved region (shown in red) forming a wall of the catalytic pocket. The remaining U resonating in the non-canonical region (from ^{1}H ^{15}N HSQC) at 10 ppm was assigned to U42 that is involved in the base triple with C25 and G2 as observed in the crystal structure.

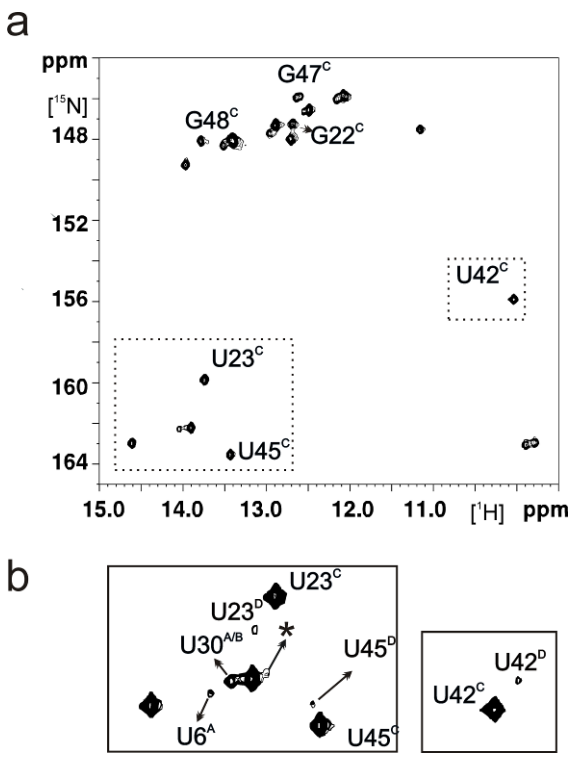

*Figure 17: a) $^{1}H,^{15}N$ HSQC of G27 MUT ribozyme in complex with ligand and Ca^{2+} ions (entry 11 in Table 4 gives experimental parameters.) Annotated cross peaks indicate resonances from the major fold C of complex population that also exhibit additional cross peaks originating from fold D of the weaker minor population. b) Boxed sections of the spectra in b at lower S/N showing weak resonances from fold D, the alternative complex conformation. Also labeled are peaks from residual free ribozyme. $U6^{A}$ is residual peak from fold A of the free form. Peaks arising from the less populated fold D are labeled with a suffix D. * denotes unassigned peaks.*

G27 MUT complex displays conformational heterogeneity. The $^{1}H,^{15}N$ HSQC of the complex showed a set of additional weak crosspeaks in the non-canonical resonance region belonging to the nucleotides from the catalytic pocket, namely U42, U45, and U23. These are labeled with superscript D in Figure 17b and indicate a second conformation, fold D, in the complex state. The FRET study also revealed conformational heterogeneity even for the A27 WT ribozyme in the complex form. In addition, resonances from the yellow stem II, namely, G22, G47 and G48 also displayed weaker resonances indicating conformational heterogeneity of stem II.

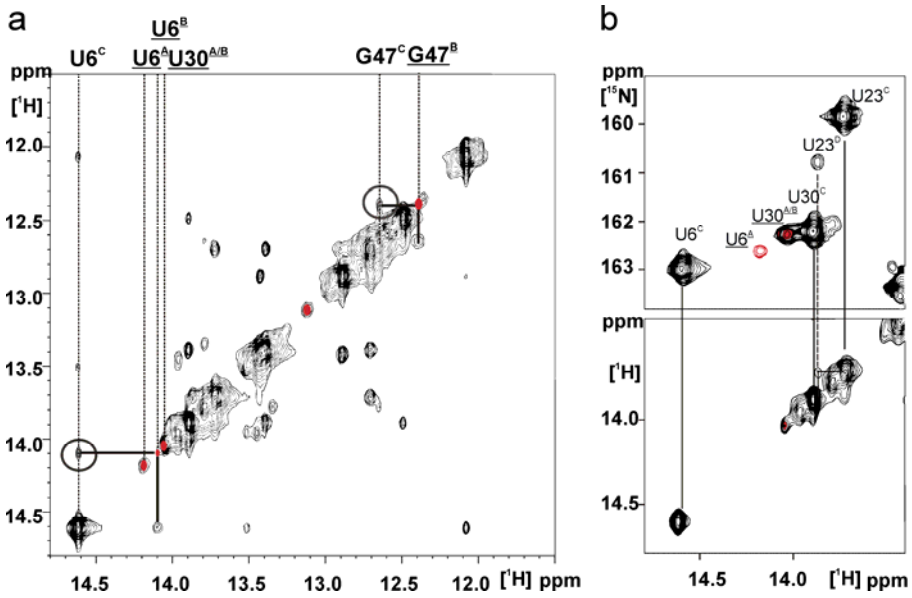

Figure 18: a) $^{1}H,^{1}H$ NOESY spectrum of imino proton region of G27 MUT complex. Diagonal peaks shown in red arise from residual free form. Exchange crosspeaks above the diagonal between complex and minor free form conformations are circled in black. Residu77al free form labels are underscored and have a suffix superscript A or B denoting folds A and B, respectively (entry 10 in Table 4 gives experiment parameters.) b) Expansion of the imino region of the $^{1}H,^{15}N$ HSQC (on top) and NOESY (bottom) spectra of the region around the U23 chemical shift arising from the G27 MUT ribozyme (0.5 mM) in complex with ligand (2 mM) and Ca^{2+} (4 mM). The vertical lines connect those resonances assigned to the same nucleotides in the two spectra. A weak crosspeak of U23 of fold C in the NOESY is shown by continuous lines. The dotted line connects the resonance labeled $U23^{D}$ in the HSQC arising from a second conformation to the weak exchange crosspeak highlighted in the NOESY. The peaks shown in red arise from residual free form population and their labels underscored.

Ligand-RNA crosspeaks. The crystal structure of G27 MUT in the presence of Mg^{2+} but absence of ligand/product showed that the RNA assumes a preformed structure (PDB:1YKQ) (Serganov et al., 2005).

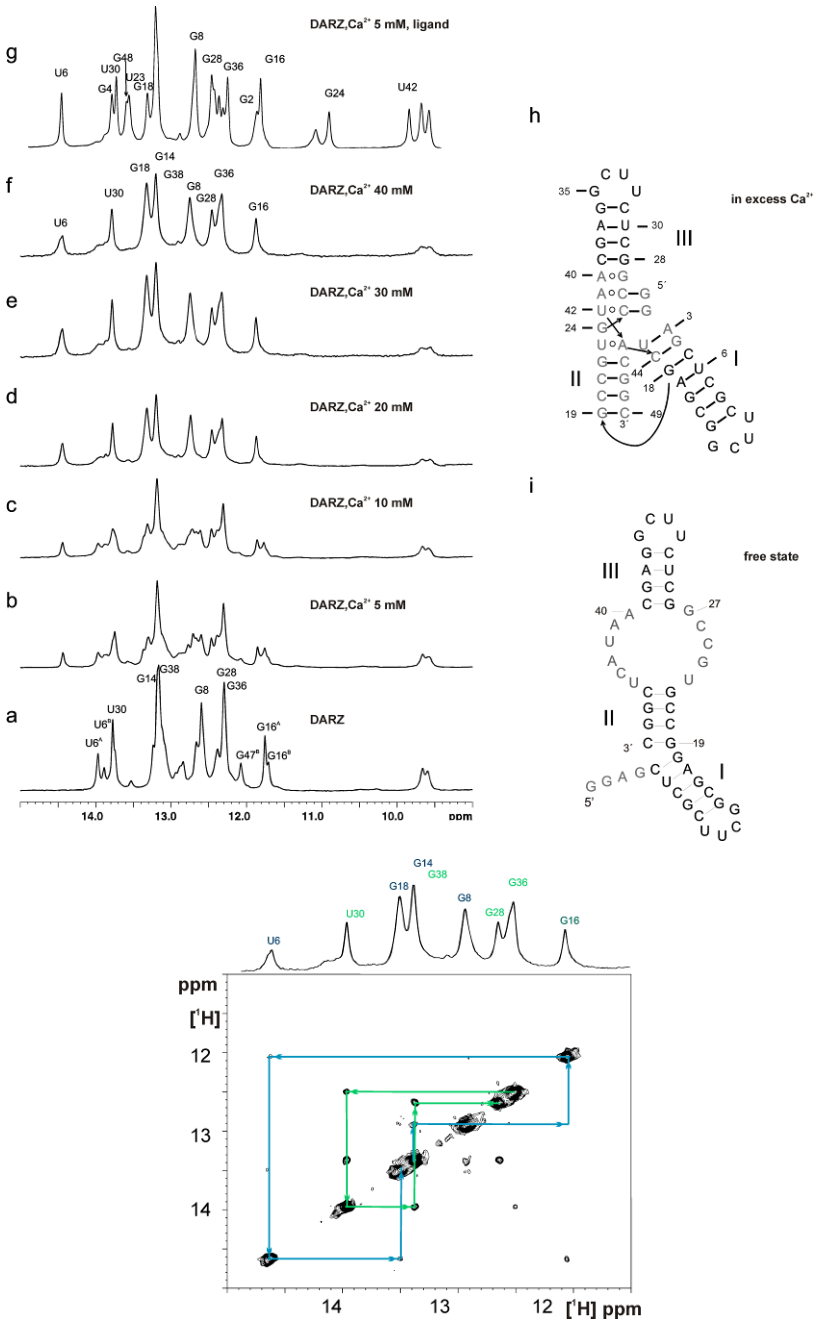

Figure 19: In the figure, on the left are 1D spectra of the imino region of G27 MUT showing titration of RNA with excess (40 mM) Ca^{2+} and comparisons with the spectra of free state (a) and complex tertiary ligand bound state.(g) In the center are the complex secondary structure layout as determined by x-ray crystallography on the top (h) and the mfold predicted free form at the bottom(i). The unassigned nucleotides are shown in light grey. $^{1}H,^{1}H$ NOESY of RNA in the presence of 40 mM Ca^{2+} measured at 283 K.

The titration experiments, however, revealed that all non-canonical Watson-Crick basepairs involved in long-distance tertiary structure interactions appeared well resolved only on the addition of ligand (Figure 19). Addition of Ca^{2+} initiates the folding of RNA into tertiary complex which is indicated by the appearance of $U6^{C.like}$ peak and fading of $U6^{A}$ and $U6^{B}$. The assignment in Figure 19f could be obtained by analysis of a NOESY spectrum (right panel in Figure 19). Stems I and III are nearly identical with the tertiary ligand bound state. But no signals are resolved from the catalytic pocket region. Also absent are the signals arising due to pairing of bases from the 5` GGAG tetranucleotide to the shorter strand of the asymmetrical bulge present in the free form. These signals are annotated in red in g, the ligand bound complex state. These are denoted by nucleotides marked in grey in panel h of the Figure 19. Significantly yellow stem II is also not resolved therefore indicating a degree of dynamics.

In order to characterize the ligand-RNA interactions, assignments were performed with the help of measurement of $^{1}H,^{1}H$ NOESY of the complex in deuterium. Deuterium exchange of the solvent was performed by freeze drying the RNA-complex and dissolving it in D_2O (99.996%). This procedure was performed 3 times to ensure complete exchange of all exchangeable protons. After measurements the RNA complex was exchanged back into H_2O and its 1D imino spectrum was recorded to verify that the complex was unchanged. The interactions of the ligand and RNA are tabulated in Table 1. Strong NOESY crosspeaks are observed from the alkyl sidechain of the ligand to the imino protons of U23, G24 and A43H2, and very weak ones to U42. The anthracene rings showed crosspeaks to the imino protons of G2, U45 and A43H2.

Table 1: List of NOE crosspeaks detected between the ligand protons and the ribozyme

AMDA ^{1}H	G27 MUT ^{1}H									
	G2-H1	A3-H2	U45-H3	A43-H2	U23-H3	G24-H1	U42-H3	NH2 (G2/C25)	NH2	H1'
H1,4			m							
H2,3			m	S						
H5,8	w	w								
H6,7	vw	w								
H9,10	s							w		
H11,1	s		vw					w		
H13			vw	s	w	s		w	w	
H14				m	w	w	vw	w	vw	w
H15			vw	m	m	w	vw	w	vw	w
H16				s	w		vw	vw		w
H17				m	s	vw	vw	vw		

NOE crosspeak intensity levels denoted as strong (s), medium (m), weak (w), very weak (vw).

Weak binding. The ligand exhibited weak binding with the RNA and additional sets of peaks are also observed arising from the protons of the alkyl side chain of the ligand. There protons are indicated in red in Figure 20.

Divalent metal ion binding sites in the G27 MUT-ligand complexes. The line broadening effect of paramagnetic Mn^{2+} ions was exploited to identify the metal ion binding sites of the ribozyme complex by $^{1}H,^{15}N$ HSQC. According to the crystal structure, at least six Mg^{2+} ions stabilize the RNA structure: While Mg1 and Mg2 are involved in the positioning of stems I and II, Mg4 and Mg6 bind in the grooves of blue stem I, Mg3 in the green stem III, and Mg5 binds near G24, the unpaired nucleotide bordering the catalytic pocket. We

performed competition experiments adding paramagnetic Mn^{2+} ions that lead to resonance broadening of imino resonances in the vicinity of the metal binding sites (Zeeb and Balbach, 2004). For the complex in the presence of Ca^{2+}, the strongest effect is seen for the resonances of G2, G24 and U42 that were broadened beyond NMR detection upon addition of 5 µM Mn^{2+} to the ribozyme complex (containing 0.220 mM RNA, 4 mM Ca^{2+} and 0.4 mM ligand (Table 4, entries 14 and 15 give NMR experiment parameters).

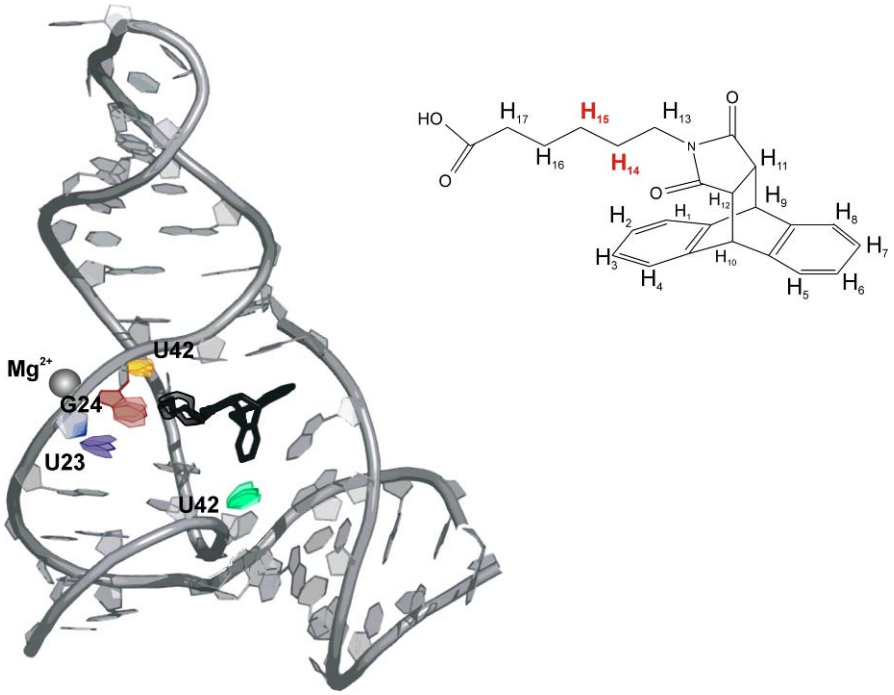

Figure 20: Cartoon representation of the crystal structure of G27 MUT is shown to demonstrate the additional weak conformation evident around the catalytic pocket. The colored bases belong to nucleotides that display additional weak peaks. Additional sets of peaks are also observed arising from the protons of the alkyl side chain of the ligand. There are labeled in red in B.

G28 also exhibited severe line broadening which is in line with the presence of an Mg^{2+} binding site in its vicinity. The characterization of metal ion binding on A27 WT studied by EPR concluded that the metal ions bind with different affinities (Kobitski et al., 2007). This finding is consistent with the data for G27 MUT, where linewidth broadening effects were not uniform at all binding sites.

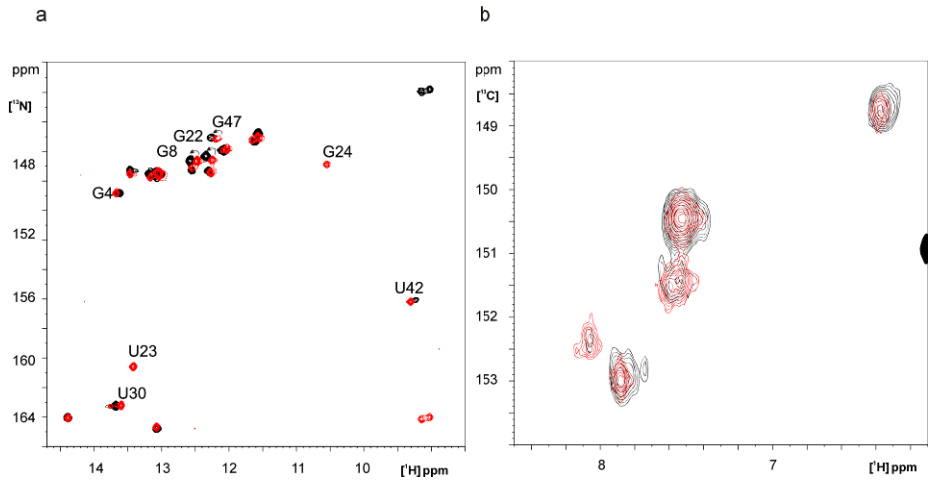

Figure 21: (a) $^{1}H,^{15}N$ HSQC (see 14 and 17 in Table 4 for experimental parameters) and (b) $^{1}H,^{13}C$-HSQC spectra (AH_2 resonance region) of the RNA complex in the presence of Mg^{2+} (peaks in black, 21 in Table 4 gives experimental parameters) and Ca^{2+} (in red, 20 in Table 4 for experimental parameters.). Those peaks that differ in intensity and chemical shift are labeled in (a).

Figure 22a and b illustrate the effects of Mn^{2+} addition on the linewidths of resonances of the G27 MUT-ligand complex folded in the presence of Ca^{2+} and Mg^{2+} ions, respectively (see entries 13, 14 and 15 in Table 4 for experimental details). Resonances arising from U23 and G24 were lost in the Mg^{2+} complex and chemical shift differences between the two complexes were also observed for peaks arising from G8, G22, U42 and G47 (see Figure 21a). Nevertheless, the $^{1}H,^{13}C$ HSQC of the aromatic region showed that the same conformation is maintained for both complexes including the reverse Hoogsteen base pair (Figure 21b). Consequently, the presence of resonance differences in the $^{1}H,^{15}N$ HSQC of the two complex forms points to differences in solvent exchange and conformational exchange differences. This observation may provide clues to the difference in catalytic activity between the two complexes. The activity reduces by 65% when Ca^{2+} is substituted for Mg^{2+} (Seelig and Jäschke, 1999). As has been established previously, metal ions do not directly participate in the reaction (Seelig and Jäschke, 1999). The significant difference in activity points to the structural characteristics of the ribozyme, specifically the dynamics of the catalytic pocket region, as an important player in the catalytic efficiency. Catalytic pocket dynamics was also proposed in the FRET study to explain the catalytic properties (Kobitski et al., 2007). The poor

spectral resolution of the Mg^{2+} complex indicates a certain degree of structural flexibility which may be essential for rapid binding and release of substrate and product of the reaction.

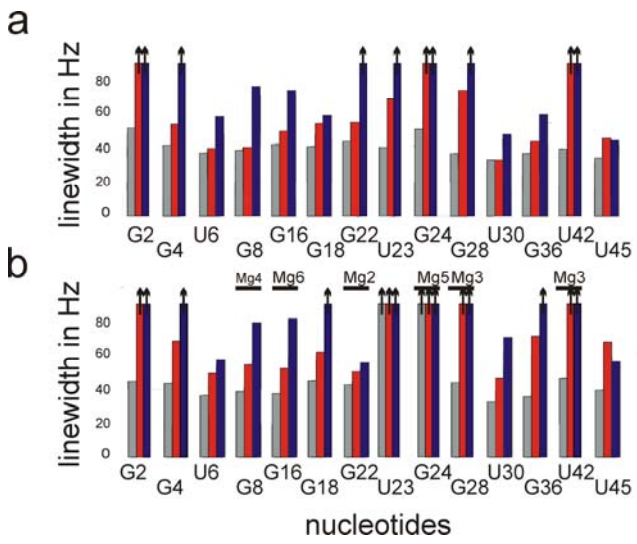

Figure 22: a) Bar chart giving linewidths of imino protons from $^{1}H,^{15}N$ HSQC spectra of the ribozyme-Ca^{2+}-ligand complex in grey. Red and blue bars are linewidths obtained on addition of 5 μM or 10 μM Mn^{2+}, respectively, to the above complex ribozyme. Bars with vertical arrows indicate peak broadening beyond NMR detection. b) Bar chart giving linewidths of imino protons from ^{1}H, ^{15}N HSQC spectra of the ribozyme-Mg^{2+}-ligand complex in grey. Bars with vertical arrows indicate peak broadening beyond NMR detection. Red and blue bars are linewidths obtained on addition of 4 μM and 10 μM Mn^{2+}, respectively, to the above complex ribozyme. Horizontal bars indicate Mg^{2+} binding sites observed in the x-ray structure. The sixth binding site cannot be ascertained due to insufficient chemical shift resolution in the NMR spectra. See entries 17, 18 and 19 in ***Table 4*** *for experimental parameters.*

3.3.2.C. G40 MUT tertiary complex characterization

G40 MUT ribozyme was titrated with metal ions and ligand as previously performed for the A27 WT and G27 MUT. It was found to display the same characteristics as G27 MUT. Well-resolved spectra were obtained for Ca^{2+} in comparison with Mg^{2+} (Figure 23c). There were no changes observed on addition of ligand alone to the RNA, indicating non-binding of ligand to RNA in its free form. G40 MUT also showed complex-like peaks on addition of metal ions in the absence of ligand. However, the ligand was found to greatly stabilize the RNA-metal ion complex.

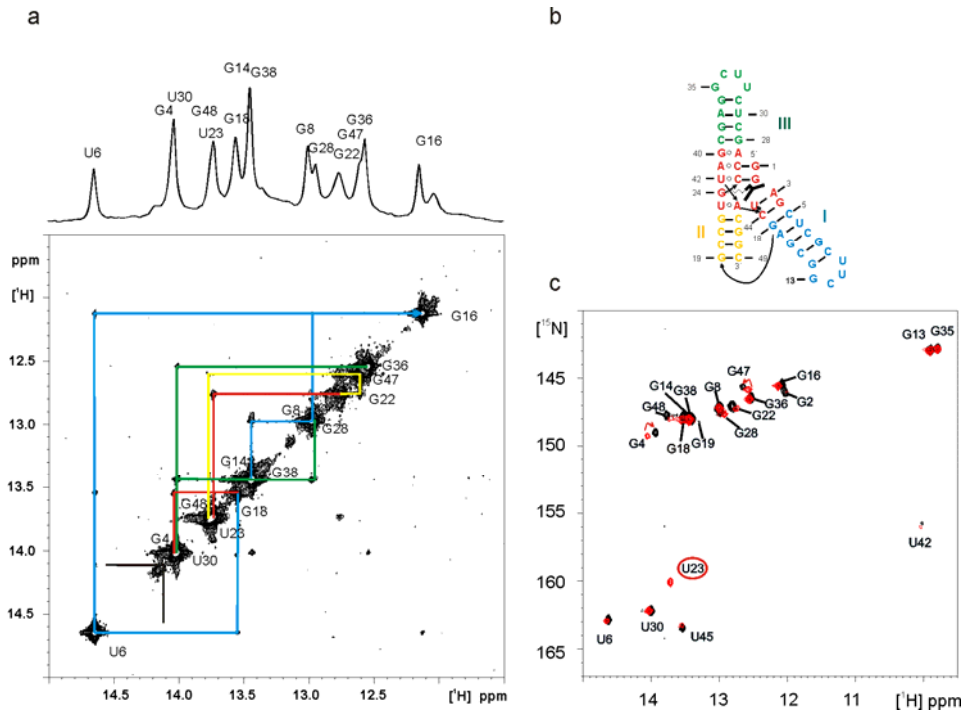

Figure 23: a) Imino region (15-9 ppm) of the G40 MUT product complex in the presence of Ca^{2+} in the ^{1}H, ^{1}H NOESY spectrum. Conc. of RNA=0.180 mM, ligand=0.8 mM, Ca^{2+}=6 mM, τ_M =100 ms, T=283 K, 800 MHz, 44 hrs. See entry 22 in Table 4 for complete NMR experiment parameters. The sequential walk for the assignment is color coded according to the secondary structure layout shown in panel b. b) secondary structure layout of the RNA in complex with ligand and metal ion proposed based on NMR assignments. C) ^{1}H, ^{15}N HSQC of G40 MUT in complex with Mg^{2+} in black (conc. of RNA=0.2 mM, Mg^{2+}=8 mM, ligand=0.8 mM.) and G40 MUT in complex with Ca^{2+} in red (conc. of RNA=0.2 mM , Ca^{2+}=8 mM, ligand=0.8mM.). Resonance labels are indicated and those circled in red indicate those resonances which are not observed in the Mg^{2+} complex. Entries 23 and 24 in Table 4 for experimental NMR parameters.

The assignment of complex G40 MUT was performed by making use of the assignments of G27 MUT. From the assignment of the G40 MUT complex, it is seen that all structural properties that were observed in G27 MUT, namely the reverse Hoogsteen of U23 and base triples formed by long range interaction of the 5` tetranucleotide strand are observed (Figure 24*b*). As expected, G28 showed a change in chemical shift since one of its neighboring base pair has changed from A40.G27 to G40.A27. The changes in chemical shifts between G40 MUT (black peaks) and G27 MUT (red peaks) are indicated in Figure 24*b* by red arrows. G24 forming the spine of the catalytic pocket between helices II and III could be detected at lower temperature but not at 283K. In conclusion, the tertiary structures of all three ribozymes are

similar, though, differences in local dynamics are observed in the catalytic pocket region. Namely, the base triple formed by G1 of the 5` end is not observed in G40 MUT due to exchange broadening. G2 and U42 also show very broad linewidth indicating weakened hydrogen bonding.

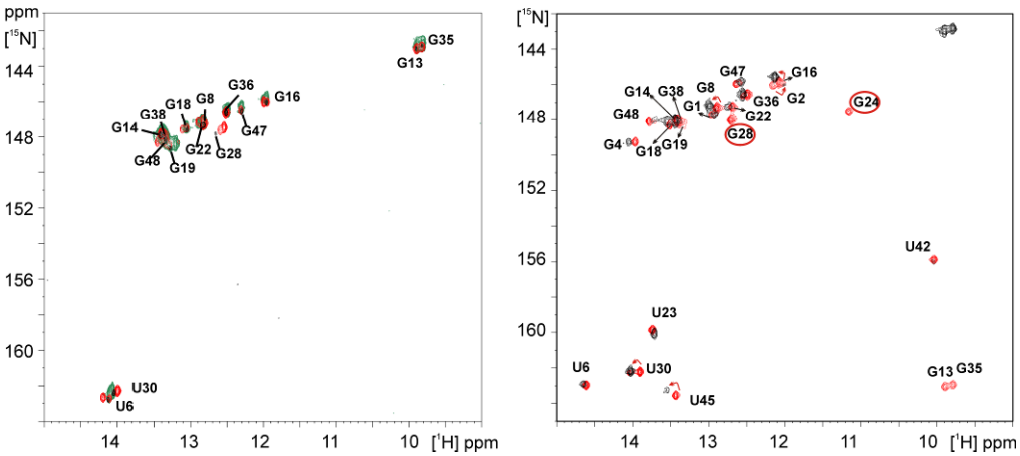

Figure 24: a) ^{1}H, ^{15}N HSQC of all three ribozymes without metal ions and ligand. Green peaks belong to G40 MUT, red to G27 MUT and black to A27 WT. b) ^{1}H, ^{15}N HSQC of G40 MUT in black (RNA=0.2 mM, Ca^{2+}=8 mM, ligand=0.8 mM.) and G27 MUT (RNA=0.4 mM , Ca^{2+}=4 mM, ligand=2 mM.) in red in complex with ligand and Ca^{2+}. Resonance labels are indicated for G27 MUT and those circled in red indicate those resonances which are not observed in G40 MUT.

Divalent metal ion binding sites in the G40 MUT-ligand complexes. Similar to the G27 MUT ribozyme, here too the competitive binding action of Mn^{2+} ions was exploited to identify the metal ion binding sites of the ribozyme complex by ^{1}H,^{15}N HSQC. The addition of paramagnetic Mn^{2+} ions leads to resonance broadening of imino resonances in the vicinity of the metal binding sites. U23 of the reverse Hoogsteen base pair and G24 the unpaired nucleotide in the catalytic pocket are exchange broadened in the Mg^{2+} complex. This was also the case with the G27 MUT.

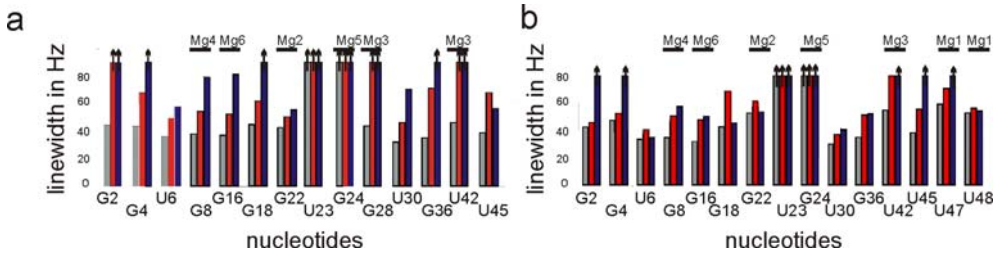

Figure 25: a) Bar chart giving linewidths of imino protons from $^{1}H,^{15}N$ HSQC spectra of the G27 MUT ribozyme-Mg^{2+}-ligand complex in grey. Red and blue bars are linewidths obtained on addition of 4 μM or 8 μM Mn^{2+}, respectively, to the above complex ribozyme (conc. of RNA=0.2 mM). Bars with vertical arrows indicate peak broadening beyond NMR detection. b) Bar chart giving linewidths of imino protons from ^{1}H, ^{15}N HSQC spectra of the G40 MUT ribozyme-Mg^{2+}-ligand complex in grey. Bars with vertical arrows indicate peak broadening beyond NMR detection. Red and blue bars are linewidths obtained on addition of 4 μM and 8 μM Mn^{2+}, respectively, to the above complex ribozyme (conc. of RNA=0.22 mM). Horizontal bars indicate Mg^{2+} binding sites observed in the x-ray structure. See entries 24, 25 and 26 in ***Table 4*** *for experimental parameters.*

Figure 25 gives the linewidth analysis of both G27 MUT and G40 MUT ribozymes in complex form in the presence of Mg^{2+} and ligand. Significant line broadening was observed for resonances arising from U42 (Mg3 binding site), U45 and U47 (Mg1 binding site). G2 and G4 belonging to the 5` tetranucleotide also showed line broadening in the presence of Mn^{2+} which was also observed for G27 MUT. No significant line broadening was observed at the binding sites of Mg4 and Mg6 in the grooves of blue stem I even at higher concentration of 8 μM Mn^{2+}. Difference in line broadening effects of the binding sites indicate different binding affinities of the Mg^{2+} ions.

Summary

In summary, all three ribozymes from the Diels-Alder ribozyme family exhibited similar tertiary structure characteristics, while distinct differences in their free form conformations were detected as discussed in section 3.3.1.D. We now have characterized the equilibrium states of the start and end states for defining the folding trajectory using time-resolved NMR experiments (Section 3.3.3).

3.3.3. Time-resolved NMR Results

3.3.3.A. A27 WT

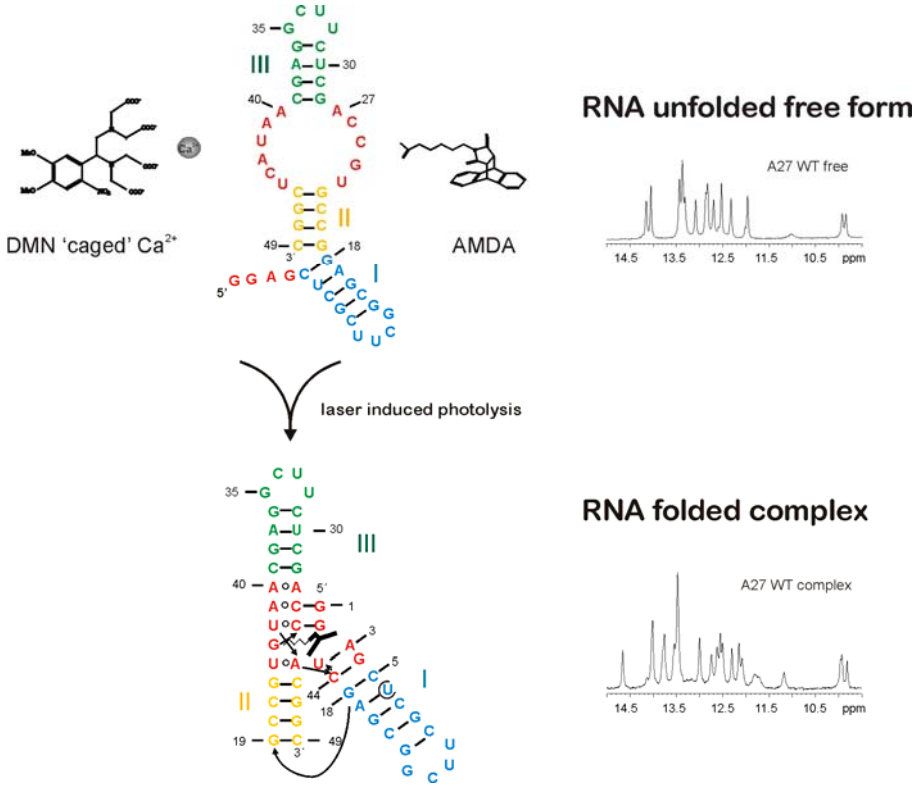

Figure 26: Schematic representation of the time-resolved NMR experiment by photocaging of the metal ion to trigger RNA folding. The RNA is in the free form conformation in the presence of DMN caged Ca^{2+} and the ligand, AMDA. On photolysis by a laser pulse, the Ca^{2+} ions are released thus allowing the RNA to assume its complex pseudoknot structure. The 1D imino spectra of the RNA in its free and complex bound form are also given.

The first system to be analyzed was the best catalyst, the wild type A27 WT. We have already discussed in the introduction the two methods of initiation of folding of RNA that has been applied here. A27 WT kinetics was investigated using the photocaging technique. A schematic representation of this is shown in Figure 26. The general outline of the procedure is as follows. The molecule is first prepared in a solution containing the high-affinity ligand, and a photolabile caged form of Ca^{2+} (DMN-Dimethoxy-nitrophen (Ellies-Davis and Kaplan, 1988), 'caged' Ca^{2+}). The 1D imino region of the RNA measured in this state is shown in panel b in Figure 27. Next, a short laser

pulse is applied. The laser pulse (350 nm, 5W) decomposes the caging compound and thus releases the metal ions (c in Figure 27). The binding affinity of the DMN photoproducts to Ca^{2+} ions is lower (K_D=3*10^{-3}M) than the binding affinity of the RNA to Ca^{2+} and much lower than the affinity of the DMN itself to Ca^{2+} ions (K_D=5*10^{-9}M). Therefore, the release of divalent ions from DMN makes them available for binding to the RNA which thus folds into its active conformation. This transition is followed by real-time NMR methods. Data collection and processing are discussed in Section 5.2.2.

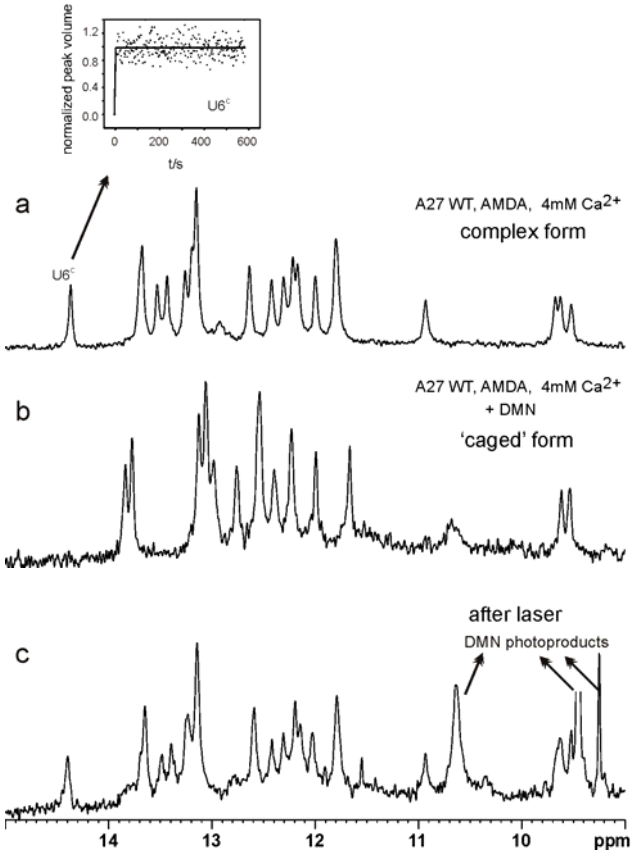

Figure 27: Imino region of 1D ^{1}H spectra recorded for the A27 WT a) in the presence of metal ion and ligand b) with photo-labile metal ion caging compound (DMN) that binds the metal ion with higher affinity than the RNA molecule and therefore leads to unfolding of the DARZ (free form) and c) after laser irradiation that induces DMN decomposition and the release of the metal ions thereby inducing folding of the RNA molecule again. The inset shows the kinetic trace of the normalized peak volume of the resonance from $U6^C$ that is plotted as a function of time in seconds.

For the A27 WT ribozyme, folding was fast and was completed in the dead time of the experiment (1.5s) in agreement with the FRET study that

showed a 100 ms timescale for transitions between RNA states in the absence of ligand (Kobitski et al., 2007). The inset in Figure 27 shows an example kinetic trace of $U6^{C}$.

3.3.3.B. G27 MUT

For the single nucleotide mutant G27 MUT ribozyme, time-resolved NMR experiments were conducted using two techniques. The first involved caging of Ca^{2+} by the photolabile metal chelator dimethyl-nitrophen, the induction of folding by application of a laser pulse (350 nm, 5W), and subsequent monitoring of the kinetics by 1D experiments. The main limitation of this technique was the amount of the Ca^{2+} required to be released in order to provide sufficient signal-to-noise ratio in the NMR measurements. This issue is discussed in detail below. The second technique was the rapid sample-mixing technique involving the use of an injection device to rapidly add Ca^{2+} to induce folding, with the NMR tube acting as the mixing chamber.

Time-resolved NMR using photo-caging technique

Figure 28a shows the various stages of the time-resolved experiment involving the photocaging technique on G27 MUT. Addition of DMN to a mixture of RNA, Ca^{2+}, and AMDA in buffer leads to a spectrum that shows all features of the RNA free form (including the two different folds A and B, compare states I and III). On laser-induced photolysis of DMN the RNA undergoes Ca^{2+}-induced folding into its ligand bound tertiary complex (compare states II and IV showing the imino region of the 1D spectra). The time-resolved NMR experiment involves monitoring of the transition from state III to state IV by recording of a series of 1D spectra. Since experimental conditions allowed for the release of only 1 mM Ca^{2+} for a laser pulse of 1.5 s duration, we titrated the ribozyme with Ca^{2+} in steps of 1 mM and used the step which showed the largest transition in terms of peak volumes for kinetics analysis (1 mM to 2 mM Ca^{2+} - see panel b in Figure 28).

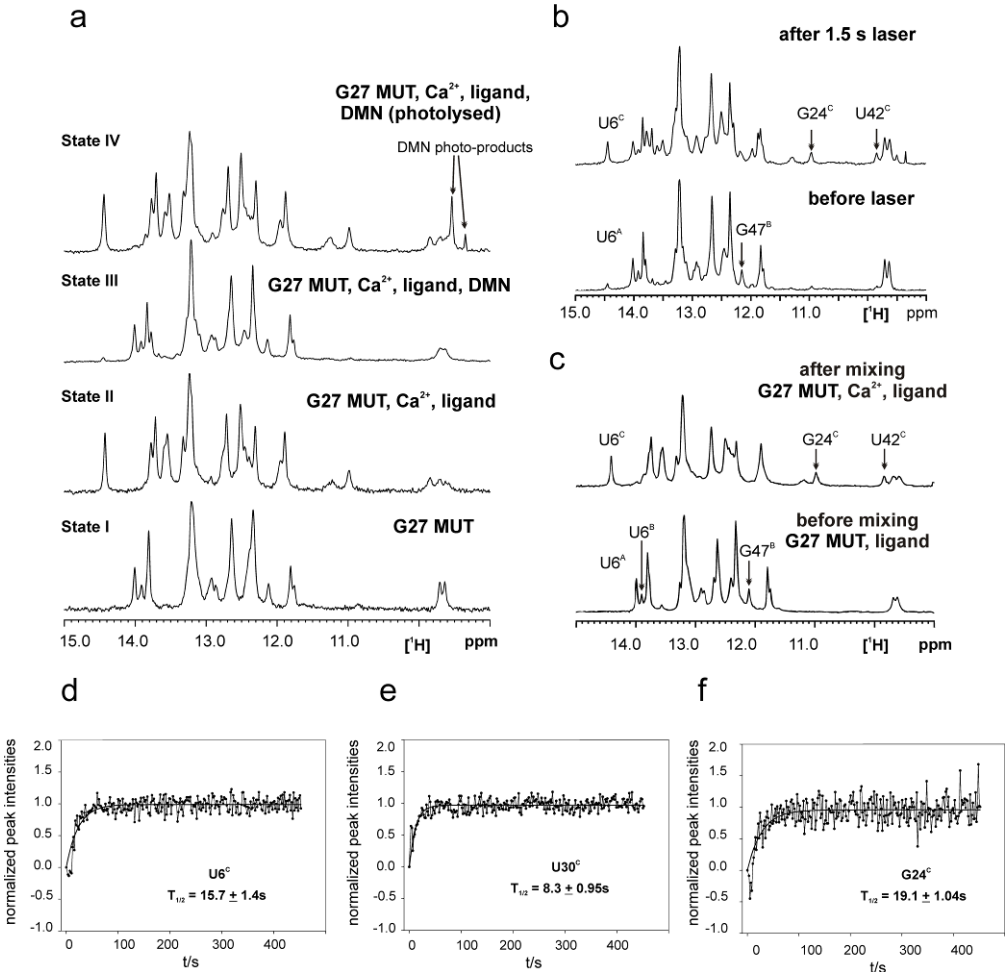

Figure 28: a) 1D imino region spectra of G27 MUT showing, bottom-up, the free state(State I), complex state (State II), Ca^{2+} caged (State III) and Ca^{2+} released (State IV) state after 4 laser-pulses of 2 s each (350 nm, 5W). b) Imino spectra generated from an experiment monitoring the kinetics of approximately 1/5th of the population. See text for detailed experimental setup. c) Imino proton region of 1D of DARZ. Top - DARZ in the presence of ligand in the ratio 1:1.5 before addition of Ca^{2+} using mixing device. Bottom – DARZ in the presence of ligand after injection of Ca^{2+} using mixing device. d,e and f) Normalized peak intensities of U6, U42 and G24 of complex conformation are plotted as a function of time after initiation of ribozyme folding. The apparent half-life of the folding reaction ($T_{1/2}$) is calculated from the pseudo first order fit of the rate curves.

Therefore, effectively folding kinetics of approximately a fifth of the total population of molecules is monitored - since at least 3 mM Ca^{2+} is required for complex tertiary folding of nearly all molecules. Three peaks, U6 ($U6^C$), U30 ($U30^C$) and G24 ($G24^C$), representative of stems I and III and the catalytic pocket respectively, were chosen for their good spectral resolution for the analysis. The plots of their kinetic traces are given in panels d, e and f in Figure 28.

Interpreting the kinetic data into structural transitions requires prior conformational information of the peaks monitored. We established (see section on tertiary complex characterization of G27 MUT) that $U6^C$ indicates tertiary complex positioning of blue stem I and probable interaction between the conserved bulge region and the 5' terminal G1G2A3G4 tetranucleotide, since this is to a large extent also dependant on ligand binding. In titration experiments G2, G4 and G24 resolve only in the presence of ligand and at least 2 mM of Ca^{2+} (see Figure 14). In the absence of ligand binding, the imino protons lining the catalytic pocket are susceptible to solvent exchange and hence the peaks arising from these protons cannot be detected by NMR. Therefore, the signal arising from $G24^C$ indicates Ca^{2+} and ligand binding induced stabilization of the catalytic pocket. Nevertheless, the data from this technique should be interpreted with caution due to the very low signal to noise ratio of the data. However, we do get a preliminary folding rate that gives us an estimate of the folding of the RNA into the complex pseudoknot structure.

Time-resolved NMR using rapid-mixing technique

We then performed time-resolved NMR using rapid-mixing experiments to monitor the kinetics of the Ca^{2+}-induced folding to the ribozyme complex. Folding was induced by addition of Ca^{2+} to a sample of RNA already containing ligand * (Figure 29c, bottom). This method was preferred over the injection of a mixture of Ca^{2+} and ligand into RNA to prevent ligand precipitation due to insolubility. Efficient mixing was achieved using a pneumatic syringe placed outside the NMR magnet which injects the Ca^{2+} into the NMR tube containing the sample, via a PTFE transfer line.

* NMR spectra showed no changes on addition of ligand to RNA in absence of divalent cations indicating absence of binding. Therefore, in the experiment the pre-mix sample contained RNA and ligand in the ratio ~1:1.5.

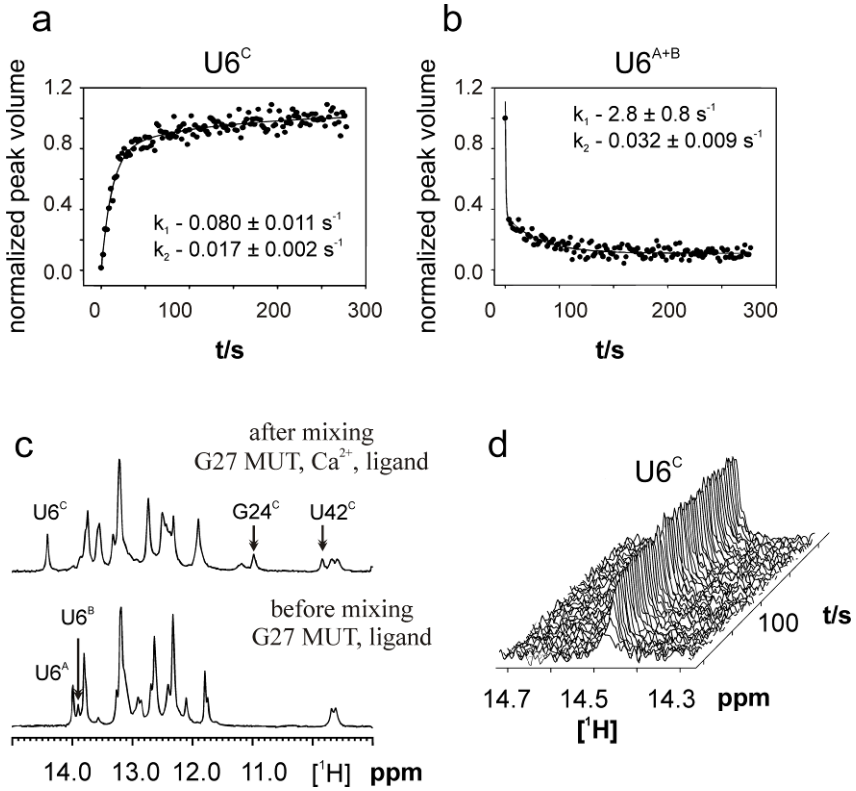

Figure 29: Normalized integrals of resonances of $U6^C$ measured after initialization of folding plotted as a function of time using a double exponential fit. b) Double exponential fit of $U6^A$ and $U6^B$ resonances arising from the free state of the ribozyme. c) Top - Imino proton region of 1D of G27 MUT in the presence of ligand in the ratio 1:1.5 before addition of Ca^{2+}. Bottom - G27 MUT in the presence of ligand after injection of Ca^{2+}. d) Stack plot of imino proton spectra as a function of time of resonance from $U6^C$.

For the A27 WT ribozyme, folding was fast and was completed in the dead time of the experiment (1.5s) in reasonable agreement with the FRET study that showed a 100 ms timescale for transitions between RNA states in the absence of ligand (Kobitski et al., 2007).On the other hand, the rates obtained for the G27 MUT were in the order of seconds. Along with slower folding kinetics of the ribozyme mutant we detected significant conformational heterogeneity both in the free and complex forms of the ribozyme as revealed by the static NMR experiments. We observe at least four conformations, two for the complex (fold C and fold D in Figure 29a) and two for the free forms (fold A and fold B in Figure 29). In the presence of Ca^{2+} ions, but without ADMA, the conformational heterogeneity is even more pronounced (Figure 13a and b). Under equilibrium conditions, at least three conformations are

observed: a complex like conformation ($C^{like}\cdot Ca^{2+}$) as well as two conformations ($A^{like}\cdot Ca^{2+}$ and $B^{like}\cdot Ca^{2+}$) that resemble the free state. The line width of the two conformations $A\cdot Ca^{2+}$ and $B\cdot Ca^{2+}$ is exchange broadened over the entire concentration range of [RNA]:[Ca^{2+}] (Figure 19a-g) and thus, the relative ratio [$A\cdot Ca^{2+}$]:[$B\cdot Ca^{2+}$] cannot be determined due to line broadening. In the absence of Ca^{2+}, A27 WT revealed only one free form conformation, while in the presence of Ca^{2+}, also additional conformational dynamics are induced (Figure 13a and b).

During the folding of the A27 WT complex, new basepairs are formed including two canonical, two non-canonical and two base triples. These triples involve long distance interactions between the unpaired nucleotides of the bulge region and the 5' tetranucleotide strand leading to a complex pseudoknot and a cavity that enables substrate binding. The forging of basepairs is accompanied by an overall structural rearrangement that involves splaying of the backbone between nucleotides G18 and G19 of stems I and II, respectively. For the G27 MUT ribozyme, a number of different states are populated after addition of Ca^{2+} to induce folding. For the major free fold A to fold into the complex, six G-C basepairs have to be broken before the correct nucleotide pairing of the yellow stem II can be achieved as required for fold C. Therefore, in addition to the long distance interactions as stated above for the A27 WT, four additional G-C basepairs have to be formed. Consequently, the rate of formation of the bound complex form should depend strongly on the rate of unfolding of fold A. The characterization of the minor fold B of the free from of G27 MUT revealed an identical fold to the wildtype ribozyme. The unfolding rate of the minor fold of G27 MUT is therefore likely to be similar to the unfolding rate of A27 WT. This hypothesis is supported by the NOESY exchange peaks observed at equilibrium between the minor free fold B and the major complex fold C with a rate constant of ~3 s^{-1}.

Table 2: Table of rates obtained from kinetic experiments using time-resolved NMR spectroscopy. A and B are amplitudes k_1 and k_2 are rate constants and Adj Rsqr the goodness of fit for the equation f=a(1-exp(-b*x))+(1-a)*(1-exp(-d*x)) for rising peaks and f=y0+a*exp(-b*x)+(1-a)*exp(-d*x) for decaying peaks.*

Peak	Temp K	A%	k_1 s^{-1}	B%	k_2 s^{-1}	Adj. Rsqr
$U6^C$	288	73.2 ± 0.10	0.08 ± 0.011	26.7 ± 3.78	0.017 ± 0.002	0.8565
$U6^C$	293	88.8 ± 0.17	0.095 ± 0.019	11.2 ± 2.24	0.02 ± 0.004	0.9048
$G24^C$	288	70.4 ± 0.07	0.094 ± 0.009	29.5 ± 2.95	0.011 ± 0.001	0.7268
$G24^C$	293	85.84 ± 0.08	0.123 ± 0.011	14.16 ± 1.33	0.016 ± 0.001	0.6404
$U23^C/G48^C$	288	86.05 ± 0.22	0.112 ± 0.028	13.95 ± 3.57	0.012 ± 0.003	0.9267
$U23^C/G48^C$	293	95.67 ± 0.28	0.137 ± 0.041	4.33 ± 1.31	0.011 ± 0.003	0.9329
$U6^{A+B}$	288	75.21 ± 0.22	2.8 ± 0.8	24.79 ± 7.33	0.032 ± 0.009	0.8743

For the fitting of the rates of folding and unfolding of the G27 MUT detected in the time-resolved NMR experiments, biexponential folding kinetics had to be assumed based on F-statistics analysis. For example, the folding rates towards the complex detected for the NMR signal of $U6^C$ arise from a fast ($0.08 \pm 0.011 s^{-1}$ for 73% population) and a slow transition ($0.017 \pm 0.002 s^{-1}$ for 27% population). The unfolding rates of $U6^{A+B}$ also revealed second order reactions in the order of $2.8 \pm 0.8 s^{-1}$ (75%) and $0.032 \pm 0.009 s^{-1}$ (25%). It should be noted that the fast rate of unfolding is within the dead time of the experiment.

3.3.3.C. G40 MUT

The reactivity of the G40 MUT ribozyme is only 30% of the wild type A27 WT. The complex form characterization showed it to assume a pseudoknot fold similar to A27 WT and G27 MUT. This experimental finding leads to the hypothesis that its reactivity is perhaps related to the dynamics of the ribozyme. Therefore to increase our understanding of the system, the folding trajectory of the G40 MUT ribozyme was delineated and analyzed

using the time-resolved experimental set up. For the G40 MUT only the rapid-mixing technique was applied as the photocaging technique was not feasible.

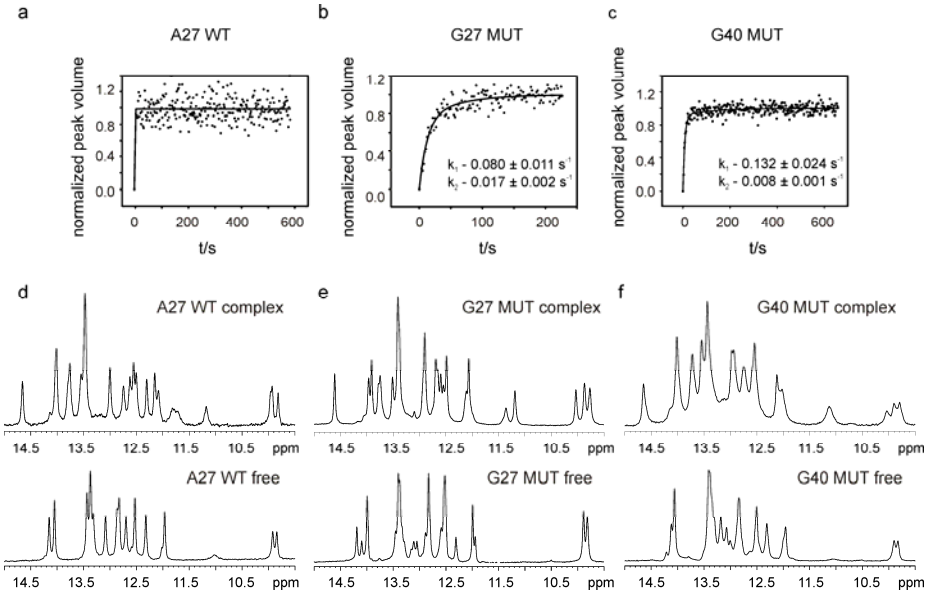

Figure 30: a) ,b) and c) Kinetic traces of a single peak U6^{C} from the wildtype and two mutant ribozymes plotted over time. d,e and f) Imino region of the 1D ^{1}H spectra of all three ribozymes in the free state and ligand bound state.

Time-resolved NMR by rapid-mixing technique

Rapid-mixing technique was applied for the time-resolved experiments of G40 MUT. Ca^{2+} was injected into an NMR tube containing a solution of ribozyme and ligand that is placed inside the NMR magnet by a pneumatic syringe from outside the magnet. Kinetic information was obtained by integration of the imino resonance peaks. Similar to G27 MUT, G40 MUT also showed biexponential kinetics showing a fast phase and an additional slow phase. The kinetic trace from U6^{C} exhibited a rate of $k_1 = 0.132 \pm 0.024$ s^{-1} with 90% population and $k_2 = 0.008 \pm 0.001$ s^{-1}. The rates obtained indicate that G40 MUT attains its tertiary complex state faster than the G27 MUT ribozyme but still on a slower time scale than those of A27 WT.

The time-resolved results agree well with the NMR characterization of the static states of the ribozyme in its free and complex form. Fold B, the major populated conformation was identified as the WT free form conformation. From mfold predictions, it was observed that the weakly populated fold A of

G40 MUT showed the yellow helix II with incorrect basepairs with respect to the tertiary complex conformation. This situation is somewhat similar to the G27 MUT free form and tertiary complex form conformations. The dissimilarities between the two systems arise in the equilibrium dynamics between the two folds. While G27 MUT showed the WT free form conformation to be the weaker populated fold, in G40 MUT at equilibrium the WT conformation is the thermodynamically more stable fold. In addition, the weaker conformation with the incorrect base pair interactions, fold A of G40 MUT, shows only 2 base-pairs that require dissociation for correct tertiary complex conformation. In the case of G27 MUT 6 basepairs should be broken for the correct tertiary conformation contributing to its slow folding kinetics.

CHAPTER IV

4. Discussion and Conclusions

4.1. Folding Model for G27 MUT

The results of the static and time-resolved NMR experiments conducted in this study were complementary to each other. The results of the time-resolved experiments revealed distinct difference of folding into the native state of the ribozymes A27 WT, G27 MUT and G40 MUT. The folding rates observed for the G27 MUT ribozyme (e.g. $U6^{C}$=0.08 ± 0.011 s^{-1}) differed by three orders of magnitude from the A27 WT folding rates (k >7 s^{-1}) and was approximately the same order of magnitude as the rates from G40 MUT (e.g. $U6^{C}$=0.132 ± 0.024 s^{-1}). The differences in the folding rates could be explained with the help of static NMR experiments. The mutant G27 MUT ribozyme that differs from the most active ribozyme by a single nucleotide reveals an additional energetically favorable conformation fold A in the free state that is slightly more stable than the folding competent fold B resembling the wildtype free fold. Also after addition of Ca^{2+}, not only a single conformation is observed, but a heterogeneous ensemble of conformations of at least three different states is adopted: namely $A^{like}\cdot Ca^{2+}$, $B^{like}\cdot Ca^{2+}$ and $C^{like}\cdot Ca^{2+}$.

The NMR signals of this counterion-induced ensemble of conformations exhibit increased line widths due to the dynamic interconversion of those states. It would be interesting to determine the relative populations of the conformations defining the ensemble, this, however, could not be done due to large line widths. From the time-resolved NMR experiments, we can infer that the barriers of interconversion between the states is still high and therefore, we deduce structural information of the folds $A^{like}\cdot Ca^{2+}$ and $B^{like}\cdot Ca^{2+}$ from the characterization in the absence of Ca^{2+}. Since fold A is stabilized by a different pattern of basepairs, the energetic barrier for conversion of this second fold into the catalytically active fold is high, since several basepairs need to be broken and formed; this leads to a decrease of the overall folding rate in the G27 MUT system.

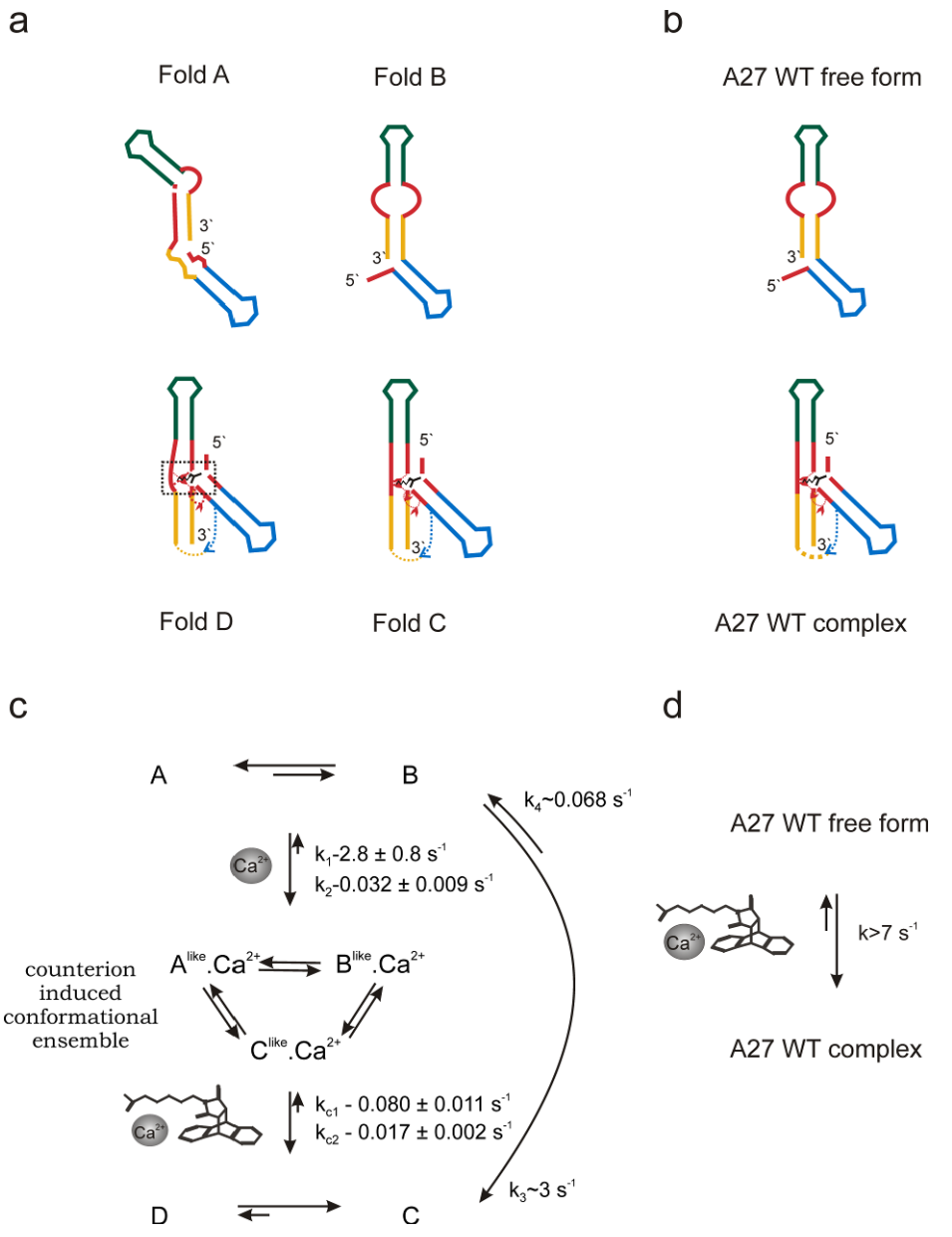

Figure 31: a) Cartoon representation of the folds as determined from static NMR experiments. A and B are the free form of the ribozyme and C and D the complex form, D being a minor conformation in the complex form with conformational differences centered around the catalytic core. Fold D is in slow exchange with fold C. b) Cartoon representation of the folds of A27 WT in free form and complex form. c) Folding model derived based on NMR experiments for G27 MUT ribozyme. The relative concentration of A and B are 3:1. On addition of cations and ligand, conformations A and B assume a counterion-induced ensemble of conformations, $A^{like}{\cdot}Ca^{2+}$, $B^{like}{\cdot}Ca^{2+}$ and $C^{like}{\cdot}Ca^{2+}$, which in turn fold into catalytically active fold C. k_1 and k_2 are rates of unfolding of $U6^{A+B}$, k_{c1} and k_{c2} are rates of folding of $U6^{C}$. k_3 and k_4 are derived from the sum of forward and reverse rates, which is obtained from the analysis of exchange induced NOE crosspeaks and K_{eq} obtained from the relation K_{eq}=Fold C/Fold B. d) Folding model of the A27 WT consistent with NMR data presented here and previously published FRET analysis.

The fundamental rate-limiting step here points to the rearrangement of secondary structures in a compact state rather than a folding mechanism involving tertiary structural rearrangements. Such behavior is not unprecedented, as both the isolated P5abc domain with a three-way junction from the *Tetrahymena* ribozyme (Wu and Tinoco Jr, 1998) and the hairpin ribozyme of the satellite RNA of tobacco ringspot virus (Rupert and Ferré-D'Amaré, 2001) showed local secondary structure rearrangement during Mg^{2+} induced folding.

In addition, the time-resolved experiments provide additional insight into the folding event. We observed biexponential kinetics without sigmoidal phase for the folding of the complex state, composed of a fast phase and a slow phase in line with the heterogeneous conformations observed for the free ribozyme. The rates for complex formation detected for the NMR signal of $U6^C$ are 0.08 ± 0.011 s^{-1} with 73% amplitude and a slow rate of 0.017 ± 0.002 s^{-1} with 27% amplitude. Despite the limited signal-to-noise in these experiments, the kinetic amplitudes of the two phases, however, are not identical to the 3:1 ratio of populations in the free state. If molecules adopting fold A were revealing slow folding kinetics, then the amplitudes of the slow phase should be 75%. To explain this, the following two additional aspects of the data were considered. From the time-resolved experiments, we had additional information on the unfolding rates (2.8 ± 0.8 s^{-1} (75%) and 0.032 ± 0.009 s^{-1} (25%)) of the two folds. The amplitudes are in agreement with the kinetic rates reporting on complex formation. From the rate obtained from the NOESY spectrum, the folding from fold B to the complex fold C proceeds at a time scale of ~3s^{-1}. Due to similarity of fold B to the fold of the free state of A27 WT, this conclusion is also strengthened by the results of A27 WT from both NMR as well as FRET studies. The signal-to-noise for NMR resonances reporting on unfolding is higher than for the peaks associated with folding. Therefore, we are not able to detect the fast folding phase in the time-resolved experiments but only in the NOESY exchange spectra.

Since there is no evidence of a sigmoidal phase in the kinetics, the data do not provide evidence for a folding intermediate but rather suggest a complex folding mechanism with different rate constants for different

conformations, once folding-competent conditions have been established after the addition of divalent cations. Therefore, we interpret the fast rate of 2.8 ± 0.8s^{-1} to arise from a divalent counterion-induced rapid collapse of both folds A and B of the ribozyme into at least three folds $A^{like}{\cdot}Ca^{2+}$, $B^{like}{\cdot}Ca^{2+}$ and $C^{like}{\cdot}Ca^{2+}$. Such counterion-induced collapse has been reported for other RNAs (Deras et al., 2000; Russell et al., 2000; Russell et al., 2002). In fact, rapid counterion-induced collapse in RNA folding is reported to induce an ensemble of heterogeneous compact conformations before the tertiary structure formation is stabilized. In such compact states, RNAs displaying interactions similar to the native final fold show faster folding kinetics while unfavorably folded compact conformations fold slower, as is also observed in this system from the folding rates of 0.08 ± 0.011 s^{-1} and 0.017 ± 0.002 s^{-1} for fold C. Therefore we cannot delineate the folding pathways of the two folds A and B into the native tertiary complex fold C given the current data resolution and in light of the existence of a collapsed state.

4.2. Folding Model for G40 MUT

Figure 32 shows the folding model derived based on static and time-resolved NMR experiments for the G40 MUT. Overall, the molecular resolution of the data for G40 MUT in both the static and time-resolved NMR experiments conducted was low when compared to that of G27 MUT, due to technical reasons. The time-resolved experiments showed biexponential kinetics with 90% population showing a fast phase and an additional slow phase. These rates were slower than A27 WT by about 2 orders of magnitude but approximately faster than G27 MUT. From the static NMR experiments, the titrations showed that addition of Ca^{2+} to the ribozyme in the absence of ligand exhibited an ensemble of conformations $A^{like}{\cdot}Ca^{2+}$, $B^{like}{\cdot}Ca^{2+}$ and $C^{like}{\cdot}Ca^{2+}$, which was also observed with G27 MUT. From time-resolved experiments, kinetic rates of the fading free form imino resonance peaks (for example, $U6^{A+B}$) could not be extracted as the rates were too fast and occurred in the dead time of the experiment. The presence of a chemical exchange crosspeak in the NOESY of the ribozyme in the presence of metal ions and ligand indicates folding at an additional fast phase that is not delineated in the time-resolved experiment.

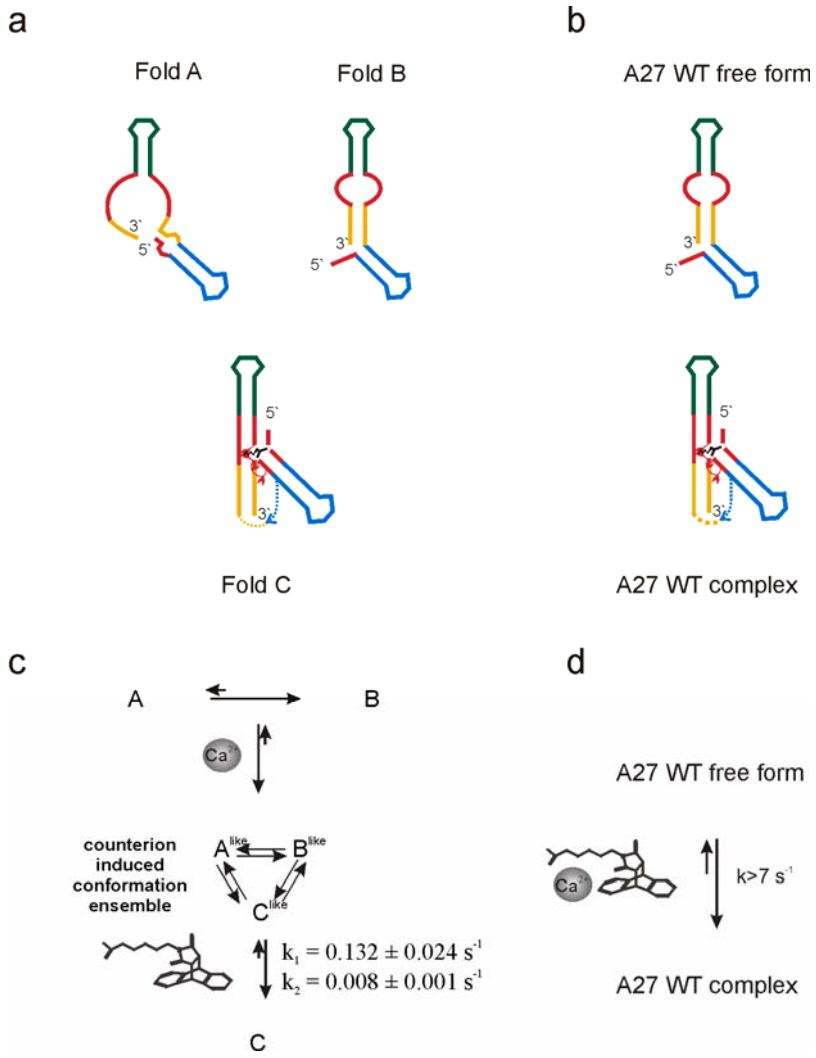

Figure 32: a) Cartoon representation of the folds as determined from static NMR experiments and mfold predictions. A and B are the free form of the G40 MUT ribozyme and C the complex form. b) Cartoon representation of the folds of A27 WT in free form and complex form. c) Folding model derived based on NMR experiments for G40 MUT ribozyme. The relative concentration of A and B are 1:4. On addition of cations and ligand, conformations A and B assume a counterion-induced ensemble of conformations, $A^{like}{\cdot}Ca^{2+}$, $B^{like}{\cdot}Ca^{2+}$ and $C^{like}{\cdot}Ca^{2+}$ which in turn fold into catalytically active fold C. d) Folding model of the A27 WT consistent with NMR data presented here and previously published FRET analysis.

Due to the low S/N of the NOESY spectrum as well as the conformational dynamics of the ensemble in the presence of Ca^{2+}, we could not determine whether the chemical exchange peak between the complex and free form arises from fold A or fold B. The rapid fading of free form resonance peaks in comparison to the slow building up of resonance peaks from the complex form instead of a sigmoidal build up points to the presence of a metal ion induced

collapsed state. This collapsed state is an ensemble of $A^{like}\cdot Ca^{2+}$, $B^{like}\cdot Ca^{2+}$ and $C^{like}\cdot Ca^{2+}$ folds. Once again, there is no evidence of an folding intermediate. The amplitude of the fast phase of the biexponential kinetic rates is approximately 90%. The ratio of the folds A and B at equilibrium in the absence of Ca^{2+} is 1:4, where fold B is the conformation of the wild type ribozyme. The proportion of the correctly folded wild type conformation, fold B (~80%) does not match with the proportion of molecules that fold with the fast rate (90%) extracted from the biexponential kinetic trace. This indicates change in the conformational ensemble dynamics attained on addition of Ca^{2+} leading to the subsequent display of faster folding kinetics by those conformations that have reached their native like folding state and slower kinetics for non-native like conformations. These results are similar to the G27 MUT results, except in the ratios of populations, which reflect the free form conformation stabilities of G40 MUT. G27 MUT also showed a fast and slow phase kinetics in the time-resolved experiments while A27 WT folding time was in the range of 100ms (Kobitski et al., 2007). For G27 MUT it is shown that the slow folding times in comparison to A27 WT are due to the presence of wrongly folded conformation in addition to the required correct conformation at equilibrium in the ratio ~3:1. For G40 MUT, at equilibrium, fold B which is the required correct secondary structure for complex structure formation is the major conformation. Therefore the influence of the fold A which may be incorrectly folded is minimal. This leads to kinetics that are overall faster than G27 MUT but slower than that of the A27 WT.

4.3. Summary

In summary, the present work considerably advances the application of time-resolved NMR spectroscopy to study biomolecular folding reactions, since for the first time RNA pseudoknot folding has been investigated by NMR spectroscopy. Based on these results, several factors appear to contribute to the 30% reduction of catalytic activity of the G27 MUT in comparison to the wildtype:

(i) In the G27 MUT ribozyme, the interaction between the Diels-Alder product and the RNA is weakened, and the ensemble displays conformational heterogeneity. We were able to identify at least one weakly populated

conformation (D in Figure 31a) which is found to be in slow exchange with major complex population. The difference between these two conformations arises from the difference in folding of the catalytic pocket and the yellow stem II regions.

(ii) The equilibrium between free and bound state of G27 MUT is shifted compared to wildtype and approximately 10% population of the free form can still be detected, leading to a decrease in activity.

(iii) The major complex (fold C in Figure 31a) is also in exchange with the minor conformation (fold B) of free form, which can be directly detected in the NOESY spectrum. Taken together with the lack of stacking interactions between the green stem III and the basepairs formed between nucleotides from the asymmetric internal bulge, these findings suggest that the core of the ribozyme is in a dynamic state in solution, a common feature of some ribozymes. For example, this model has been proposed in the case of the hammerhead ribozyme (Blount and Uhlenbeck, 2005a) based on ^{1}H- and ^{31}P-NMR (Suzumura et al., 2000), ^{19}F-NMR (Hammann et al., 2001) and residual dipolar coupling measurements (Bondensgaard et al., 2002). Further, the observed differences between the Ca^{2+}- and Mg^{2+}-bound complexes reveal conformational dynamics in the catalytic pocket as an important factor for efficient catalysis.

The reduction in catalytic activity of the G40 MUT by 75% in comparison to the WT is less clear from this study. The observed folding rates of G40 MUT are faster than the rates observed in G27 MUT. This could satisfactorily be explained from the conformations of the ribozymes in the free form state. Static NMR characterization of the tertiary complex conformation of G40 MUT exhibited all the base pair interactions that are observed for A27 WT and G27 MUT. One significant difference observed is the conformational dynamics of the catalytic pocket region. The unpaired nucleotide, G24, that forms one wall of the catalytic pocket showed a higher degree of conformational dynamics compared to the G27 MUT ribozyme indicating internal motions.

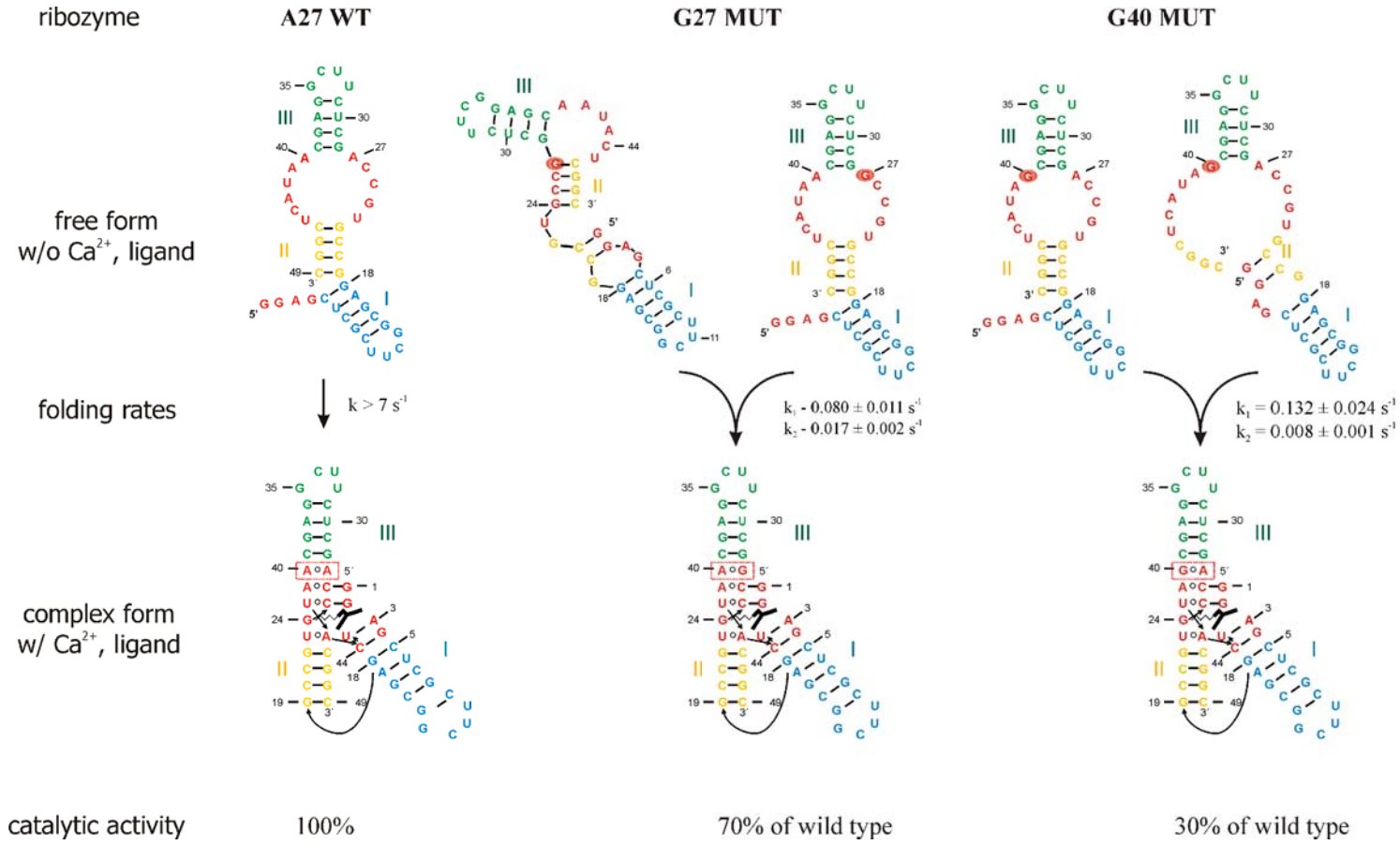
ribozyme
A27 WT
G27 MUT
G40 MUT
free form
w/o Ca2+, ligand
folding rates
k > 7 s-1
k1 - 0.080 ± 0.011 s-1
k2 - 0.017 ± 0.002 s-1
k1 = 0.132 ± 0.024 s-1
k2 = 0.008 ± 0.001 s-1
complex form
w/ Ca2+, ligand
catalytic activity
100%
70% of wild type
30% of wild type

Figure 33: A schematic representation of all three Diels-Alder ribozyme systems investigated in this thesis with their results are shown. The mfold predicted free forms in the absence of Ca2+ and ligand and validated by static NMR experiments are depicted. Also shown are the A27 WT and G27 MUT complex forms in the presence of Mg2+ and ligand as determined by x-ray crystallography and validated by static NMR. The predicted complex form of G40 MUT by NMR investigation is given in the third system. The kinetic rates of folding derived from time-resolved NMR experiments (G27 MUT and G40 MUT) and FRET (A27 WT) are shown.

The resonance crosspeak from the G24 in the ^{1}H, ^{15}N HSQC experiment could only be observed at low temperatures, lower than 278K. Therefore, to fully understand the catalytic behavior of G40 MUT additional experiments showing ligand interactions with the catalytic pocket are required. Possible future work includes molecular dynamics (MD) simulations for understanding the catalytic core of the ribozyme. MD simulations have proven useful in analyzing those dynamics that are not captured by biophysical structural studies. They have been used for example to study the catalytic behavior of the hairpin ribozyme (Ditzler et al., 2009) and the hepatitis delta virus ribozyme (Liu et al., 2007).

The detailed NMR analysis detects a number of differences in the structure and conformational dynamics of the single nucleotide mutants of the most efficient Diels-Alder-ribozyme. The effect of this single point mutation is dramatic as several conformations in the free and the complex state are populated as the result of a single point mutation. The energetic difference in free enthalpy is small, but the barrier of interconversion is high and therefore prolongs the lifetime of the two free states and of the bound states of the ribozyme, respectively. Therefore, the slow refolding kinetics of RNAs, (Fürtig et al., 2007) compared to the situation for proteins, amplify a small destabilizing effect in the ground state energies of the ribozymes.

These differences suggest that during the *in vitro* SELEX procedure, evolution of RNA sequences that rapidly fold into the catalytically active conformation constitutes an important evolutionary restraint to gain high turn-over for the best ribozymes. Even single point mutations lead to very significant differences in folding rates spanning three orders of magnitude; these differences are linked to structural differences in the free form of both

ribozymes, where the free form of the slower folding mutant ribozymes populate two detectable conformations with high barriers for conformational transition. It is tempting to suggest that optimal fit and fast folding kinetics are evolutionary restraints selected for in the SELEX experiments.

Current work in RNA therapeutics is a multi pronged approach that includes such areas as RNA interference, antisense RNA, ribozymes and aptamers. The various selection and engineering procedures *in vitro* selection and evolution in combination with rational designing fuel this effort. Functionality of these interesting molecules is as dependent on folding dynamics as on their equilibrium conformational states. Here, we have conducted time-resolved NMR experiments on selected members of the Diels-Alder ribozyme family in addition to the characterization of the ligand bound and free states. Combination of structure and kinetics results allows interpretation of the relationship between the primary sequences, the folding kinetics and functionality. Even single nucleotide mutations are observed to be detrimental to the functionality. This raises the possibility of designing of RNA that include the advantages of high throughput combinatorial techniques and high molecular resolution structure and kinetics detection techniques for better engineering of molecules.

CHAPTER V

5. Material and Methods

5.1. RNA Preparation Overview

^{15}N, ^{13}C-labelled and unlabelled G27 MUT were prepared by *in vitro* transcription with T7 RNA polymerase from linearized plasmid DNA templates. DNA templates were prepared and purified following literature procedures. (Varani et al., 1996). The crude run-off transcript was purified by an anion-exchange column step for removal of abortive products and unused nucleotides, (Stoldt et al., 1999) followed by 'ion-pair'-reversed phase HPLC (Pingoud et al., 1987). The obtained RNA was freeze-dried and desalted using Centricon-10 micro-concentrators (Amicon). Folding of the RNA was achieved by denaturing at 95°C followed by 10-fold dilution and cooling on ice cold water for an hour and verified by native gel electrophoresis. Finally, the folded RNA was exchanged into the NMR buffer containing 25 mM Tris-HCl buffer at pH 7.5 using Centricon-10 micro-concentrators. The chemically synthesized unlabelled A27 WT was purchased from Chemical Synthesis Service (Craigavon, UK). The *in vitro* transcription yield was 12% for G27 MUT and 15% for G40 MUT calculated as a percentage of all nucleotides.

5.1.1. General Protocol for preparation of G27 MUT and G40 MUT

Primers and templates for preparation of double stranded DNA template were purchased from MWG-Biotech (Ebersberg) and are given in Table 3. The double stranded DNA which includes the T7 promoter segment was subsequently prepared by the PCR (Polymerase Chain Reaction) using *Pfx* Polymerase. The preparation and protocol are given in Scheme 1.

Table 3: Primers used for preparation of ds DNA template for G27 MUT in vitro transcription.

Forward Primer	5' - GAG AAT TCT AAT ACG ACT CAC TAT A GG AG -3'
Reverse Primer	5´- TCCATATGG GCG CCG AGT ATT GCT CCG AAG - 3´
Template	5' -G ACT CAC TAT AGG AGC TCG CTT CGG CGA GGC CGT GCC AGC TCT TCG GAG CAA TAC TC – 3'

Scheme 1: Protocol used for preparation of ds DNA using Polymerase Chain Reaction

41 µl H2O
5 µl 10 X Pfx Buffer
1 µl Reverse Primer
1 µl Template (Diluted 1/500)
1 µl Forward Primer
0.4 µl Pfx Polymerase

– 94°C – 2 mins
– 94°C – 1 min DENATURE
– 55°C –1 min ANNEAL
– 68°C – 2 min ELONGATE
Loop 25 times
– 68°C – 1 min
– 4°C – End

5' - GAG AAT TCT AAT ACG ACT CAC TAT AGG AGC TCG CTT CGG CGA GGC CGT GCC GGC TCT TCG GAG CAA TAC TCG GCG CCC ATA TGG A – 3'

Eco R1 T7 Promoter Coding Region Sfo 1 NdeI

5' - GAG AAT TCT AAT ACG ACT CAC TAT AGG AGC TCG CTT CGG CGA GGC CGT GCC AGC TCT TCG GAG CGA TAC TCG GCG CCCATATGGA – 3'

Eco RI T7 Promoter Coding Region Sfo 1 NdeI

Figure 34: ds DNA template for G27 MUT and G40 MUT containing the recognition sites needed for ligation into the vector and the promoter recognition site for the T7 polymerase.

The PCR products were agarose gel (Scheme 2) extracted. The gel extraction kit from Qiagen was used according to the manufacturer's instructions for PCR product. The double stranded DNA was then digested with enzymes Eco RI and NdeI (ordered from New England Biolabs) to create 'sticky' ends for cloning. The digested PCR fragment was cloned into PUC19 vector using the ligation and transformation procedures given in Scheme 3.

Scheme 2: Preparation and setup of 2% Agarose Gel

Preparation

- Agarose 1gm
- 1xTAE Buffer 50ml

Running conditions

- Buffer- 1xTAE
- Power – 130V

Scheme 3: Protocol followed for cloning of dsDNA

Ligation

- 0.25µl puc19-Digested
- 1µl Digested PCR fragment
- 8.8µl H_2O
- 10µl Quick Ligase buffer
- 1µl Ligase

5 mins @ Room temperature

Transformation

- 1µl Ligation mixture
- 9µl H_2O

On ice 5 mins

- Add 50 µl DH5α Cells to above

On ice for 30 mins.

Heat Shock @ 42°C for 45 seconds

On ice for 2 mins

- Add SOC Medium 125µl

Incubate @ 37°C for 1 hour

50µl applied to LB medium plates containing Ampicillin and incubated @ 37°C overnight.

The next step is to confirm the sequence of the clone. For sequencing an initial 'mini' preparation of DNA was performed. A colony from the LB medium plates was transferred to 5ml LB medium containing 0.1mg/ml Ampicillin and incubated for 12-16 hrs at 37°C, agitating at 320 rpm. Next, the cells were centrifuged at 5000G for 5 mins and the pellet collected. Qiagen mini prep purification kit was used to obtain the plasmid from the cell pellets. The DNA plasmid was then sequenced using the universal M13 forward and reverse primer (SRD, Oberursel). On obtaining positive sequence, the DNA template required for *in vitro* transcription was prepared from larger volumes of LB medium (usually 2 Litres) with all other steps remaining the same as in the 'mini' preparation. Qiagen Mega Prep purification kit was used to obtain DNA pellet. The average yield was 5 mg. For in vitro transcription the DNA was prepared as shown in Scheme 4

Scheme 4: Plasmid DNA linearization and purification

Plasmid DNA digestion with SfoI	***Chloroform/Phenol Purification***
• DNA 2ml (2.5 mg/ml) • SfoI 160µl • Neb2 buffer 1 ml • H_2O 7 ml • @ 37°C ON	• Add 0.5 volume of CHCl3/Phenol, mix well and centrifuge @ 8000G 2 mins (phase separation). • Solution divides into lower viscous phase (denatured protein) and upper watery phase. Remove the watery half and use for the next steps. • Repeat Step 1 and 2 twice. • Add 1 volume of CHCl3, mix well (vortex slightly) and centrifuge @ 8000 G for 2 mins. • Remove upper watery phase and repeat Step 4 two more times. • Add 1 Vol of Isopropanol • Precipitate DNA at -20°C for two hours. • Centrifuge at 8000 G for 30 mins. Discard supernatant and air dry pellet. • Dissolve the pellet in H^2O (~2ml)

To avoid RNAse contamination, disposable plastic ware and RNAse-free water was used. Analytical *in vitro* transcription was performed to optimize Mg^{2+}, DNA and NTP-mix to obtain the best yield of RNA. A sample Mg^{2+} optimization step of in vitro transcription is shown in Scheme 5. The yield was verified with a denaturant Polyacrylamide (PAA) gel and quantified by HPLC. A sample transcription result on a 15% PAA gel is shown in Figure 35b. The yield was 12%, calculated as a percentage of total nucleotides.

Scheme 5: Analytical in vitro transcription

Content	**Stock**	**Vol. added**	**Final**
Spermidin	200 mM	0.5 µl	4 mM
DTT	1 M	1 µl	10 mM
5X-X-Script*		20 µl	1X
NTP mix**	100 mM each	5 µl	~2.5 mM
MgCl2	300 mM	-	5-30 mM
DNA		1 µl	2.5 µg
T7 poly	30mg/ml	0.1 µl	
H2O		16.9 µl	50 µl

*5X-x-Script Buffer - 500mM Tris-glutamic acid, pH 8.1

** NTP-mix composition according to RNA composition

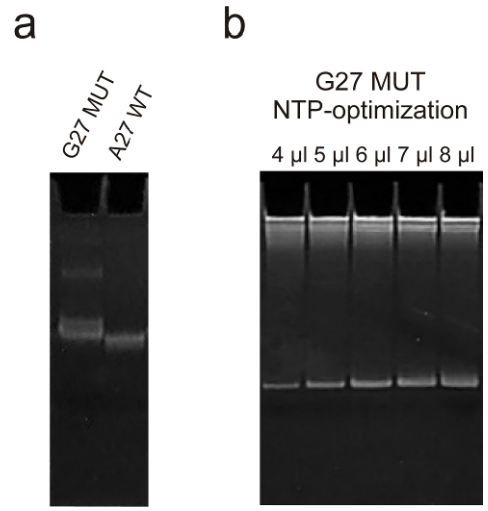

Figure 35: Native gel electrophoresis (Scheme 6): RNA was loaded in a buffer containing 50 mM Tris–acetate, 100 mM sodium acetate (pH 8.0) (running buffer). Electrophoresis was performed in 15% acrylamide:bisacrylamide gels in running buffer at room temperature at less than 1 W for 5 h. The gel was stained with ethidium bromide. G27 MUT exhibits dimer formation and also a double band at the expected monomer position indicating two folded populations. b) 15 % PAA-Gel electrophoresis (Scheme 6) of an in vitro transcription reaction of G27 MUT in 7M Urea. The 5 lanes represent the reaction at different concentration of NTPs

Scheme 6: Denaturant PAA Gel and Polyacrylamide Native gel preparation

Stock Solution (Denaturant)

- 4.2 gms Urea
- 5 ml Acrylamide (Stock 30%)
- 1 ml 10x TBE *
- H_20 – to make up 10ml

To be added just before use

- 100µl AMPS
- 10µl Temed

Loading buffer composition-

- 99% Formamid
- 0.1% Bromophenolblau
- 0.1% Xylencyanol FF

Running Buffer – 1 X TBE

Running Conditions – 35mA

Stock Solution Preparation (Native)

- 5 ml Acrylamide (30%)
- 1 ml 10X TAE **
- 4 ml H_20

Before running gel

- 100µl AMPS
- 10 µl Temed

Loading buffer composition-

- 99% Glycerin
- 0.1% Bromophenolblau
- 0.1% Xylencyanol FF

Running Buffer – 1 X TAE

Running Conditions - < 3watts usually

50mA and 50V.

** TBE – 134 mM Tris, 45 mM Boric Acid, 2.5 mM EDTA*

*** TAE - 50 mM Tris–acetate, 100 mM sodium acetate –pH 8.0*

Preparative *in vitro* transcription: Using the optimized analytical transcriptions, the preparative transcription was performed as shown in Scheme 1. All ingredients were added together except T7 polymerase and DTT in a 50ml Falcon tube. It was then placed

Scheme 7: Preparative in vitro transcription of unlabelled G27 MUT

Content	Stock	Vol. added	FinalC
Spermidin	200 mM	0.25 ml	4 mM
DTT	1 M	0.5 ml	10 mM
5X-X-Script		10 ml	1X
NTP mix	100 mM each	4 ml	
MgCl2	300 mM	0.835 ml	10 mM
DNA		1 ml	2.5 mg
T7 poly	30mg/ml	0.05 ml	
H2O		8.4 ml	25 ml

in a water bath at 37°C for 20 min on a magnetic stir plate. Next T7 polymerase and DTT are added to the mix and transcription was allowed to proceed for ~5 hours. Centrifuge for 20 min @9000g in case of visible precipitate in transcription solution. The crude run-off supernatant was purified by an anion-exchange column step (Scheme 8) for removal of abortive products and unused nucleotides (Stoldt et al., 1999), before 'ion-pair'-reversed phase HPLC (Pingoud et al., 1987) (Scheme 9). The obtained RNA was freeze-dried and desalted using Centricon-10 microconcentrators (Amicon) as given in Scheme 10. Folding was done by denaturing at 95°C followed by 10-fold dilution and cooling on ice cold water for an hour and verified by native gel electrophoresis (Figure 35a) Scheme 11. Finally, the folded RNA was exchanged into the NMR buffer containing 25mM Tris-HCl buffer at pH 7.5 using Centricon-10 microconcentratiors. The *in vitro* transcription yield calculated as the percentage of total nucleotides was 12%.

Scheme 8: First purification step of crude run-off transcription.

- **to remove polymerase, abortive products etc.:**
  - glass column, ø 2.5 cm, ~50ml volume
  - DEAE sepharose FF (Amersham)

- 0.1% DEPC in water
- 3M NaOAc, pH 5.5, and appropriate dilutions (see below)

- **Method:**
  - pour a 10 – 15 mL DEAE Sepharose in column
  - wash with 100ml water
  - wash with 0.1% DEPC in water and let sit over night
  - wash with hot (>60 °C) water to destroy residual DEPC
  - equilibrate with 10 volumes of 0.1M NaOAc, pH 5.5
  - load combined supernatant from transcription reaction
  - collect flow through.
  - develop column with
    - 5 volumes of 0.6M
    - 5 volumes of 1M,
    - 6 volumes of 2M
    - 2 volumes of 3M NaOAc, pH 5.5
- collect 10 mL fractions and monitor UV absorbance @ 260 nm
  - RNA containing fractions determined from denaturing PAA gels (here, 1M and 2M)
  - precipitated RNA over night at -20°C using 20x volume of ethanol
  - if no salt has precipitated (if yes, add more ethanol and precipitate RNA again), spin down RNA @ 8000g (or more) for 30 min @ 4 °C
  - supernatant removed and pellet air dried.
  - dissolve RNA to approx. 150 OD260/mL in water

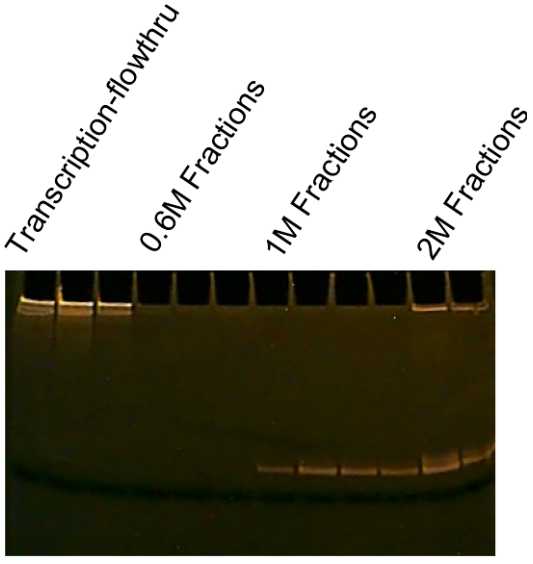

15% Denaturant PAA Gel

Scheme 9: RP-HPLC Purification

Column:	1cm x 25cm C18 column (Vydac 218TP510)
Buffer A:	50 mM K-phosphate, pH 5.9 2mM tetra-butyl-ammonium-hydrogen sulfate
Buffer B:	as above plus 60% (v/v) acetonitrile
Temperature:	60 °C
Flowrate:	5mL/min

Scheme 10:Desalting of HPLC purified RNA.

- Lyophylization (takes ~2 days)
- Dissolve the freeze dried RNA in H_2O
- Desalt using YM10 Centriprep, followed by YM10 Centricon for concentrating the RNA (~0,5ml)
- Precipitate RNA with 5 volumes of 2% (w/v) $LiClO_4$ in acetone @ -20 °C over-night.

Scheme 11: RNA folding

- Collect precipitated RNA from previous step by centrifugation for 30 min @ 8000 – 10.000g @ 4 °C
- Wash RNA pellet with 2x ice cold 70% ethanol
- Centriguge for 10 min @8000 – 10.000g @ 4 °C
- Dissolve RNA in water or 25mM Tris-HCl Buffer at pH 7.5

RNA Folding in NMR Buffer/water

RNA diluted 10 fold

Heat RNA to 95 °C for 5 min

Let sit RNA on ice for 60 mins

Concentrate RNA using YM10 CENTRICON up to desired concentration

5.2. Data Acquisition

5.2.1. NMR data acquisition for static NMR experiments

NMR measurements were performed on Bruker 600, 700, 800, and 900 MHz spectrometers with 5 mm HCN cryogenic probes and z-axis gradients. Bruker Topspin and Accelyrs Felix2004 software programs were used for data processing and analysis. All NMR samples contained 10% D_2O and were measured at a temperature of 288 K, except when otherwise stated. The final RNA concentrations ranged between 0.2 mM and 0.9 mM as determined by UV spectroscopy at 260 nm. For the bound state, we used AMDA (anthracene-maleimidocaproic acid Diels-Alder adduct) as a Diels-Alder product (Stuhlmann and Jaschke, 2002). The compound was dissolved in DMSO for better solubility prior to complex formation. Therefore, all RNA samples contained DMSO at a concentration of approximately 1%. The $^{1}H,^{1}H$-NOESY (Stonehouse et al., 1994) spectra of the A27 WT was measured with a mixing time of 80 ms at a temperature of 283 K, while a mixing time of 150 ms was used for $^{1}H,^{1}H$-NOESY spectra of the G27 MUT and 100ms for G40 MUT, the temperature was set to 288 K. The $^{1}H,^{15}N$ HSQC (Furtig et al., 2003; Wijmenga and van Buuren, 1998) and HNN-COSY experiment measured for G27 MUT to infer the base-pairing pattern of the RNA and to characterize the hydrogen bonding pattern within base-pairs were performed as given in (Dingley and Grzesiek, 1998) and (Noeske, 2005). The software packages XWINNMR, Topspin and Sparky were used for processing and analyzing experimental data.

5.2.2. Laser induced time-resolved NMR data acquisition

All time-resolved NMR experiments were performed on an 800 MHz spectrometer equipped with 5 mm HCN cryogenic probe and z-axis gradients. The time-resolved experiments were pseudo 3D experiments consisting of 2 planes of 256 1D-spectra each, measured at 288 K (Furtig et al., 2007). Restricted volume NMR Shigemi tubes of a diameter of 3 mm and 5 mm with sample volumes of 65 µl and 150 µl, respectively, were used for the measurements. The laser set-up (Kuhn and Schwalbe, 2000) used pulses of

monochromatic light (350 nm, 5W) from a CW argon ion laser (Spectra Physics) with durations of 1.5 - 2 s introduced by a glass-fiber and a pencil tip into the NMR-tube located in the spectrometer. 1D-imino proton spectra were recorded with a jump-return echo pulse sequence (Sklenar and Bax, 1987). In the kinetic experiments, each 1D spectrum was measured from 8 scans using Ernst angle excitation. (Ernst et al., 1990). The jump-return echo sequence provide imino-proton-selective excitation due to its excitation profile. The optimal parameters for pulse flip angle and relaxation delay were determined for every run of the system. The first 256 scans were recorded and served as a blank experiment, followed by irradiation with a single laser pulse of duration of 1.5 s and the recording of another 256 scans. Each 1D experiment, consisting of eight scans, was recorded at an interval of 1.76 seconds. The resulting pseudo 3D data-set was subjected to Fourier-Transform with 2K data-points in the direct dimension after multiplication with a squared cosines window function. The resulting 1D-spectra were submitted to phasing, polynomial base-line correction and peak-integration of the imino-proton signals in the chemical shift range 9–15 ppm. For the kinetic analysis, the baseline corrected and normalized peak intensities were plotted as a function of time. Residual baseline was determined by averaging the intensity values of the first 256 pre-laser scans, (recorded before laser pulsing) at the position of the selected signal and subtracting this from the scans recorded after irradiation. Normalized imino proton signal intensities were plotted as a function of time. The data curves were fit to the rate law of a reversible, uni-molecular reaction and half-times were obtained using a pseudo first order equation approximation from the formula $t_{1/2} = \ln(2)/k$. Kinetic plots and pseudo first order reaction fittings were plotted using SigmaPlot 10. FELIX (Accelrys) software was used for processing and analyzing the kinetic data.

5.2.3. Rapid sample-mixing induced time-resolved NMR

The rapid sample-mixing time-resolved NMR experiments were set-up as described in (Mok et al., 2003). A 50 µL volume of 50 mM Ca^{2+} in NMR buffer (pH 7.5), was injected into 330 µL of NMR buffer containing 0.43 mM RNA and 1 mM AMDA in 10% D_2O. The final concentrations were between 0.37 mM for RNA, 0.7 mM for AMDA and 8 mM for Ca^{2+}. The NMR

experiments consisted of a pseudo 3D experiment of 2 planes with 128 1D spectra each. A single injection of 50ms duration followed the recording of the first plane and the second plane thus monitored Ca^{2+} induced folding with a time resolution of 2.2 s. The pseudo 3D data-set was Fourier-transformed with 4K data-points in the direct dimension after multiplication with a squared cosines window function. The resulting 1D-spectra were submitted to phasing, polynomial base-line correction and peak-integration of the imino-proton signals in the chemical shift range 9–15 ppm. For the kinetic analysis, the baseline corrected and normalized peak intensities were plotted as a function of time. Residual baseline was determined by averaging the intensity values of the first 256 pre-laser scans, (recorded before laser pulsing) at the position of the selected signal and subtracting this from the scans recorded after irradiation. In addition, corrections for baseline distortions caused by fluid turbulence after injection were performed. The baseline was determined by averaging the area under the curve in a position where no peaks were observed and subtracting this from both rising and fading peaks. Normalized imino proton signal intensities were plotted as a function of time. The data curves were fit to the rate law of a reversible, unimolecular reaction and half-times were obtained using a pseudo first order equation approximation from the formula $t_{1/2} = \ln(2)/k$. Kinetic plots and pseudo first order reaction fittings were plotted using SigmaPlot 10. FELIX (Accelrys) software was used for processing and analyzing the kinetic data.

Table 4: Parameters of NMR Experiments

SN	Expt.	Mole.	Field MHz	Indirect Dimension			Direct Dimension			NS	D1 s	τ_M ms	Acq. Time	Temp K	Conc. mM
				SW ppm	t1	Carrier ppm	SW ppm	t2	Carrier ppm						
1	*$^{1}H,^{15}N$ HSQC*	*A27 WT*	*800*	*30*	*256*	*152.5*	*24*	*2048*	*4.7*	*512*	*1*	*-*	*41h*	*283*	*RNA-0.9*
2	*$^{1}H,^{15}N$ HSQC*	*G27 MUT*	*800*	*30*	*128*	*152.5*	*24*	*2048*	*4.7*	*32*	*1*	*-*	*1h 16m*	*283*	*RNA-0.7*
3	*$^{1}H,^{1}H$ NOESY*	*A27 WT*	*800*	*24*	*700*	*4.698*	*24*	*4096*	*4.698*	*144*	*1.5*	*80*	*47h*	*283*	*RNA-0.9*
4	*$^{1}H,^{1}H$ NOESY*	*G27 MUT*	*800*	*14.5*	*1024*	*4.699*	*21*	*4096*	*4.699*	*64*	*2.2*	*150*	*45h*	*288*	*RNA-0.6*
5	*HNN-COSY*	*G27 MUT*	*700*	*100*	*192*	*185*	*23.9*	*2048*	*4.698*	*384*	*1*	*-*	*23h 41m*	*283*	*RNA-0.7*
6	*$^{1}H,^{13}C$ HSQC*	*G27 MUT*	*600*	*28*	*256*	*143*	*16*	*2048*	*4.689*	*32*	*1.5*	*-*	*49m*	*288*	*RNA-0.4*
7	*$^{1}H,^{1}H$ NOESY*	*G40 MUT*	*800*	*12.5*	*1024*	*4.701*	*20*	*4096*	*4.701*	*64*	*2.0*	*150*	*48h*	*288*	*RNA-0.3*
8	*$^{1}H,^{15}N$ HSQC*	*G40 MUT*	*600*	*30*	*256*	*152*	*24*	*2048*	*4.698*	*8*	*1.5*	*-*	*55m*	*283*	*RNA-0.3*
9	*$^{1}H,^{1}H$ NOESY*	*A27 WT*	*900*	*22*	*1024*	*4.7*	*12*	*4096*	*4.7*	*128*	*1.5*	*150*	*60h*	*283*	*RNA-0.4, Mg^{2+}-5, Ligand- 0.6*
10	*$^{1}H,^{1}H$ NOESY*	*G27 MUT*	*800*	*24*	*800*	*4.701*	*24*	*4096*	*4.701*	*104*	*1.5*	*150*	*41h*	*293*	*RNA-0.4, Ca^{2+}-4, Ligand-2.*
11	*$^{1}H,^{15}N$ HSQC*	*G27 MUT*	*600*	*20*	*224*	*154*	*20*	*2048*	*4.695*	*192*	*1.3*	*-*	*17h*	*293*	*RNA-0.4, Ca^{2+}-4, Ligand-2.*
12	*HNN-COSY*	*G27 MUT*	*600*	*95*	*264*	*187.5*	*22*	*2048*	*4.695*	*256*	*1*	*-*	*22h*	*283*	*RNA-0.4, Ca^{2+}-4, Ligand-2.0*
13	*$^{1}H,^{15}N$ HSQC*	*G27 MUT*	*700*	*29*	*128*	*152*	*24*	*2048*	*4.7*	*32*	*1.5*	*-*	*1h 51m*	*283*	*RNA-0.22, Ca^{2+}-4., Ligand-0.4*

SN	Expt.	Mole.	Field MHz	Indirect Dimension			Direct Dimension			NS	D1 s	τ_M ms	Acq. Time	Temp K	Conc. mM
				SW ppm	t1	Carrier ppm	SW ppm	t2	Carrier ppm						
14	*$^{1}H,^{15}N$ HSQC*	*G27 MUT*	*700*	*29*	*128*	*152*	*24*	*2048*	*4.7*	*32*	*1.5*	*-*	*1h 51m*	*283*	*RNA-0.22, Ca^{2+}-4.0, Ligand-0.4, Mn^{2+}-5 μM*
15	*$^{1}H,^{15}N$ HSQC*	*G27 MUT*	*700*	*29*	*128*	*152*	*24*	*2048*	*4.7*	*32*	*1.5*	*-*	*1h 51m*	*283*	*RNA-0.2, Ca^{2+}-4.0,Ligand-0.4, Mn^{2+}-10 μM*
16	*$^{1}H,^{15}N$ HSQC*	*G27 MUT*	*800*	*29*	*128*	*152*	*22*	*2048*	*4.7*	*32*	*1*	*-*	*1h 17m*	*283*	*RNA-0.2, Mg^{2+}-8, Ligand-0.6*
17	*$^{1}H,^{15}N$ HSQC*	*G27 MUT*	*800*	*29*	*128*	*152*	*22*	*2048*	*4.7*	*32*	*1*	*-*	*1h 17m*	*283*	*RNA-0.2, Mg^{2+}-8.0, Ligand-0.6, Mn^{2+}-4 μM*
18	*$^{1}H,^{15}N$ HSQC*	*G27 MUT*	*800*	*29*	*128*	*152*	*22*	*2048*	*4.7*	*32*	*1*	*-*	*1h 17m*	*283*	*RNA-0.2, Mg^{2+}-8.0, Ligand-0.6, Mn^{2+}-10 μM*
19	*$^{1}H,^{13}C$ HSQC*	*G27 MUT*	*900*	*30*	*256*	*141*	*11.9*	*2048*	*4.702*	*8*	*1.29*	*-*	*49m*	*283*	*RNA-0.4, Ca^{2+}-4, Ligand-2.0*
20	*$^{1}H,^{13}C$ HSQC*	*G27 MUT*	*400*	*41*	*256*	*141*	*16*	*2048*	*4.735*	*128*	*1.54*	*-*	*12h 10m*	*288*	*RNA-0.2, Mg^{2+}-6, Ligand-0.6,*
21	*$^{1}H,^{1}H$ NOESY*	*G40 MUT*	*800*	*24*	*930*	*4.70*	*8.25*	*4096*	*4.700*	*64*	*2*	*100*	*44h*	*283*	*RNA-0.18, Ca^{2+}-6, Ligand-0.8.*
22	*$^{1}H,^{15}N$ HSQC*	*G40 MUT*	*700*	*28*	*256*	*153*	*24*	*2048*	*4.7*	*32*	*1.2*	*-*	*3h*	*283*	*RNA-0.2, Ca^{2+}-8.0, Ligand-0.6*
23	*$^{1}H,^{15}N$ HSQC*	*G40 MUT*	*800*	*29*	*128*	*153*	*22*	*2048*	*4.75*	*16*	*1*	*-*	*48m*	*283*	*RNA-0.2, Mg^{2+}-10, Ligand-0.9*
24	*$^{1}H,^{15}N$ HSQC*	*G40 MUT*	*800*	*29*	*128*	*153*	*22*	*2048*	*4.75*	*16*	*1*	*-*	*38m*	*283*	*RNA-0.22, Mg^{2+}-8, Ligand-0.6*
25	*$^{1}H,^{15}N$ HSQC*	*G40 MUT*	*800*	*29*	*128*	*153*	*22*	*2048*	*4.75*	*16*	*1*	*-*	*38m*	*283*	*RNA-0.22, Mg^{2+}-8.0, Ligand-0.6, Mn^{2+}-4 μM*

SN	Expt.	Mole.	Field MHz	Indirect Dimension			Direct Dimension			NS	D1 s	τ_M ms	Acq. Time	Temp K	Conc. mM
				SW ppm	t1	Carrier ppm	SW ppm	t2	Carrier ppm						
26	*$^{1}H,^{15}N$ HSQC*	*G40 MUT*	*800*	*29*	*128*	*153*	*22*	*2048*	*4.75*	*16*	*1*	*-*	*38m*	*283*	*RNA-0.22, Mg^{2+}-8.0, Ligand-0.6, Mn^{2+}-10 µM*

Zusammenfassung

Trotz der bekannten Bedeutung der Ribonukleinsäuren (RNA) in der Zellbiologie ist es erstaunlich, dass neue grundlegende Funktionen von RNAs erst vor kurzem entdeckt wurden. Einer der Hauptgründe für die vielen Funktionen der RNA ist ihre Eigenschaft, verschiedene Konformationen, auch Faltungen genannt, anzunehmen. Die Sequenz der RNA, ein lineares Polymer aus vier verschiedenen wiederholten Einheiten, kann sich falten in alternative Sekundär-Struktur-Motive, die unter Ausbildung weitreichender Wechselwirkungen komplexe tertiäre Strukturen einnehmen. Liganden wie Metallionen oder Metaboliten mit niederem Molekulargewicht, aber auch Proteine oder Peptide können an RNA binden und dadurch Veränderungen der tertiären Konformation induzieren.

In prokaryotischen Zellen partizipiert RNA an der Regulation der Genexpression in Form von Riboswitches. Riboswitches sind Bestandteile der nicht-translatierten Regionen der Boten-RNA (mRNA) und nehmen unterschiedliche Konformationen an, je nach Vorhandensein oder Fehlen von spezifischen Metaboliten. Wenn ein Metabolit oberhalb einer bestimmten Konzentration vorliegt, induziert die Bindung dieses Metaboliten eine Konformationsänderung im jeweiligen Riboswitch. Damit ändert sich die Genexpression.

RNA-Thermometer partizipieren in der Zelle am translationalen Mechanismus durch eine ähnliche Strategie. Die Ribosomenbindungsregion (Shine-Darlargno, SD-Sequenz) befindet sich in der 5'-nicht-translatierten Region und ist verantwortlich für den Start der Translation; im ersten Schritt bindet eine Untereinheit des Ribosoms an diese Region. Bei niedrigen Temperaturen wird die Bindung des Ribosoms an die SD-Sequenz durch die Bildung von Basenpaaren in der SD-Sequenz verhindert.

Daher ist die Charakterisierung der Kinetik und der Faltungswege der RNA wichtig zum Verstehen der Funktion der RNA und ein wichtiger Beitrag zum Verständnis der grundlegenden Funktionen der RNA in der Zelle. RNA-Konformationsänderungen treten über einen großen Bereich von Zeitskalen auf. Je nach der Zeitskala können verschiedene biophysikalischen Techniken verwendet werden, um Konformationsänderungen der RNA zu untersuchen. In biophysikalischen Studien stellt das Erreichen einer hohen strukturellen und zeitlichen Auflösung häufig

Probleme dar. Zum Beispiel liefert Einzel-Molekül FRET-Spektroskopie hohe zeitliche Auflösung im Millisekundenbereich bei hoher Empfindlichkeit, aber nicht atomare Auflösung. Jüngste Fortschritte im Bereich der Kernresonanzspektroskopie (engl. nuclear magnetic resonance, NMR) ermöglichen es, tertiäre Faltung von RNA mit atomarer Auflösung aufzulösen.

Diese Dissertation widmet sich der NMR-spektroskopischen Untersuchung der Faltung von RNA-Molekülen. Kinetische Experimente erfordern die rasche Induktion der Kinetik, gefolgt vom der Detektion des Reaktionsverlaufs. In dieser Arbeit wurden zwei unterschiedliche Techniken zur Faltungeinleitung angewendet, nämlich **Photocaging** und **rasche Vermischung**.

Die Methode des Photocaging ist gut etabliert und baut auf dem folgenden Prinzip auf: Eine photolabile Schutzgruppe wird in einem Molekül so eingeführt, dass eine spezifische Interaktion verhindert wird. Nach Bestrahlung des Moleküls mit Laser-Licht einer bestimmten Wellenlänge wird die Photoschutzgruppe abgespalten. Zusammen mit der Gruppe von Prof. S. Pitsch, ETH Lausanne, konnten wir photolabile RNA-Nukleotidderivate entwickeln und mittels zeitaufgelöster NMR-Spektroskopie untersuchen (ähnliche RNAs wurden in der Gruppe von Prof. A. Heckel entwickelt).

Schnelle und möglichst spurenlose Freisetzung der photolabilen Vorläufer-Verbindung mit einem Laserpuls induziert die Faltung der RNA und die Bildung des nativen Zustand der RNA wird durch NMR-Signale beobachtet, die charakteristisch für den nativen Zustand der RNA sind. Durch optische Kopplung eines Lasers an einen NMR-Magneten kann das oben beschriebene Verfahren in-situ erfolgen und die Kinetik durch NMR aufgezeichnet werden. Mehrere verschiedene Moleküle können mit einer photolabilen Schutzgruppe versehen werden: Die Photoschutzgruppe kann direkt an RNA kovalent gebunden werden. Solche photolabil modifizierten Nukleotide können an strategischen Positionen der Ziel-RNA eingeführt werden, deren Faltungseigenschaften untersucht werden sollen. Die Photoschutzgruppe kann auch an einem Liganden angebracht werden: Wenn die RNA-Faltung von Ligandbindung abhängig ist, kann diese Bindung durch die Photoschutzgruppe unterbunden werden.

In dieser Arbeit wird eine alternative Methode für das so genannte „Photocaging“ eingeführt. Metallionen, die für manche RNA einen wesentlichen Kofaktor für die Faltung darstellen, werden in der Form des photolabilen Metall-DM-Nitrophen (DMN)-Komplexes chelatisiert. Photolyse des DMN setzt diese Metallionen frei, wodurch RNA-Faltung initiiert wird.
In der Mischtechnik wird eine der Komponenten, die für die Faltung der RNA notwendig ist, schnell in ein NMR-Proberöhrchen durch Einsatz eines pneumatischen Injektions-Gerätes in situ injiziert.

Die Diels-Alder Ribozym-Familie wurde in der Gruppe von A. Jäschke, Univ. Heidelberg entwickelt und die Faltung mittels der oben genannten Techniken charakterisiert. Das Diels-Alder Ribozym ist eine *in-vitro* selektierte RNA, die die Cycloaddition eines Anthracen-Diens an das Dienophil Maleimid katalysiert. Aus verschiedenen Gründen ist die Untersuchung dieses Systems sehr interessant:

• Das Diels-Alder Ribozym ist ein nicht-natürlicher Katalysator, der durch *in-vitro*-Selektionsverfahren entwickelt wurde. Als Grundlage für seine katalytische Aktivität zeigt er eine interessante „pseudoknot“-Struktur auf, die häufig in natürlichen Ribozymen gefunden wird.

• Die tertiäre Faltung des Diels-Alder Ribozyms in die katalytisch aktive Form ist Mg^{2+}-abhängig, und stellt damit ein gutes System dar, um sowohl die „photocaging“-Methode als auch die Mischtechnik anzuwenden.

• Reaktivität und Eigenschaften des Ribozyms sind bereits auf der Basis einer Vielzahl von biochemischen Analysen sehr gut bekannt. Darüber hinaus ist die Kristallstruktur des Diels-Alder Ribozyms sowohl in der apo- als auch der holo-Form bekannt. Für die NMR-spektroskopische Untersuchung sind die Resonanzen der Iminoprotonen wichtige Sondensignale. Erste NMR-Experimente zeigen eine hohe chemische Verschiebungsdispersion und große Änderungen bei Zugabe von Ionen und Inhibitor, so dass man die Kinetik der RNA-Faltung anhand einer Reihe von Signale bestimmen kann.

• Zeitgleich wurde das Diels-Alder Ribozym auch mit komplementären biophysikalischen Methoden wie Fluorescence Resonance Energy Transfer (FRET) und Elektronenspin-Resonanz (EPR) untersucht. Dabei ergaben sich wertvolle

Informationen über die Energien der an der Faltung beteiligten Konformationen und die Anzahl von Metallionenbindungsstellen.

In der vorliegenden Arbeiten wurden drei Ribozyme aus der Diels-Alder-Familie untersucht. Die Faltung der Wildtypsequenz (A27 WT) wurde zunächst mittels der „photocaging"-Technik untersucht. Dabei zeigte sich, dass die Metallionen induzierte Faltung zu schnell ist, um mittels zeitaufgelöster NMR-Spektroskopie untersucht werden zu können. Deshalb wurde eine Einzelnukleotidmutante (G27 MUT) ausgewählt und die Kinetik ihrer Faltung mit beiden Methoden untersucht. Die Kristallstrukturen der holo-Zustände von A27 WT und G27 MUT sind gleich, die Mutante weist allerdings eine um 30% reduzierte katalytische Aktivität auf. Eine zweite Einzelnukleotidmutante (G40 MUT) wurde aufgrund der Ähnlichkeit zu G27 MUT untresucht. G40 MUT ist eine interessante Mutante, da sie sich von G27 MUT nur in der Lage der G und der A-Nukleotide unterscheidet, was allerdings zu einer Reduktion der Aktivität um 70% im Vergleich zur Wildtypribozym führt.

Statische NMR-Ergebnisse zeigten, dass beide Mutanten im apo-Zustand (ohne Metallionen) konformationelle Heterogenität aufwiesen. Diese konformationelle Heterogenität im Apo-Zustand der beiden Mutanten-Ribozyme hat signifikanten Einfluss auf ihre Faltungs-Raten und ihre Faltungswege. Die Metallionen-induzierten Faltungsraten für beide Mutanten werden durch die Auflösung von ungünstigen, nicht-nativen Basenpaaren im Apo-Zustand des Diels-Alder Ribozyms im ratenbestimmenden Schritt beeinflusst. Die zeitaufgelösten Experimente zeigten eine biexponentielle Kinetik für beide Mutanten. Die beobachteten Faltungsraten unterschieden sich um drei Größenordnungen von der Kinetik der Faltung von A27 WT.

Ein Modell auf der Grundlage der Charakterisierung der metallfreien sowie der Substrat- und Metall- gebundenen Formen der Ribozyme wird vorgeschlagen, das den Unterschied in der Faltung zwischen Wildtyp und den beiden anderen Ribozymen erklärt. Außerdem gibt es Hinweise, dass die Aktivität des Ribozyms moduliert ist aufgrund der örtlichen Dynamik rund um die katalytische Tasche für das G27 MUT Ribozym.

Publications

List of publications part of thesis in Frankfurt am Main

Fürtig B, Buck J, Manoharan V,Bermel W, Jäschke A, Wenter P, Pitsch S, Schwalbe H. Time-resolved NMR studies of RNA folding. *Biopolymers*, Volume 86; NUMBER 5-6, pages 360-383. **2007**

Manoharan, V, Fürtig, B, Jäschke, A, Schwalbe, H. Metal-Induced Folding of Diels-Alderase Ribozymes Studied by Static and Time-Resolved NMR Spectroscopy. *J. Am. Chem. Soc.*, 131 (17), pp 6261–6270. **2009**

List of previous publications

Ganapathiraju, M., Manoharan, V. and Klein-Seetharaman, J. BLMT. Statistical Sequence Analysis Using N-Grams. *Applied Bioinformatics. Volume 3 (2-3): 193-200.* **2004**

Ganapathiraju, M., Manoharan, V., Reddy, R. and Klein-Seetharaman, J. Collaborative Discovery through Biological Language Modeling Interface. *Lecture Notes in Computer Science*, Volume 3864: 300-321. **2006**

Budyak, I., Mironova, O., Yanamala, N., Manoharan, V., Bueldt, G., Schlesinger, R. and Klein-Seetharaman, J. Flexibility of the Cytoplasmic Domain of the Phototaxis Transducer II from Natronomonas pharaonis. *Journal of Biophysics*. Volume 2008. Article ID 267912, 11 pages. doi:10.1155/2008/267912. **2008**

References

Akasaka, K. (2003). Highly fluctuating protein structures revealed by variable-pressure nuclear magnetic resonance. Biochemistry *42*, 10875-10885.

Akke, M., Fiala, R., Jiang, F., Patel, D., and Palmer, A.G., 3rd (1997). Base dynamics in a UUCG tetraloop RNA hairpin characterized by 15N spin relaxation: correlations with structure and stability. RNA (New York, NY *3*, 702-709.

Al-Hashimi, H.M. (2005). Dynamics-based amplification of RNA function and its characterization by using NMR spectroscopy. Chembiochem *6*, 1506-1519.

Al-Hashimi, H.M., and Walter, N.G. (2008). RNA dynamics: it is about time. Curr Opin Struct Biol *18*, 321-329.

Ansel-McKinney, P., and Gehrke, L. (1997). Footprinting RNA—Protein Complexes with Hydroxyl Radicals In mRNA Formation and Function J.D. Richter, ed., pp. 285-303.

Auclair, K., Sutherland, A., Kennedy, J., Witter, D.J., Van den Heever, J.P., Hutchinson, C.R., and Vederas, J.C. (2000). Lovastatin nonaketide synthase catalyzes an intramolecular Diels-Alder reaction of a substrate analogue. J Am Chem Soc *122*, 11519–11520.

Balbach, J., Forge, V., van Nuland, N.A., Winder, S.L., Hore, P.J., and Dobson, C.M. (1995). Following protein folding in real time using NMR spectroscopy. Nat Struct Biol *2*, 865-870.

Bartel, D.P., and Szostak, J.W. (1993). Isolation of new ribozymes from a large pool of random sequences [see comment]. Science *261*, 1411-1418.

Beaudry, A.A., and Joyce, G.F. (1990). Minimum secondary structure requirements for catalytic activity of a self-splicing group I intron. Biochemistry *29*, 6534-6539.

Bédoyère, C.D.l. (2005). The Discovery of DNA, Illustrated edn (Evans Brothers).

Blount, K.F., and Uhlenbeck, O.C. (2005a). The structure-function dilemma of the hammerhead ribozyme. Annu Rev Biophys Biomol Struct *34*, 415-440.

Blount, K.F., and Uhlenbeck, O.C. (2005b). The structure-function dilemma of the hammerhead ribozyme. Annual review of biophysics and biomolecular structure *34*, 415-440.

Bondensgaard, K., Mollova, E.T., and Pardi, A. (2002). The global conformation of the hammerhead ribozyme determined using residual dipolar couplings. Biochemistry *41*, 11532-11542.

Braisted, A.C., and Schultz, P.G. (1990). An antibody-catalyzed bimolecular Diels-Alder reaction. J Am Chem Soc *112*, 7430-7431.

Breaker, R.R. (1997). In Vitro Selection of Catalytic Polynucleotides. Chem Rev *97*, 371-390.

Brenowitz, M., Chance, M.R., Dhavan, G., and Takamoto, K. (2002). Probing the structural dynamics of nucleic acids by quantitative time-resolved and equilibrium hydroxyl radical "footprinting". Curr Opin Struct Biol *12*, 648-653.

Buck, J., Furtig, B., Noeske, J., Wohnert, J., and Schwalbe, H. (2007). Time-resolved NMR methods resolving ligand-induced RNA folding at atomic resolution. Proc Natl Acad Sci USA *104*, 15699.

Butcher, S.E. (2001). Structure and function of the small ribozymes. Curr Opin Struct Biol *11*, 315-320.

Carmi, N., Shultz, L.A., and Breaker, R.R. (1996). In vitro selection of self-cleaving DNAs. Chemistry & biology *3*, 1039-1046.

Cech, T.R. (1990). Self-splicing of group I introns. Annual review of biochemistry *59*, 543-568.

Cole, P.E., and Crothers, D.M. (1972). Conformational changes of transfer ribonucleic acid. Relaxation kinetics of the early melting transition of methionine transfer ribonucleic acid (Escherichia coli). Biochemistry *11*, 4368-4374.

Cole, P.E., Yang, S.K., and Crothers, D.M. (1972). Conformational changes of transfer ribonucleic acid. Equilibrium phase diagrams. Biochemistry *11*, 4358-4368.

Coutts, S.M. (1971). Thermodynamics and kinetics of G-C base pairing in the isolated extra arm of serine-specific transfer RNA from yeast. Biochim Biophys Acta *232*, 94-106.

Craig, M.E., Crothers, D.M., and Doty, P. (1971). Relaxation kinetics of dimer formation by self complementary oligonucleotides. J Mol Biol *62*, 383-401.

Crothers, D.M., Cole, P.E., Hilbers, C.W., and Shulman, R.G. (1974). The molecular mechanism of thermal unfolding of Escherichia coli formylmethionine transfer RNA. J Mol Biol *87*, 63-88.

Dahm, R. (2005). Friedrich Miescher and the discovery of DNA. Developmental biology *278*, 274-288.

Dam, E., Pleij, K., and Draper, D. (1992). Structural and functional aspects of RNA pseudoknots. Biochemistry *31*, 11665-11676.

Deras, M.L., Brenowitz, M., Ralston, C.Y., Chance, M.R., and Woodson, S.A. (2000). Folding mechanism of the Tetrahymena ribozyme P4-P6 domain. Biochemistry *39*, 10975-10985.

DeRose, V.J. (2002). Two decades of RNA catalysis. Chemistry & biology *9*, 961-969.

Diegelman-Parente, A., and Bevilacqua, P.C. (2002). A mechanistic framework for co-transcriptional folding of the HDV genomic ribozyme in the presence of downstream sequence. J Mol Biol *324*, 1-16.

Dingley, A.J., and Grzesiek, S. (1998). Direct observation of hydrogen bonds in nucleic acid base pairs by internucleotide (2)J(NN) couplings. J Am Chem Soc *120*, 8293-8297.

Ditzler, M.A., Sponer, J., and Walter, N.G. (2009). Molecular dynamics suggest multifunctionality of an adenine imino group in acid-base catalysis of the hairpin ribozyme. RNA (New York, NY *15*, 560-575.

Doudna, J.A., and Cech, T.R. (2002). The chemical repertoire of natural ribozymes. Nature *418*, 222-228.

Draper, D.E. (1996). Parallel worlds. Nat Struct Biol *3*, 397-400.

Draper, D.E. (1999). Themes in RNA-protein recognition. J Mol Biol *293*, 255-270.

Draper, D.E., Grilley, D., and Soto, A.M. (2005). Ions and RNA folding. Annual review of biophysics and biomolecular structure *34*, 221-243.

Eddy, S.R. (2001). Non-coding RNA genes and the modern RNA world. Nature reviews *2*, 919-929.

Edwards, T.E., and Sigurdsson, S.T. (2005). EPR spectroscopic analysis of U7 hammerhead ribozyme dynamics during metal ion induced folding. Biochemistry *44*, 12870-12878.

Ellies-Davis, G.C.R., and Kaplan, J.H. (1988). J Org Chem *53*, 1966-1969.

Ellington, A.D., and Szostak, J.W. (1990). In vitro selection of RNA molecules that bind specific ligands. Nature *346*, 818-822.

Ernst, R.R., Bodenhausen, G., and Wokaun, A. (1990). Principles of Nuclear Magnetic Resonance in One and Two Dimensions (Oxford University Press).

Famulok, M., and Jenne, A. (1998). Oligonucleotide libraries--variatio delectat. Current opinion in chemical biology *2*, 320-327.

Fedor, M.J. (2002). The role of metal ions in RNA catalysis. Curr Opin Struct Biol *12*, 289-295.

Fedorova, O., and Zingler, N. (2007). Group II introns: structure, folding and splicing mechanism. Biol Chem *388*, 665-678.

Felden, B. (2007). RNA structure: experimental analysis. Current opinion in microbiology *10*, 286-291.

Ferre-D'Amare, A.R. (2004). The hairpin ribozyme. Biopolymers *73*, 71-78.

Ferre-D'Amare, A.R., Zhou, K., and Doudna, J.A. (1998). Crystal structure of a hepatitis delta virus ribozyme. Nature *395*, 567-574.

Fresco, J.R., Adams, A., Ascione, R., Henley, D., and Lindahl, T. (1966). Tertiary structure in transfer ribonucleic acids. Cold Spring Harbor symposia on quantitative biology *31*, 527-537.

Furtig, B., Buck, J., Manoharan, V., Bermel, W., Jaschke, A., Wenter, P., Pitsch, S., and Schwalbe, H. (2007). Time-resolved NMR studies of RNA folding. Biopolymers *86*, 360-383.

Furtig, B., Richter, C., Schell, P., Wenter, P., Pitsch, S., and Schwalbe, H. (2008). NMR-spectroscopic characterization of phosphodiester bond cleavage catalyzed by the minimal hammerhead ribozyme. RNA biology *5*, 41-48.

Furtig, B., Richter, C., Wohnert, J., and Schwalbe, H. (2003). NMR spectroscopy of RNA. ChemBioChem *4*, 936-962.

Fürtig, B., Wenter, P., Reymond, L., Richter, C., Pitsch, S., and Schwalbe, H. (2007). Conformational dynamics of bistable RNAs studied by time-resolved NMR spectroscopy. J Am Chem Soc *129*, 16222-16229.

Gilbert, W. (1986). Origin of life: The RNA world. Nature *319*, 618.

Gillet, R., and Felden, B. (2001). Emerging views on tmRNA-mediated protein tagging and ribosome rescue. Molecular microbiology *42*, 879-885.

Grosshans, C.A., and Cech, T.R. (1989). Metal ion requirements for sequence-specific endoribonuclease activity of the Tetrahymena ribozyme. Biochemistry *28*, 6888-6894.

Guerrier-Takada, C., Gardiner, K., Marsh, T., Pace, N., and Altman, S. (1983). The RNA moiety of ribonuclease P is the catalytic subunit of the enzyme. Cell *35*, 849-857.

Guimaraes, C.R.W., Udier-Blagovic, M., and Jorgensen, W.L. (2005). Macrophomate Synthase: QM/MM Simulations Address the Diels-Alder versus Michael-Aldol Reaction Mechanism. J Am Chem Soc *127*, 3577-3588.

Hammann, C., Norman, D.G., and Lilley, D.M.J. (2001). Dissection of the ion-induced folding of the hammerhead ribozyme using 19F NMR. Proc Natl Acad Sci USA *98*, 5503–5508.

Hammond, S.M., Bernstein, E., Beach, D., and Hannon, G.J. (2000). An RNA-directed nuclease mediates post-transcriptional gene silencing in Drosophila cells. Nature *404*, 293-296.

Hampel, K.J., and Burke, J.M. (2001). Time-resolved hydroxyl-radical footprinting of RNA using Fe(II)-EDTA. Methods *23*, 233-239.

Hannon, G.J., Rivas, F.V., Murchison, E.P., and Steitz, J.A. (2006). The expanding universe of noncoding RNAs. Cold Spring Harbor symposia on quantitative biology *71*, 551-564.

Hawkins, E.R., Chang, S.H., and Mattice, W.L. (1977). Kinetics of the renaturation of yeast tRNA3 leu. Biopolymers *16*, 1557-1566.

Heilman-Miller, S.L., and Woodson, S.A. (2003). Effect of transcription on folding of the Tetrahymena ribozyme. RNA (New York, NY *9*, 722-733.

Herschlag, D. (1995). RNA chaperones and the RNA folding problem. The Journal of biological chemistry *270*, 20871-20874.

Hiley, S.L., and Collins, R.A. (2001). Rapid formation of a solvent-inaccessible core in the Neurospora Varkud satellite ribozyme. Embo J *20*, 5461-5469.

Hilvert, D., Hill, K.W., Nared, K.D., and Auditor, M.T.M. (1989). Antibody catalysis of the Diels-Alder reaction. J Am Chem Soc *111*, 9261-9262.

Hobartner, C., and Micura, R. (2003a). Bistable secondary structures of small RNAs and their structural probing by comparative imino proton NMR spectroscopy. J Mol Biol *325*, 421-431.

Hobartner, C., and Micura, R. (2003b). Bistable secondary structures of small RNAs and their structural probing by comparative imino proton NMR spectroscopy. J Mol Biol *325*, 421-431.

Hobartner, C., Mittendorfer, H., Breuker, K., and Micura, R. (2004). Triggering of RNA secondary structures by a functionalized nucleobase. Angew Chem Int Ed Engl *43*, 3922-3925.

Hobartner, C., and Silverman, S.K. (2005). Modulation of RNA tertiary folding by incorporation of caged nucleotides. Angewandte Chemie (International ed *44*, 7305-7309.

Hoeltzli, S.D., and Frieden, C. (1995). Stopped-flow NMR spectroscopy: real-time unfolding studies of 6-19F-tryptophan-labeled Escherichia coli dihydrofolate

reductase. Proceedings of the National Academy of Sciences of the United States of America *92*, 9318-9322.

Hoeltzli, S.D., and Frieden, C. (1996). Real-time refolding studies of 6-19F-tryptophan labeled Escherichia coli dihydrofolate reductase using stopped-flow NMR spectroscopy. Biochemistry *35*, 16843-16851.

Hoogstraten, C.G., Legault, P., and Pardi, A. (1998). NMR solution structure of the lead-dependent ribozyme: evidence for dynamics in RNA catalysis. J Mol Biol *284*, 337-350.

Huq, I., Tamilarasu, N., and Rana, T.M. (1999). Visualizing tertiary folding of RNA and RNA-protein interactions by a tethered iron chelate: analysis ofHIV-1 Tat-TAR complex. Nucleic acids research *27*, 1084-1093.

Ilin, S., Hoskins, A., Ohlenschlager, O., Jonker, H.R., Schwalbe, H., and Wohnert, J. (2005). Domain reorientation and induced fit upon RNA binding: solution structure and dynamics of ribosomal protein L11 from Thermotoga maritima. Chembiochem *6*, 1611-1618.

Illangasekare, M., Sanchez, G., Nickles, T., and Yarus, M. (1995). Aminoacyl-RNA synthesis catalyzed by an RNA. Science *267*, 643-647.

Isaacs, F.J., Dwyer, D.J., Ding, C., Pervouchine, D.D., Cantor, C.R., and Collins, J.J. (2004). Engineered riboregulators enable post-transcriptional control of gene expression. Nature biotechnology *22*, 841-847.

Jacob, F., and Monod, J. (1961). Genetic regulatory mechanisms in the synthesis of proteins. J Mol Biol *3*, 318-356.

Jäschke, A. (2001). RNA-catalyzed carbon-carbon bond formation. Biol Chem *382*, 1321–1325.

Jenne, A., and Famulok, M. (1998). A novel ribozyme with ester transferase activity. Chemistry & biology *5*, 23-34.

Joyce, G.F. (2004). Directed evolution of nucleic acid enzymes. Annual review of biochemistry *73*, 791-836.

Juneau, K., Podell, E., Harrington, D.J., and Cech, T.R. (2001). Structural basis of the enhanced stability of a mutant ribozyme domain and a detailed view of RNA--solvent interactions. Structure *9*, 221-231.

Kaplan, J.H., and Ellis-Davies, G.C.R. (1988). Photolabile Chelators for the Rapid Photorelease of Divalent Cations. Proc Natl Acad Sci USA *85*, 6571-6575.

Katayama, K., Kobayashi, T., Oikawa, H., Honma, M., and Ichihara, A. (1998). Enzymatic activity and partial purification of solanapyrone synthase: first enzyme catalyzing Diels–Alder reaction. Biochim Biophys Acta *1384*, 387-395.

Keenan, R.J., Freymann, D.M., Stroud, R.M., and Walter, P. (2001). The signal recognition particle. Annual review of biochemistry *70*, 755-775.

Keiper, S., Bebenroth, D., Seelig, B., Westhof, E., and Jäschke, A. (2004). Architecture of a Diels-Alderase Ribozyme with a Preformed Catalytic Pocket. Chem Biol *11*, 1217-1227.

Kim, S.P., Leach, A.G., and Houk, K.N. (2002). The Origins of Noncovalent Catalysis of Intermolecular Diels-Alder Reactions by Cyclodextrins, Self-Assembling Capsules, Antibodies, and RNAses. J Org Chem *67*, 4250-4260.

Kisseleva, N., Kraut, S., Jäschke, A., and Schiemann, O. (2007). Characterizing multiple metal ion binding sites within a ribozyme by cadmium-induced EPR silencing. HFSP J *1*, 127-136.

Kleinman, M.E., Yamada, K., Takeda, A., Chandrasekaran, V., Nozaki, M., Baffi, J.Z., Albuquerque, R.J., Yamasaki, S., Itaya, M., Pan, Y.*, et al.* (2008). Sequence- and target-independent angiogenesis suppression by siRNA via TLR3. Nature *452*, 591-597.

Kobitski, A.Y., Nierth, A., Helm, M., Jaschke, A., and Nienhaus, G.U. (2007). Mg 2+-dependent folding of a Diels-Alderase ribozyme probed by single-molecule FRET analysis. Nucleic Acids Res *35*, 2047.

Koduvayur, S.P., and Woodson, S.A. (2004). Intracellular folding of the Tetrahymena group I intron depends on exon sequence and promoter choice. RNA (New York, NY *10*, 1526-1532.

Koizumi, M., and Ohtsuka, E. (1991). Effects of phosphorothioate and 2-amino groups in hammerhead ribozymes on cleavage rates and Mg2+ binding. Biochemistry *30*, 5145-5150.

Korzhnev, D.M., Salvatella, X., Vendruscolo, M., Di Nardo, A.A., Davidson, A.R., Dobson, C.M., and Kay, L.E. (2004). Low-populated folding intermediates of Fyn SH3 characterized by relaxation dispersion NMR. Nature *430*, 586-590.

Kruger, K., Grabowski, P.J., Zaug, A.J., Sands, J., Gottschling, D.E., and Cech, T.R. (1982). Self-splicing RNA: autoexcision and autocyclization of the ribosomal RNA intervening sequence of Tetrahymena. Cell *31*, 147-157.

Kuhn, T., and Schwalbe, H. (2000). Monitoring the Kinetics of Ion-Dependent Protein Folding by Time-Resolved NMR Spectroscopy at Atomic Resolution. J Am Chem Soc *122*, 6169-6174.

Laggerbauer, B., Murphy, F.L., and Cech, T.R. (1994). Two major tertiary folding transitions of the Tetrahymena catalytic RNA. Embo J *13*, 2669-2676.

Latham, J.A., and Cech, T.R. (1989). Defining the inside and outside of a catalytic RNA molecule. Science *245*, 276-282.

Legault, P., Hoogstraten, C.G., Metlitzky, E., and Pardi, A. (1998). Order, dynamics and metal-binding in the lead-dependent ribozyme. J Mol Biol *284*, 325-335.

Leontis, N.B., and Westhof, E. (2001). Geometric nomenclature and classification of RNA base pairs. RNA (New York, NY *7*, 499-512.

Lerner, R.A., Benkovic, S.J., and Schultz, P.G. (1991). At the crossroads of chemistry and immunology: catalytic antibodies. Science *252*, 659-667.

Lescoute, A., and Westhof, E. (2006). The interaction networks of structured RNAs. Nucleic Acids Res *34*, 6587-6604.

Leulliot, N., Baumruk, V., Abdelkafi, M., Turpin, P.Y., Namane, A., Gouyette, C., Huynh-Dinh, T., and Ghomi, M. (1999). Unusual nucleotide conformations in GNRA and UNCG type tetraloop hairpins: evidence from Raman markers assignments. Nucleic Acids Res *27*, 1398-1404.

Leulliot, N., and Varani, G. (2001). Current topics in RNA-protein recognition: control of specificity and biological function through induced fit and conformational capture. Biochemistry *40*, 7947-7956.

Lipfert, J., and Doniach, S. (2007). Small-angle X-ray scattering from RNA, proteins, and protein complexes. Annual review of biophysics and biomolecular structure *36*, 307-327.

Liu, H., Robinet, J.J., Ananvoranich, S., and Gauld, J.W. (2007). Density functional theory investigation on the mechanism of the hepatitis delta virus ribozyme. The journal of physical chemistry *111*, 439-445.

Lorsch, J.R., and Szostak, J.W. (1994). In vitro evolution of new ribozymes with polynucleotide kinase activity. Nature *371*, 31-36.

Lynch, D.C., and Schimmel, P.R. (1974). Cooperative binding of magnesium to transfer ribonucleic acid studied by a fluorescent probe. Biochemistry *13*, 1841-1852.

Maas, S., and Rich, A. (2000). Changing genetic information through RNA editing. Bioessays *22*, 790-802.

Mahen, E.M., Harger, J.W., Calderon, E.M., and Fedor, M.J. (2005). Kinetics and thermodynamics make different contributions to RNA folding in vitro and in yeast. Molecular cell *19*, 27-37.

Mathews, D.H., Sabina, J., Zuker, M., and Turner, D.H. (1999). Expanded sequence dependence of thermodynamic parameters improves prediction of RNA secondary structure. J Mol Biol *288*, 911-940.

McCray, J.A., Fidler-Lim, N., Ellis-Davies, G.C., and Kaplan, J.H. (1992). Rate of release of Ca2+ following laser photolysis of the DM-nitrophen-Ca2+ complex. Biochemistry *31*, 8856-8861.

McKay, D.B. (1996). Structure and function of the hammerhead ribozyme: an unfinished story. RNA (New York, NY *2*, 395-403.

Menger, M., Eckstein, F., and Porschke, D. (2000). Dynamics of the RNA hairpin GNRA tetraloop. Biochemistry *39*, 4500-4507.

Merino, E.J., Wilkinson, K.A., Coughlan, J.L., and Weeks, K.M. (2005). RNA structure analysis at single nucleotide resolution by selective 2'-hydroxyl acylation and primer extension (SHAPE). J Am Chem Soc *127*, 4223-4231.

Meroueh, M., and Chow, C.S. (1999). Thermodynamics of RNA hairpins containing single internal mismatches. Nucleic Acids Res *27*, 1118-1125.

Mironov, A.S., Gusarov, I., Rafikov, R., Lopez, L.E., Shatalin, K., Kreneva, R.A., Perumov, D.A., and Nudler, E. (2002). Sensing small molecules by nascent RNA: a mechanism to control transcription in bacteria. Cell *111*, 747-756.

Mohr, S., Stryker, J.M., and Lambowitz, A.M. (2002). A DEAD-box protein functions as an ATP-dependent RNA chaperone in group I intron splicing. Cell *109*, 769-779.

Mok, K.H., Nagashima, T., Day, I.J., Jones, J.A., Jones, C.J.V., Dobson, C.M., and Hore, P.J. (2003). Rapid Sample-Mixing Technique for Transient NMR and Photo-CIDNP Spectroscopy: Applications to Real-Time Protein Folding. J Am Chem Soc *125*, 12484-12492.

Nagel, J.H., Gultyaev, A.P., Oistamo, K.J., Gerdes, K., and Pleij, C.W. (2002). A pH-jump approach for investigating secondary structure refolding kinetics in RNA. Nucleic Acids Res *30*, e63.

Nahvi, A., Sudarsan, N., Ebert, M.S., Zou, X., Brown, K.L., and Breaker, R.R. (2002). Genetic control by a metabolite binding mRNA. Chemistry & biology *9*, 1043.

Nakano, S., Chadalavada, D.M., and Bevilacqua, P.C. (2000). General acid-base catalysis in the mechanism of a hepatitis delta virus ribozyme. Science *287*, 1493-1497.

Neidle, S. (2008). Principles of Nucleic Acid Structure (Elsevier).

Neudecker, P., Zarrine-Afsar, A., Choy, W.Y., Muhandiram, D.R., Davidson, A.R., and Kay, L.E. (2006). Identification of a collapsed intermediate with non-native long-range interactions on the folding pathway of a pair of Fyn SH3 domain mutants by NMR relaxation dispersion spectroscopy. J Mol Biol *363*, 958-976.

Nikolcheva, T., and Woodson, S.A. (1999). Facilitation of group I splicing in vivo: misfolding of the Tetrahymena IVS and the role of ribosomal RNA exons. J Mol Biol *292*, 557-567.

Nissen, P., Hansen, J., Ban, N., Moore, P.B., and Steitz, T.A. (2000). The structural basis of ribosome activity in peptide bond synthesis. Science *289*, 920-930.

Noeske, J.R., C.; Grundl, M. A.; Nasiri, H.R.; Schwalbe, H.; Wöhnert. J. (2005). An intermolecular base triple as the basis of ligand specificity and affinity in the guanine- and adenine-sensing riboswitch RNAs. Proc Natl Acad Sci USA *102*, 1372-1377.

Nölting, B. (2006). Protein folding kinetics - Biophysical Methods, Edition: 2, illustrated edn (Birkhäuser).

Ose, T., Watanabe, K., Mie, T., Honma, M., Watanabe, H., Yao, M., Oikawa, H., and Tanaka, I. (2003). Insight into a natural Diels-Alder reaction from the structure of macrophomate synthase. Nature *422*, 185-189.

Pan, T., Artsimovitch, I., Fang, X.W., Landick, R., and Sosnick, T.R. (1999). Folding of a large ribozyme during transcription and the effect of the elongation factor NusA. Proceedings of the National Academy of Sciences of the United States of America *96*, 9545-9550.

Peattie, D.A., and Gilbert, W. (1980). Chemical probes for higher-order structure in RNA. Proceedings of the National Academy of Sciences of the United States of America *77*, 4679-4682.

Perrotta, A.T., Shih, I., and Been, M.D. (1999). Imidazole rescue of a cytosine mutation in a self-cleaving ribozyme. Science *286*, 123-126.

Pindur, U., Lutz, G., and Otto, C. (1993). Acceleration and selectivity enhancement of Diels-Alder reactions by special and catalytic methods. Chem Rev *93*, 741-761.

Pingoud, A., Fließ, A., and Pingoud, V. (1987). HPLC of oligonucleotides. Anal BioanalChem *327*, 22-23.

Pleij, C.W., Rietveld, K., and Bosch, L. (1985). A new principle of RNA folding based on pseudoknotting. Nucleic Acids Res *13*, 1717-1731.

Pley, H.W., Flaherty, K.M., and McKay, D.B. (1994). Three-dimensional structure of a hammerhead ribozyme. Nature *372*, 68-74.

Porschke, D., and Eigen, M. (1971). Co-operative non-enzymic base recognition. 3. Kinetics of the helix-coil transition of the oligoribouridylic--oligoriboadenylic acid system and of oligoriboadenylic acid alone at acidic pH. J Mol Biol *62*, 361-381.

Price, M.A., and Tullius, T.D. (1992). Using hydroxyl radical to probe DNA structure. Methods in enzymology *212*, 194-219.

Prody, G.A., Bakos, J.T., Buzayan, J.M., Schneider, I.R., and Bruening, G. (1986). Autolytic Processing of Dimeric Plant Virus Satellite RNA. Science *231*, 1577-1580.

Pyle, A.M., and Green, J.B. (1995). RNA folding. Curr Opin Struct Biol *5*, 303-310.

Qin, P.Z., and Dieckmann, T. (2004). Application of NMR and EPR methods to the study of RNA. Curr Opin Struct Biol *14*, 350-359.

Regis, E. (2008). What is Life?: Investigating the Nature of Life in the Age of Synthetic Biology (Farrar, Straus, and Giroux).

Repsilber, D., Wiese, S., Rachen, M., Schroder, A.W., Riesner, D., and Steger, G. (1999). Formation of metastable RNA structures by sequential folding during transcription: time-resolved structural analysis of potato spindle tuber viroid (-)-stranded RNA by temperature-gradient gel electrophoresis. RNA (New York, NY *5*, 574-584.

Rick Russell, X.Z., Hazen P. Babcock, Ian S. Millett, Sebastian Doniach, Steven Chu, and Daniel Herschlag (2002). Exploring the folding landscape of a structured RNA. PNAS *99*, 6.

Riesner, D., Maass, G., Thiebe, R., Philippsen, P., and Zachau, H.G. (1973). The conformational transitions in yeast tRNAPhe as studied with tRNAPhe fragments. European journal of biochemistry / FEBS *36*, 76-88.

Roelfes, G., and Feringa, B.L. (2005). DNA-Based Asymmetric Catalysis. Angew Chem, Int Ed *44*, 3230-3232.

Romero-Lopez, C., Barroso-delJesus, A., Puerta-Fernandez, E., and Berzal-Herranz, A. (2005). Interfering with hepatitis C virus IRES activity using RNA molecules identified by a novel in vitro selection method. Biol Chem *386*, 183-190.

Rupert, P.B., and Ferré-D'Amaré, A.R. (2001). Crystal structure of a hairpin ribozyme- inhibitor complex with implications for catalysis. Nature *410*, 780-786.

Russell, R., Millett, I.S., Doniach, S., and Herschlag, D. (2000). Small angle X-ray scattering reveals a compact intermediate in RNA folding. Nat Struct Mol Biol *7*, 367-370.

Russell, R., Millett, I.S., Tate, M.W., Kwok, L.W., Nakatani, B., Gruner, S.M., Mochrie, S.G.J., Pande, V., Doniach, S., Herschlag, D.*, et al.* (2002). Rapid compaction during RNA folding. Proc Natl Acad Sci USA *99*, 4266-4271.

Saenger, W. (1984). Principles of Nucleic Acid Structure.

Saville, B.J., and Collins, R.A. (1990). A site-specific self-cleavage reaction performed by a novel RNA in Neurospora mitochondria. Cell *61*, 685-696.

Schroeder, R., Grossberger, R., Pichler, A., and Waldsich, C. (2002). RNA folding in vivo. Curr Opin Struct Biol *12*, 296-300.

Schwalbe, H., Buck, J., Furtig, B., Noeske, J., and Wohnert, J. (2007). Structures of RNA switches: insight into molecular recognition and tertiary structure. Angewandte Chemie (International ed *46*, 1212-1219.

Sclavi, B., Sullivan, M., Chance, M.R., Brenowitz, M., and Woodson, S.A. (1998a). RNA folding at millisecond intervals by synchrotron hydroxyl radical footprinting. Science *279*, 1940-1943.

Sclavi, B., Woodson, S., Sullivan, M., Chance, M., and Brenowitz, M. (1998b). Following the folding of RNA with time-resolved synchrotron X-ray footprinting. Methods in enzymology *295*, 379-402.

Sclavi, B., Woodson, S., Sullivan, M., Chance, M.R., and Brenowitz, M. (1997). Time-resolved synchrotron X-ray "footprinting", a new approach to the study of nucleic acid structure and function: application to protein-DNA interactions and RNA folding. J Mol Biol *266*, 144-159.

Scott, W.G., Finch, J.T., and Klug, A. (1995). The crystal structure of an all-RNA hammerhead ribozyme: a proposed mechanism for RNA catalytic cleavage. Cell *81*, 991-1002.

Seelig, B., and Jäschke, A. (1999). A small catalytic RNA motif with Diels-Alderase activity. Chem Biol *6*, 167-176.

Seelig, B., Keiper, S., Stuhlmann, F., and Jäschke, A. (2000). Enantioselective Ribozyme Catalysis of a Bimolecular Cycloaddition Reaction. Angew Chem, Int Ed *39*, 4576-4579.

Serganov, A., Keiper, S., Malinina, L., Tereshko, V., Skripkin, E., Höbartner, C., Polonskaia, A., Phan, A.T., Wombacher, R., Micura, R*., et al.* (2005). Structural basis for Diels-Alder ribozyme-catalyzed carbon-carbon bond formation. Nat Struct Mol Biol *12*, 218-224.

Sklenar, V., and Bax, A. (1987). Spin-echo water suppression for the generation of pure-phase two-dimensional NMR spectra. J Magn Reson *74*, 469-479.

Soto, C. (2003). Unfolding the role of protein misfolding in neurodegenerative diseases. Nat Rev Neurosci *4*, 49-60.

Soukup, J.K., and Soukup, G.A. (2004). Riboswitches exert genetic control through metabolite-induced conformational change. Curr Opin Struct Biol *14*, 344-349.

Stoldt, M., Wöhnert, J., Ohlenschläger, O., Görlach, M., and Brown, L.R. (1999). The NMR structure of the 5S rRNA E-domain- protein L25 complex shows preformed and induced recognition. EMBO J *18*, 6508-6521.

Stonehouse, J., Shaw, G.L., and Keeler, J. (1994). Improving solvent suppression in jump-return NOESY experiments. J Biomol NMR *4*, 799-805.

Storz, G. (2002). An expanding universe of noncoding RNAs. Science *296*, 1260-1263.

Stuhlmann, F., and Jaschke, A. (2002). Characterization of an RNA Active Site: Interactions between a Diels-Alderase Ribozyme and Its Substrates and Products. J Am Chem Soc *124*, 3238-3244.

Suzumura, K., Warashina, M., Yoshinari, K., Tanaka, Y., Kuwabara, T., Orita, M., and Taira, K. (2000). Significant change in the structure of a ribozyme upon introduction of a phosphorothioate linkage at P9: NMR reveals a conformational fluctuation in the core region of a hammerhead ribozyme. FEBS Lett *473*, 106-112.

Szostak JW, E.R. (1993). In vitro selection of functional RNA sequences. In The RNA World A.J. Gesteland RF, ed. (Cold Spring Harbor, NY: Cold Spring Harbor Laboratory Press), pp. 511-533.

Tarasow, T.M., Tarasow, S.L., and Eaton, B.E. (1997). RNA-catalysed carbon-carbon bond formation. Nature *389*, 54.

Theimer, C.A., and Feigon, J. (2006). Structure and function of telomerase RNA. Curr Opin Struct Biol *16*, 307-318.

Treiber, D.K., and Williamson, J.R. (1999). Exposing the kinetic traps in RNA folding. Curr Opin Struct Biol *9*, 339-345.

Tuerk, C., and Gold, L. (1990). Systematic evolution of ligands by exponential enrichment: RNA ligands to bacteriophage T4 DNA polymerase. Science *249*, 505-510.

Tullius, T.D., and Dombroski, B.A. (1986). Hydroxyl radical "footprinting": high-resolution information about DNA-protein contacts and application to lambda repressor and Cro protein. Proceedings of the National Academy of Sciences of the United States of America *83*, 5469-5473.

Turner, B., Melcher, S.E., Wilson, T.J., Norman, D.G., and Lilley, D.M. (2005). Induced fit of RNA on binding the L7Ae protein to the kink-turn motif. RNA (New York, NY *11*, 1192-1200.

Tzeng, T.H., Tu, C.L., and Bruenn, J.A. (1992). Ribosomal frameshifting requires a pseudoknot in the Saccharomyces cerevisiae double-stranded RNA virus. Journal of virology *66*, 999-1006.

Valadkhan, S., and Manley, J.L. (2001). Splicing-related catalysis by protein-free snRNAs. Nature *413*, 701-707.

Valadkhan, S., Mohammadi, A., Wachtel, C., and Manley, J.L. (2007). Protein-free spliceosomal snRNAs catalyze a reaction that resembles the first step of splicing. RNA (New York, NY *13*, 2300-2311.

van Belkum, A., Abrahams, J.P., Pleij, C.W., and Bosch, L. (1985). Five pseudoknots are present at the 204 nucleotides long 3' noncoding region of tobacco mosaic virus RNA. Nucleic Acids Res *13*, 7673-7686.

Varani, G. (1995). Exceptionally Stable Nucleic Acid Hairpins. Annu Rev Biophys Biomol Struct *24*, 379-404.

Varani, G., Aboul-ela, F., and Allain, F.H.T. (1996). NMR investigation of RNA structure. Prog Nucl Magn Reson Spectrosc *29*, 51-127.

Verma, S., Vaish, N.K., and Eckstein, F. (1997). Structure-function studies of the hammerhead ribozyme. Current opinion in chemical biology *1*, 532-536.

Volkin, E., and Astrachan, L. (1956). Phosphorus incorporation in Escherichia coli ribo-nucleic acid after infection with bacteriophage T2. Virology *2*, 149-161.

Waldsich, C., and Schroeder, R. (2005). *In Vivo* Determination of RNA Structure by Dimethylsulfate. In Handbook of RNA Biochemistry, R. Hartmann, A. Binereif, A. Schoen, and E. Westhof, eds. (Wiley-VCH), p. 973.

Walter, N.G., Harris, D.A., Pereira, M.J., and Rueda, D. (2001). In the fluorescent spotlight: global and local conformational changes of small catalytic RNAs. Biopolymers *61*, 224-242.

Walter, P., and Blobel, G. (1982). Signal recognition particle contains a 7S RNA essential for protein translocation across the endoplasmic reticulum. Nature *299*, 691-698.

Watanabe, K., Mie, T., Ichihara, A., Oikawa, H., and Honma, M. (2000). Detailed Reaction Mechanism of Macrophomate Synthase. Extraordinary enzyme catalyzing five-step transformation from 2-pyrones to benzoates. J Biol Chem *275*, 38393-38401.

Weeks, K.M., and Cech, T.R. (1996). Assembly of a ribonucleoprotein catalyst by tertiary structure capture. Science *271*, 345-348.

Wenter, P., Furtig, B., Hainard, A., Schwalbe, H., and Pitsch, S. (2005). Kinetics of Photoinduced RNA Refolding by Real-Time NMR Spectroscopy. Angew Chem Int Ed *44*, 2600-2603.

Wenter, P., Furtig, B., Hainard, A., Schwalbe, H., and Pitsch, S. (2006). A Caged Uridine for the Selective Preparation of an RNA Fold and Determination of its Refolding Kinetics by Real-Time NMR. ChemBioChem *7*, 417-420.

Wijmenga, S.S., and van Buuren, B.N.M. (1998). The use of NMR methods for conformational studies of nucleic acids. Prog Nucl Magn Reson Spectrosc *32*, 287-387.

Williamson, J.R. (2000). Induced fit in RNA-protein recognition. Nat Struct Biol *7*, 834-837.

Winkler, W., Nahvi, A., and Breaker, R.R. (2002a). Thiamine derivatives bind messenger RNAs directly to regulate bacterial gene expression. Nature *419*, 952-956.

Winkler, W.C., Cohen-Chalamish, S., and Breaker, R.R. (2002b). An mRNA structure that controls gene expression by binding FMN. Proceedings of the National Academy of Sciences of the United States of America *99*, 15908-15913.

Winkler, W.C., Nahvi, A., Roth, A., Collins, J.A., and Breaker, R.R. (2004). Control of gene expression by a natural metabolite-responsive ribozyme. Nature *428*, 281-286.

Woese, C. (1968). The Genetic Code. (Harper & Row).

Wombacher, R., Keiper, S., Suhm, S., Serganov, A., Patel, D.J., and Jäschke, A. (2006). Control of stereoselectivity in an enzymatic reaction by backdoor access. Angew Chem Int Ed *45*, 2469–2472.

Woodson, S.A. (2000). Recent insights on RNA folding mechanisms from catalytic RNA. Cell Mol Life Sci *57*, 796-808.

Wu, M., and Tinoco Jr, I. (1998). RNA folding causes secondary structure rearrangement. Proc Natl Acad Sci USA *95*, 11555-11560.

Xi, X., Sun, Y., Karim, C.B., Grigoryants, V.M., and Scholes, C.P. (2008). HIV-1 nucleocapsid protein NCp7 and its RNA stem loop 3 partner: rotational dynamics of spin-labeled RNA stem loop 3. Biochemistry *47*, 10099-10110.

Zarrinkar, P.P., Wang, J., and Williamson, J.R. (1996). Slow folding kinetics of RNase P RNA. RNA (New York, NY *2*, 564-573.

Zeeb, M., and Balbach, J. (2004). Protein folding studied by real-time NMR spectroscopy. Methods *34*, 65-74.

Zhang, B., and Cech, T.R. (1997). Peptide bond formation by in vitro selected ribozymes. Nature *390*, 96-100.

Zhuang, X., Bartley, L.E., Babcock, H.P., Russell, R., Ha, T., Herschlag, D., and Chu, S. (2000). A single-molecule study of RNA catalysis and folding. Science *288*, 2048-2051.

Zhuang, X., and Rief, M. (2003). Single-molecule folding. Current opinion in structural biology *13*, 88-97.

Zuker, M. (2003). Mfold web server for nucleic acid folding and hybridization prediction. Nucleic Acids Res *31*, 3406-3415.

Curriculum Vitae

Name: VIJAYALAXMI MANOHARAN
Gender: Female
DOB: 24 February 1977
Nationality: Indian
Email: vijimanoharan@gmail.com

UNIVERSITY EDUCATION

Bachelor of Engineering, University of Madras, **India** Jun 94 – Apr 98

SCHOOLING

Good Shepherd Matriculation Higher Secondary School, (High School), Chennai, **India** Jun 92 - Apr 94

Good Shepherd Matriculation, (Primary School), Chennai, **India** Jun 82 - Apr 92

EMPLOYMENT HISTORY

Systems Programmer, Dept. of Pharmacology, Univ. of Pittsburgh**, USA** Sep 02 - May 05

Programmer Analyst, Smartsoft Technologies Ltd., **USA** Apr 02 - Aug 02

Senior Systems Executive, Global Infoserv Limited, **India** Jun 00 - Sep 01

Programmer, Korel Communications, **India** Jan 99 - May 00

Technical Writer, Domex Technologies Ltd., **India** May 98 - Dec 98

ACADEMIC TEACHERS

Prof. C Rajamanickam, Lect. Sathurappan, Dr. K Kannan, Dr. M. Lakshmi, Dr. S Mahalakshmi, Dr. Judith Klein-Seetharaman, Dr. Vanathi Gopalakrishnan, Prof. John Rosenberg, Prof. Gordon Rule, Prof. Ivet Bahar, Prof. Tom Mitchell, Prof. Ziv Bar Joseph, Prof. Roger Hendrix, Prof. Maria Kurnikova, Prof. Alan Waggoner, Prof. Daniel Zuckerman, Prof. Dr. Harald Schwalbe, Prof. Dr. Jens Wöhnert.